

# JNMMM

Journal of Nuclear Materials Management

- Cosmic-ray Muon Imaging of Spent Nuclear Fuel in Dry Storage Casks 5  
 J. Matthew Durham, Elena Guardincerri, Christopher L. Morris,  
 Daniel Poulson, Jeffrey D. Bacon, Joseph Fabritius, Shelby Fellows,  
 Kenie Plaud-Ramos, Deborah Morley, David Chichester, and Philip Winston
- Nuclear Materials Attribution for Reprocessed Uranium 13  
 Christopher Grove, Connah Johnson, and Kevin Hesketh
- Np/Pu Seeding of U in the Breeder Regions in an ASTRID-type Sodium 20  
 Fast Reactor to Avoid Production of Very High-quality Fissile Material  
 Christopher Grove and Kevin Hesketh
- Modeling and Analysis Methods for an On-Line Enrichment Monitor 27  
 L. Eric Smith, Kenneth D. Jarman, Richard S. Wittman, Mital A. Zalavadia, and  
 José March-Leuba
- Comparison of an Exact to an Approximate Sample Size 45  
 Calculation for Attribute Testing  
 Thomas Krieger and Tom L. Burr
- Simulation Study for Detection of Pin Diversion with the 49  
 Differential Die-away Instrument Using Fresh Nuclear Fuel  
 Alison V. Goodsell, Vladimir Henzl, Martyn T. Swinhoe, and  
 William S. Charlton





## Check out INMM's Career Center

**JOB SEEKERS:** Connect with employers who are looking for YOUR skills and experience with INMM's new Career Center.

- Tired of searching through hundreds of random job postings to find your next opportunity? Your search is about to become a whole lot easier with our new Career Center.
- Find targeted opportunities.
- Post your resume anonymously.
- Create job alerts.

**EMPLOYERS:** Make your Hire. Start at INMM's new Career Center. The INMM Career Center meets all your recruitment needs.

- Easily POST jobs.
- Search the RESUME BANK – Pay only for resumes of jobseekers interested in your position.
- ACCESS highly-qualified, professional candidates.
- Set-up PRE-SCREEN FILTERS to deliver the best candidates.

**INMM MEMBERS:** Post jobs at a substantial discount!



Visit the INMM's new **Career Center** today.

## Keep up with INMM news and activities!

Read the Communicator  
Published three times a year



The INMM Communicator

February 2016

The

## Communicator

The Institute of Nuclear Materials Management

### In This Issue

- 2 Inspiring Workshop on Mountain Landscape  
Susan Cohen-Unger
- 2 Inside Insights  
Corey Hinderstein
- 3 A Critical Turn in Japan's Nuclear Trajectory?  
Imminent Energy Decision-making Amid a Diversity of Interests  
Kathleen Araújo
- 3 Civilian Nuclear Energy Transparency and Stakeholder Engagement  
Katherine Bachner
- 5 Vulnerability Assessment Tools Workshop Summary  
Joe Rivers
- 5 Student Chapter Highlights  
University of Ibn Tofail, Morocco
- 7 Upcoming Events
- 7 INMM & WNTI Launch PATRAM Proceedings



57<sup>th</sup>

Institute of Nuclear Materials Management  
**Annual Meeting**



**Save the Date!**

July 24 – 28, 2016

Atlanta Marriott Marquis  
Atlanta, Georgia USA



**Technical Editor**

Markku Koskelo

**Technical Editor Emeritus**

Dennis Mangan

**Managing Editor**

Patricia Sullivan

**Associate Editors**

Sarah Frazar, Education and Training  
 Jeff Chapman, Facilities Operations  
 Gotthard Stein and Irmgard Niemeier,  
 International Safeguards  
 Louise Worrall and Rian Bahrán, Materials Control  
 and Accountability  
 Leslie Fishbone, Nonproliferation  
 and Arms Control  
 Felicia Durán, Nuclear Security and  
 Physical Protection  
 Glenn Abramczyk, Packaging, Transportation and  
 Disposition

**Book Review Editor**

Walter Kane

**INMM Executive Committee**

Larry Satkowiak, President  
 Corey Hinderstein, Vice President  
 Chris Pickett, Secretary  
 Robert U. Curl, Treasurer  
 Ken Sorenson, Immediate Past President

**Members At Large**

Jill N. Cooley  
 Cary Crawford  
 Ken Sanders  
 Steven Wyrick

**Design**

Shirley Soda

**Layout**

Brian McGowan

**Digital Interface**

GTXcel

**Advertising Contact**

Patricia Sullivan  
 INMM, One Parkview Plaza, Suite 800  
 Oakbrook Terrace, IL 60181 USA  
 Phone: +1-847-688-2236  
 Fax: +1-847-688-2251  
 Email: psullivan@inmm.org

JNMM (ISSN 0893-6188) is published four times a year by the Institute of Nuclear Materials Management Inc. The Institute of Nuclear Materials Management (INMM) is an international professional society dedicated to development and promulgation of practices for the safe, secure and effective stewardship of nuclear materials through the advancement of scientific knowledge, technical skills, policy dialogue, and enhancement of professional capabilities.

**DIGITAL SUBSCRIPTION RATES:** Annual (United States, Canada, and Mexico) \$200 for individuals. Institutional subscriptions are \$500 per year. Single copy of the proceedings of the Annual Meeting (United States and other countries) \$200. Send subscription requests to JNMM, One Parkview Plaza, Suite 800, Oakbrook Terrace, IL 60181 USA. Make checks payable to INMM.

**DISTRIBUTION** and delivery inquiries should be directed to JNMM, One Parkview Plaza, Suite 800, Oakbrook Terrace, IL 60181 USA, or contact Amy Lydic at +1-847-686-2236; fax, +1-847-686-2251; or email, inmm@inmm.org.

Opinions expressed in this publication by the authors are their own and do not necessarily reflect the opinions of the editors, Institute of Nuclear Materials Management, or the organizations with which the authors are affiliated, nor should publication of author viewpoints or identification of materials or products be construed as endorsement by this publication or by the Institute.

Topical Papers

|  |           |
|--|-----------|
| <b>Cosmic-ray Muon Imaging of Spent Nuclear Fuel in Dry Storage Casks</b>  | <b>5</b>  |
| <i>J. Matthew Durham, Elena Guardincerri, Christopher L. Morris, Daniel Poulson, Jeffrey D. Bacon, Joseph Fabritius, Shelby Fellows, Kenie Plaud-Ramos, Deborah Morley, David Chichester, and Philip Winston</i> |           |
| <b>Nuclear Materials Attribution for Reprocessed Uranium</b>   | <b>13</b> |
| <i>Christopher Grove, Connah Johnson, and Kevin Hesketh</i>  |           |
| <b>Np/Pu Seeding of U in the Breeder Regions in an ASTRID-type Sodium Fast Reactor to Avoid Production of Very High-quality Fissile Material</b>   | <b>20</b> |
| <i>Christopher Grove and Kevin Hesketh</i>   |           |
| <b>Modeling and Analysis Methods for an On-Line Enrichment Monitor</b>   | <b>27</b> |
| <i>L. Eric Smith, Kenneth D. Jarman, Richard S. Wittman, Mital A. Zalavadia, and José March-Leuba</i>  |           |
| <b>Comparison of an Exact to an Approximate Sample Size Calculation for Attribute Testing</b>  | <b>45</b> |
| <i>Thomas Krieger and Tom L. Burr</i>  |           |
| <b>Simulation Study for Detection of Pin Diversion with the Differential Die-away Instrument Using Fresh Nuclear Fuel</b>  | <b>49</b> |
| <i>Alison V. Goodsell, Vladimir Henzl, Martyn T. Swinhoe, and William S. Charlton</i>  |           |

Institute News

|                         |   |
|-------------------------|---|
| President's Message     | 2 |
| Technical Editor's Note | 4 |

Departments

|   |    |
|---|----|
| Book Review:<br><i>Building the H Bomb: A Personal History</i>                            | 55 |
| Taking the Long View in a Time of Great Uncertainty<br><i>Rehearsing Possible Futures</i> | 58 |
| Author Submission Guidelines  | 62 |
| Calendar  | 62 |



## An Exceptional Year

By *Larry Satkowiak*  
INMM President



We are rapidly approaching another Annual Meeting. For those of us in the international nuclear materials management community, it has been a busy and exciting year. There are a couple of events that stand out. In July 2015, negotiators from Iran and the P5+1 countries (the U.S., UK, France, Russia, and China plus Germany), along with the European Union, announced completion of a comprehensive nuclear agreement with Iran—otherwise known as the Joint Comprehensive Plan of Action (JCPOA). Then, in March 2016, the United States hosted the fourth, and, most likely final Nuclear Security Summit in Washington, DC, USA, with senior delegations from fifty-two countries represented. These two events affected most of us in the international nuclear materials management community either directly or indirectly.

The intent of the JCPOA was to deter Iran from obtaining nuclear weapons. Some of the highlights of the agreement included Iran eliminating their stockpiles of medium enriched uranium, cut its stockpile of LEU by 98 percent, reduce the number of centrifuges, plus more. In order to monitor the agreement the International Atomic Energy Agency (IAEA) will have regular access to all Iranian nuclear facilities. In return, Iran will

receive relief from nuclear-related sanctions. The implications of this agreement from nuclear materials management perspective will certainly be a topic of discussion at multiple technical sessions (not to mention in the hallways and eating and drinking establishments!) at this year's INMM Annual Meeting. For example, is this the new "gold standard" for safeguards agreements? What is the impact of extending safeguards to mining and milling? How much more will this tax the already strained safeguards department and its inspectorate? These are just a few of the questions that will be discussed and, quite fortunately, Tero Varjoranta, the Deputy Director General and Head of the Department of Safeguards at the IAEA, will be one of our opening plenary speakers to help answer them.

The other significant nuclear materials management event this year was the Nuclear Security Summit (NSS). I will not try to enumerate the amazing accomplishments that the NSS process has yielded over the years but will instead just focus on a few of the successes of the 2016 event. For example, some countries involved in the NSS that were interested in taking a specific security theme a step further developed 'gift baskets,' extra initiatives. The idea

is for presenters of such gift baskets to acquire the backing of as many countries as possible, which will in turn function as role models for a given aspect of security. This year's summit had more than twenty of these gift baskets including the following subject areas: countering nuclear smuggling, cyber security, forensics in nuclear security, HEU minimization, insider threat mitigation, security of high activity radioactive sources, transport security, and many more. Most, if not all, of the topics identified in gift baskets presented are within the scope of the Institute and will be topics of discussion at this summer's meeting, both formally and informally. Corey Hinderstein, our vice president, was actively engaged in the preparation and execution of this year's NSS. Again, we are fortunate to have Anne Harrington, Deputy Administrator for Defense Nuclear Nonproliferation within the U.S. National Nuclear Security Administration as one of our plenary speakers, both Anne and Corey will be available to answer NSS related questions. In addition, I would like to mention that the INMM had an information booth stationed at the NSS venue and several INMM volunteers answered questions and provided written materials to NSS participants. My thanks to all those that participated.

### Looking Back

In January, I participated in a World Institute for Nuclear Security (WINS) workshop, *Nuclear Security Summit: Enhancing Radiological Security, at Scandic Holmenkollen Park in Oslo, Norway*. This

### Mission Statement

The INMM is an international professional society dedicated to development and promulgation of practices for the safe, secure and effective stewardship of nuclear materials through the advancement of scientific knowledge, technical skills, policy dialogue, and enhancement of professional capabilities.

workshop was held in preparation for the 2016 Nuclear Security Summit to discuss how the signatory countries have met or will meet the commitments of one of the 'gift baskets' identified above. The objectives of the workshop included discussing the status of actions taken or planned, challenges encountered and to share experiences, common practices, and lessons learned.

In April, I attended the *A Technical Meeting on Nuclear Energy and Cyber Security* held at the U.S. Naval Academy (USNA) in Annapolis, Maryland, USA, to recognize the first USNA graduating class of nuclear engineering and cyber security majors. This meeting was a joint effort by INMM, USNA, American Nuclear Society, and the USNA American Nuclear Society Student Chapter, in association with the National Cybersecurity Institute. This was a terrific meeting that had participation by midshipmen and West Point cadets with a focus on nuclear energy, reactor designs, nuclear materials, nonproliferation and arms control, material control and accounting, and much more. My thanks to Charlie Harmon who led the INMM efforts to make this workshop a success.

Also in April, the Texas A&M Student Chapter in conjunction with the International Safeguards Technical Division and the Southwest Regional Chapter, held a *Safeguards Culture Workshop* at Texas A&M University, College Station, Texas,

USA. The workshop explored what is meant by "safeguards culture," to assess the degree to which safeguards can be incorporated into the culture of an organization, and to identify research areas that need additional focus.

### Looking Forward

This year's INMM Annual Meeting will be held at the Marriott Marquis in Atlanta, Georgia, USA, July 24–28. We have just completed the final review of the program, and quite honestly, I can't wait. From the opening to the closing plenary, the quality of the abstracts and breadth of topical areas is impressive. Our Monday morning opening plenary, *Connecting Science, Technology, Policy and Culture for Effective Nuclear Materials Management* will consist of Tero Varjoranta, Anne Harrington, and Rob Floyd (Director General, Australian Safeguards and Nonproliferation Office, Barton, Australia). For the closing plenary, *Integrated Cyber/Physical Threat Scenario*, we are trying a totally new format. A team of international experts from Idaho National Laboratory, Pacific Northwest National Laboratory and Lofty Perch will present an integrated cyber/physical threat scenario to demonstrate the potential adverse impact on nuclear security (and safety) associated with such an attack. It should be fabulous!

The 18th International Symposium on the Packing and Transportation of

Radioactive Materials (PATRAM) will be held on September 18-23, 2016, at the Kobe Portopia Hotel in Kobe, Japan. PATRAM brings together experts from governments, industries and research organizations worldwide to exchange information on all aspects of packaging and transport of radioactive materials around the globe.

### Final Thought

I am continually impressed with the INMM membership. We are a professional society, whether we volunteer to serve on a committee, work within a technical division, submit technical papers, or serve in some leadership position either in a chapter or at the corporate level, each person contributing their own personal time to the greater good of the Institute and its mission. We do what we do because we think it is important, important to the nuclear materials management community, and quite frankly to the safety and security of the world. Thank you!

### 2015-2016 INMM Executive Committee

*President:* Larry Satkowiak  
*Vice President:* Corey Hinderstein  
*Secretary:* Chris Pickett  
*Treasurer:* Robert Curl  
*Immediate Past President:* Ken Sorenson

### Members-at-Large:

Jill Cooley  
 Cary Crawford  
 Ken Sanders  
 Steven Wyrick



# Making the Measurements

*By Markku Koskelo  
JNMM Technical Editor*

To paraphrase the mission and objectives of the INMM, safe, secure, and effective stewardship of nuclear materials requires among other things accurate measurement and accounting of such materials under all aspects of the civilian nuclear fuel cycle. As the technologies associated with the use of nuclear materials change, and the number of countries using nuclear technology increase, there is a need to develop new, more accurate or more cost effective ways to make measurements to know where the nuclear materials are and how much nuclear material is present at any given time.

While this is not a special issue, you will note that this issue contains well-researched and thoughtful papers on the current practices of how to make such measurements, how to develop a sampling scheme when not everything can be measured, and how to improve the measurement technology. The papers in this issue include mathematics of the concepts, results of modeling of the proposed concept, and comparisons of the modeling results with actual measurements to show that the concept can actual work in practice. Each of the papers also provides a wealth of references for anyone who wishes to research the top-

ic and the basis for the methodology and the conclusions further.

Please note also the last paper of this issue, which is the 2015 J.D. Williams Student Paper Winner from the 2015 Annual Meeting of the INMM. It is nice to see that the next generation of nuclear materials stewards is capable of publishing quality work.

*JNMM Technical Editor Markku Koskelo can be reached at [mkoskelo@aquilagroup.com](mailto:mkoskelo@aquilagroup.com).*



# Cosmic-ray Muon Imaging of Spent Nuclear Fuel in Dry Storage Casks

*J. Matthew Durham, Elena Guardincerri, Christopher L. Morris, Daniel Poulson, Jeffrey D. Bacon, Joseph Fabritius, Shelby Fellows, Kenie Plaud-Ramos, and Deborah Morley  
Los Alamos National Laboratory, Los Alamos, New Mexico USA*

*David Chichester and Philip Winston  
Idaho National Laboratory, Idaho Falls, Idaho USA*

## Abstract

Cosmic-ray muon radiography has been used to identify the absence of spent nuclear fuel bundles inside a sealed dry storage cask. The large amounts of shielding that dry storage casks use to contain radiation from the highly radioactive contents impedes typical imaging methods, but the penetrating nature of cosmic-ray muons allows them to be used as an effective radiographic probe. This technique was able to successfully identify missing fuel bundles inside a sealed Westinghouse MC-10 cask. This method of fuel cask verification may prove useful for international nuclear safeguards inspectors. Muon radiography may find other safety and security or safeguards applications, such as arms control verification.

## Introduction

The nuclear energy policy decision to suspend spent fuel reprocessing in the United States, along with the lack of a permanent repository for high-level nuclear waste, has led to the presence of ~15,000 metric tons of irradiated fuel rods in above-ground dry cask storage at various sites throughout the country.<sup>1</sup> In other parts of the world, where spent fuel reprocessing does occur, dry casks are still in use for interim storage of irradiated fuel. This large amount of highly radioactive fuel presents a potential global security risk if any of it were diverted for illicit purposes. A continual chain of accountability and verification is a necessary safeguard.

The International Atomic Energy Agency (IAEA) typically maintains continuity-of-knowledge (CoK) of spent fuel through surveillance of storage sites and periodic checks of tamper-indicating devices on cask lids.<sup>2</sup> When independent, standalone confirmation of a dry storage cask's contents is needed (either to recover from loss of CoK or to verify a member state's declaration of cask contents) the cask must be moved to a storage

pool to be opened and visually inspected. This procedure is invasive, costly, time-consuming, and potentially dangerous. A non-destructive radiographic method for determining a cask's contents is therefore a desirable safeguard tool. Previous studies, however, have shown that the cask's heavy shielding hinders inspection with typical radiographic techniques.<sup>3</sup>

Cosmic-ray muons offer an alternative tomographic probe. Since muons are colorless leptons, they have no hadronic interaction with nucleons, and their relatively large mass of 105.6 MeV/c<sup>2</sup> limits energy loss due to bremsstrahlung radiation. These properties allow energetic muons to penetrate large amounts of material that are inaccessible to other particles. Muons do possess an electric charge and undergo Coulomb scattering off nuclei as they pass through matter. Cosmic ray interactions in the upper atmosphere produce muons that arrive at the surface of the Earth at a rate of ~1/cm<sup>2</sup>/min, with a mean energy of ~4 GeV.<sup>4</sup>

The first use of cosmic-ray muons for radiography was in 1955, when George measured muon attenuation to determine the overburden of rock above a tunnel.<sup>5</sup> This was followed by Alvarez *et al.*, who used this method to confirm the Second Pyramid of Giza did not contain any undiscovered chambers,<sup>6</sup> and more recently by several groups examining geologic features.<sup>7-11</sup> A different method, developed at Los Alamos National Laboratory, uses measurements of the multiple scattering angle of individual muons passing through an object to create tomographic images of the object's interior structure.<sup>12</sup> This technique was originally developed to inspect cargo containers for illicit trafficking of nuclear material,<sup>13,14</sup> and has since been applied to studies of nuclear weapons, industrial corrosion,<sup>15</sup> nuclear reactors,<sup>16-18</sup> and is being explored as a method to determine the condition of the damaged cores of the Fukushima Daiichi nuclear power plant.<sup>19,20</sup> A related technique, which



uses muon-induced fission to tag fissile materials, is being explored as a technology for treaty verification.<sup>21</sup>

While there has been considerable interest in cosmic-ray muon radiography of nuclear waste in storage containers,<sup>22-27</sup> there have been no actual measurements made in the field to date. Here we present the first results from cosmic-ray muon radiography of spent fuel inside a partially loaded dry storage cask at Idaho National Laboratory. With this technique, we show that it is possible to determine if several fuel bundles are missing inside the sealed cask.

## Measurement

Muons that pass through matter undergo multiple Coulomb scattering off nuclei. The angular distribution of these scattered particles can be approximated by a Gaussian of width

$$\sigma_{scat} = \frac{14.1 \text{ MeV}}{\beta c p} \sqrt{\frac{l}{X_0}}$$

where  $\beta c$  and  $p$  are the velocity and momentum of the incoming  $l/X_0$  muon and is the material's thickness in radiation lengths.<sup>4, 28-31</sup> The radiation length of a material has a strong dependence on the atomic number  $Z$  of the scattering center; for example, one radiation length of typical shielding concrete is 10.7 cm, for iron,  $X_0^{Fe} = 1.76$  cm, and in uranium,  $X_0^{Ue} = 0.32$  cm. This makes multiple scattering tomography especially sensitive to high- $Z$  objects (i.e., uranium fuel), even if surrounded by low- $Z$  material (concrete shielding). The scattering angles are

determined by measuring the trajectories of individual muons before and after they pass through the object under inspection. Data from an ensemble of trajectories gives tomographic information on the object's internal structure. For details on image reconstruction algorithms, see References 12, 14 and 32.

The incoming and outgoing muon trajectories are measured with two identical drift tube tracking detectors, which are placed on opposite sides of the object under inspection. The individual tubes are made of aluminum, are 1.2 m long with an outer diameter of 5.08 cm and wall thickness of 0.89 mm, and are filled with 1 bar of a 47.5 percent Ar, 42.5 percent  $CF_4$ , 7.5 percent  $C_2H_6$ , 2.5 percent He gas mixture (see Figure 1a). A single 30-micron diameter gold-plated tungsten anode wire runs down the center of each tube. Muons passing through the tubes ionize the gas, and the resulting electrons drift towards the wire where they are multiplied through an avalanche process in the high electric field near the surface of the wire, producing a measureable signal.

The single tube efficiency as a function of anode wire voltage is shown in Figure 1b. This was measured by stacking three tubes vertically and requiring coincident hits in the top and bottom tubes, indicating that a muon had passed through the stack of three tubes. When this trigger fired, the middle tube was examined for a coincident signal. The ratio of three-level coincidences between all tubes to the number of two-level coincidences between the outer tubes gives the efficiency of the middle tube. During operation, the wire is held at a voltage of +2585 V relative to the tube wall, which gives the tubes an ef-

**Figure 1.** Cutaway drawing of a single drift tube detector, showing the anode wire inside the 5.08 cm OD tube (a). The muon detection efficiency of a single tube as a function of anode wire voltage (b).

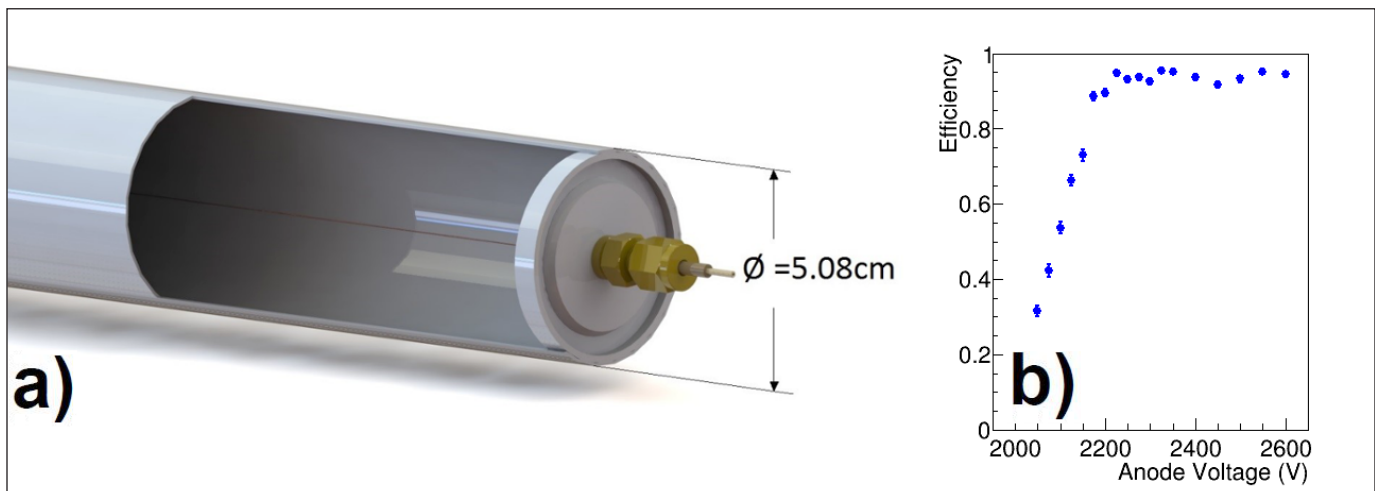
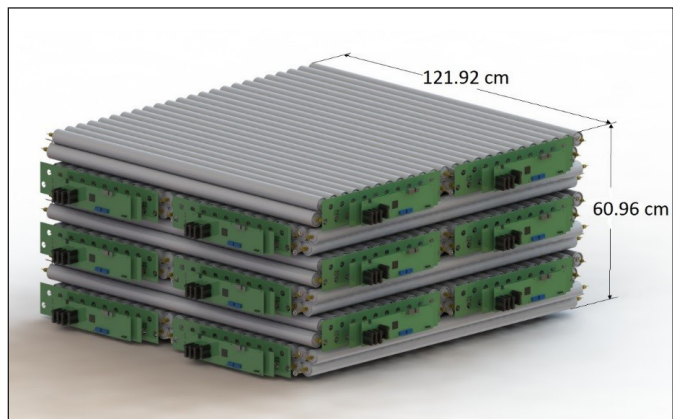


**Figure 2.** A drawing of one muon tracker, consisting of 288 individual drift tubes with read out electronics. Multiple layers of tubes in alternating orientations allow multi-dimensional particle tracking. Support structures are not shown for clarity.



efficiency >90 percent and sufficient gain to satisfy signal thresholds in the readout electronics.

Each individual drift tube measures the radial distance from the wire where the muons passed with an accuracy of ~few hundred microns. The inherent left/right ambiguity in single tubes is resolved by using double layers of tubes, which are offset in the radial direction by a distance equal to one tube radius. Stacks of six double layers, arranged with orientations alternating by 90 degrees in order to provide sensitivity in two coordinates, form a complete tracker (see Figure 2). Muon tracks are reconstructed by fitting patterns of hits in the tube layers.

The object under inspection for this measurement was a partially loaded Westinghouse MC-10 spent fuel cask located at the Idaho National Laboratory.<sup>33</sup> The MC-10 is a vertical storage cask that is 4.8 m high and 2.7 m in diameter. The cask has a basket for twenty-four pressurized water reactor fuel assemblies inside a 25-cm thick forged-steel cylindrical container that is surrounded by a layer of BISCO NS-3 neutron shielding and an outer stainless steel skin. Two identical muon tracking detectors were placed on opposite sides of the cask in order to record the incoming and outgoing tracks of muons which traverse the cask. Since the cosmic-ray muon flux is approximately proportional to  $\cos^2 \theta_z$ , where  $\theta_z$  is the angle from the zenith, one detector was elevated by 1.2 m relative to the other to increase muon counting rates. A larger elevation of the upper detector would decrease the sampled zenith angle and therefore increase the muon flux through both detectors; however, considerations of the ease of setup and stability of the detector

**Figure 3.** Muon tracking detectors in weatherproof enclosures around the MC-10 cask at Idaho National Laboratory. One detector is elevated relative to the other to take advantage of the higher muon flux at smaller zenith angles.



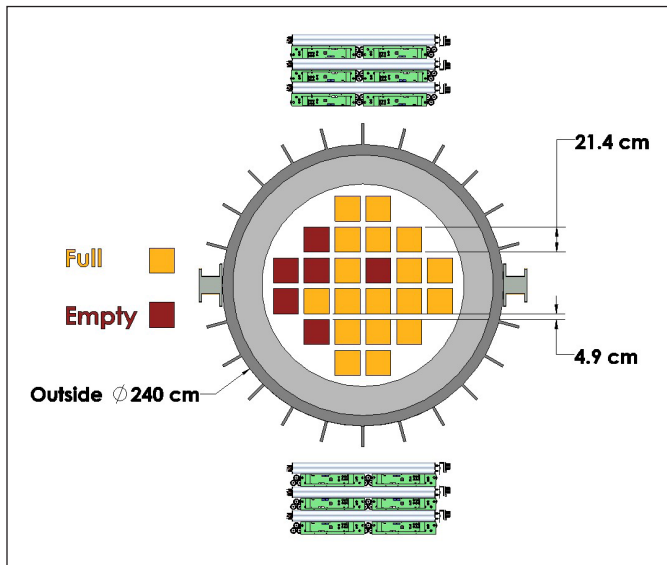
on the stand limited the allowed height. The instruments were placed in thin-walled weatherproof enclosures to protect them from precipitation during the measurement. Figure 3 shows a photograph of the setup around the MC-10 cask.

Despite the heavy shielding, there is still a significant radiation field outside the MC-10 cask that can potentially interfere with muon tracking. Measurements showed ~0.1 mSv/h (10 mrem/h) of neutrons and ~0.1 mSv/h of gamma ray activity on contact with the cask surface. Compton scattered electrons can produce spurious hits in single drift tubes, which can affect the track reconstruction algorithms. To remove this background, a trigger was added in the data acquisition system that required hits in neighboring tubes within a time window of 600 ns in order to be considered as part of a track candidate. In standalone tests away from the cask, it was found that inefficiencies in this trigger requirement reduced track counting rates by ~50 percent. During the measurement, cosmic ray tracks that went through both detectors and the cask were recorded at a rate of ~0.25 Hz. Data was collected around the MC-10 cask for ~200 hours, recording  $1.62 \times 10^5$  muon tracks that passed through the cask and both detectors.

The loading profile of the MC-10 cask is shown in Figure 4, relative to the muon tracking detector placement. The detectors are not large enough to image the entire cask body, so they were positioned such that the field of view covered the columns of most interest, which contain one, six, five, and four intact spent fuel bundles. The bundles that are present in the cask are Westinghouse 15 x 15 pressurized water reactor fuel, with nominal burn up of 30,000 MWd. Each of the bundles are



**Figure 4.** Top-down view of the loading profile of the MC-10 cask at Idaho National Laboratory. Approximate locations of the two muon tracking detectors are shown for comparison.

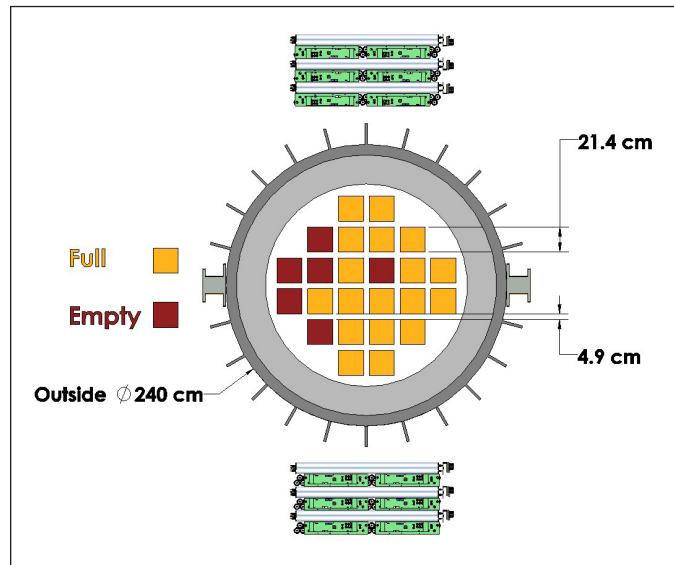


21 cm on each side with a total height of 4.06 m, of which the fuel column is 3.66 m. Twenty of the 225 possible rod locations in each assembly are occupied by guide tubes for control rods, and the centermost spot is used for in-core instrumentation. The remaining 204 slots are filled with 1.07 cm diameter fuel rods. These assemblies were removed from a U.S. commercial power reactor in the early 1980s.

## Results and Discussion

The measured muon trajectories are projected to a plane parallel to the detectors positioned near the center of the cask. This plane is divided into 2-cm x 2-cm voxels. Each voxel has a corresponding histogram, where the scattering angles of each track that pass through that voxel are collected. From the expression previously given for  $\sigma_{\text{scat}}$  we see that the scattering angles are highly dependent on the muon's momentum. The scattering histograms are fit with amplitudes corresponding to seven different groups of muon momentum, which provides a more realistic representation of the cosmic-ray muon energy spectrum (see Reference 32 for details). A typical scattering angle histogram is shown in Figure 5. The radiation length weighted areal density  $I / X_0$ , which is closely related to the thickness in units of radiation length traversed by muons that pass through that voxel, is extracted from the fit information.

**Figure 5.** A typical scattering angle histogram, along with the multigroup fit. These histograms are stored for each voxel and are used to determine the areal density traversed by muons that pass through the cask.



An image of the cask in terms of the areal density extracted from each voxel is shown in Figure 6a. From left to right, the columns within the muon tracker's field of view contain one, six, five, and four assemblies (see Figure 4). It is apparent that the column with only one fuel assembly has significantly less areal density than the neighboring column with six assemblies.

For comparison, Monte Carlo simulations were performed with GEANT4,<sup>34</sup> for three different spent fuel loading configurations, and the areal density image was obtained using identical analysis techniques. Figure 6b shows the image obtained with 10 million simulated muon trajectories through the MC-10 cask with the same partial defect in loading as the measurement. Figures 6c and 6d show the image that would be obtained for fully-loaded and empty casks, respectively.

The individual fuel assemblies contained in the cask are near uniform in the vertical direction. The cask body is also uniform in this direction over the field of view of this measurement. Therefore, the areal densities shown in Figure 6 are not expected to vary with height. Recognizing this, the two-dimensional areal density data are projected (summed over the voxel data) onto the horizontal axis and shown in Figure 7. This vertically integrated areal density metric is sensitive to the total amount of material along the path the muons take between the two detectors.

**Figure 6.** Image of the cask in terms of areal density, for the measured MC-10 cask (a) and GEANT4 simulations of three different loading configurations (b-d)

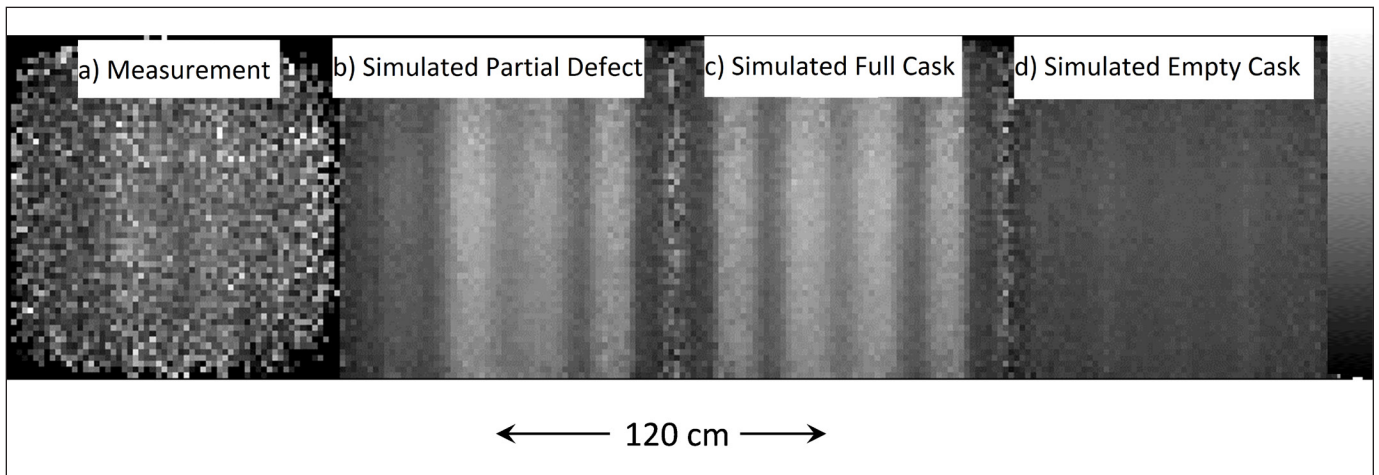
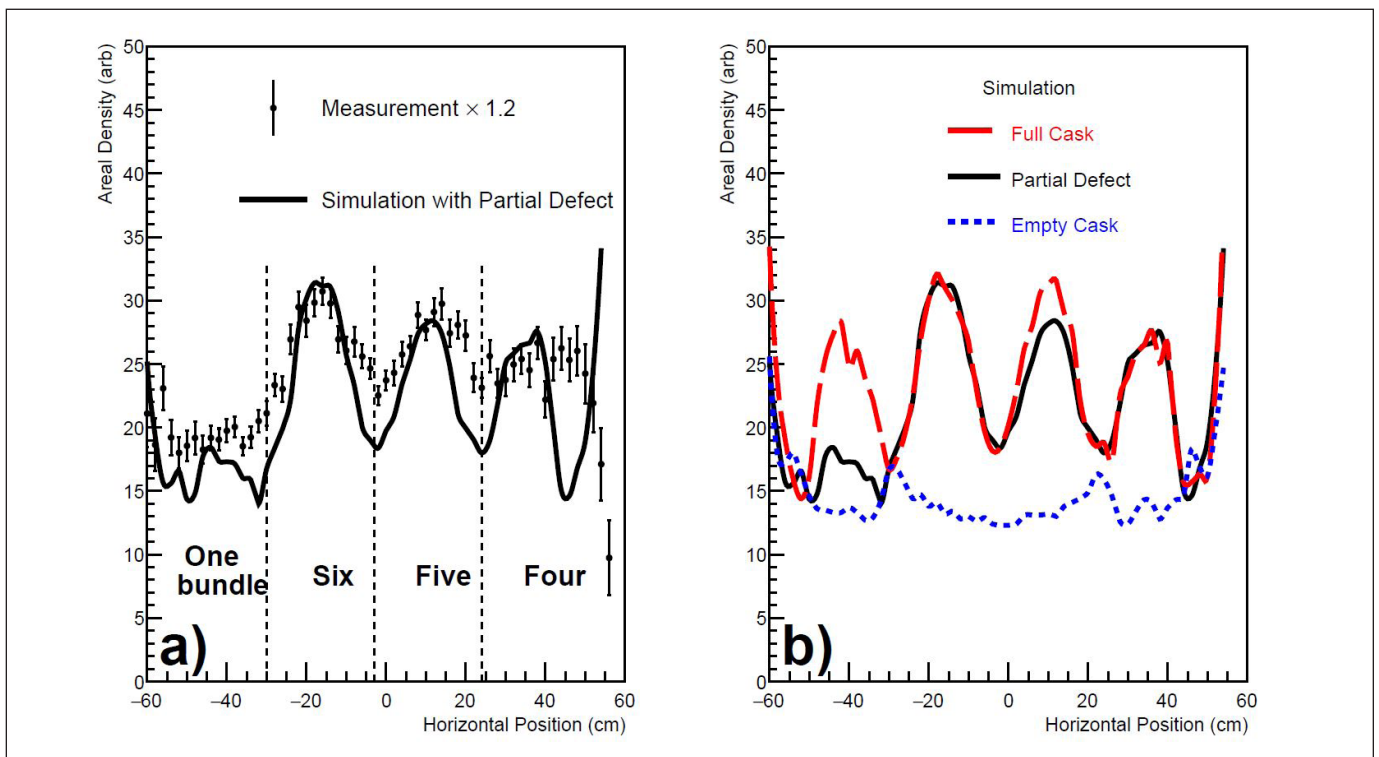


**Figure 7.** The measured areal density through the cask (a), compared to a GEANT4 simulation of a cask with the same partial defect in loading. Dashed lines show the approximate boundaries of columns in the fuel basket. Simulations of a completely full and empty cask are shown in panel (b) for comparison.



A clear difference is seen between the columns with different loading profiles. The column with only one fuel assembly on the left edge of the field of view shows a significantly smaller areal density than all the other columns. As expected, the fully loaded column with six fuel assemblies shows the greatest areal density, and is clearly distinguishable from the

columns with one and four fuel bundles. The statistical uncertainties on the data prevent a definitive statement from being made about the column with five assemblies; however, the simulations show that higher statistics measurements will be able to effectively identify that defect.





The simulated model of the fully loaded cask shows the expected variation across the view of the fuel basket, with the columns containing four fuel bundles on the edges and two fuel bundles in the center. The partially loaded cask shows clear variation, with similar structure to the measurement. The data shown in Figure 7 was scaled by a factor of 1.2 to more closely resemble the scale of the simulation. This is likely due to differences in the muon momentum spectrum used in the simulation and the actual muon momentum that is present in nature at the measurement site. There is little existing data on the muon momentum spectrum at large zenith angles and momenta less than 10 GeV/ $c$  that can be used to constrain models of cosmic-ray muon distributions in this region, so in this regard the simulation may not accurately depict reality. Near the edge of the field of view, the detector acceptance is limited and biased towards tracks which cross long path lengths through the cask, resulting in unphysically large areal densities within ~5cm of the edges of the field of view. However, no conclusions are drawn from the data affected by these artifacts.

We also note that a precise alignment of the muon tracking detectors with the fuel columns in the cask was not performed. There may be offsets of ~several cm between the center of the detector and the center of the cask, as well as misalignment between the plane in between the detectors and the fuel columns. These misalignments can introduce aberrations in the reconstructed images and areal densities that contribute to differences between the data and simulation. A more precise alignment will be performed in future measurements.

## Summary and Outlook

We have shown that cosmic-ray muon scattering angles can be used to infer the areal density of loaded dry storage casks, and thereby determine if fuel assemblies are present or missing in certain configurations. The data shown was collected over a period of ~200 hours on a partially loaded MC-10 cask at Idaho National Laboratory. This technique may be a useful tool for maintaining CoK of spent fuel in dry cask storage.

Simulations show that measurements with better statistical precision will be able to more effectively discriminate between fully loaded and partially loaded fuel columns, and may be able to determine if portions of individual fuel bundles are missing, however, additional studies are needed to determine absolute sensitivities of the technique to partial defects in individual fuel bundles. In addition, a more precise alignment of the muon tracking detectors and the fuel columns will reduce

aberrations in the reconstructed images. The density analysis performed here is integrated through the cask in the direction between the two muon tracking detectors, and therefore can locate columns where assemblies are missing, but does not measure the depth within the cask. If additional data is taken with the detectors rotated around the cask, the position ambiguities could be resolved and missing assemblies could be located in three dimensions. Future measurements to collect additional data from several viewing angles with a more careful alignment are currently being planned.

We note here that the two planar muon trackers used for this measurement are not optimized for measurements of relatively large cylindrical objects. A muon tracking detector could be designed such that it surrounds the cask completely and simultaneously measures muons coming from all azimuthal angles, giving a complete tomography of the cask's interior. Increasing muon detector coverage and decreasing the sampled zenith angle would also decrease the counting time necessary for statistically significant results. Designs and analysis of such an optimized instrument that could be fielded by international safeguards inspectors are currently underway.

## Acknowledgements

This work is funded by the National Nuclear Security Administration's Office of Defense Nuclear Nonproliferation Research and Development. We thank P. Kurnadi and L. Tovey of Decision Sciences International Corporation and W. Schwendiman of INTEC for valuable assistance. This document is released under LA-UR-15-26861.

**Keywords:** dry cask storage, muon radiography, cosmic-ray muons

## References

1. Hamilton, L. H., B. Scowcroft, et al. 2012. Blue Ribbon Commission on America's Nuclear Future Report to the Secretary of Energy.
2. Zuccaro-Labelarte, G., and R. Fagerholm. 1996. Safeguards at Research Reactors, Current Practices, Future Directions, *IAEA Bulletin*, Vol. 38, No 4.
3. Ziock, K. P., et al., 2005. Radiation Imaging of Dry-Storage Casks for Spent Nuclear Fuel, *Nuclear Science Symposium Conference Record, 2005 IEEE*, pp. 1163-1167.
4. Olive, K. A., et al. 2014. The Review of Particle Physics, *Chinese Physics C*, vol. 38, no. 090001.





5. George, E. P. 1955. Cosmic Rays Measure Overburden of Tunnel, *Commonwealth Engineer*, pp. 455-457.
6. Alvarez, L. W., et al. 1970. Search for Hidden Chambers in the Pyramids, *Science*, vol. 167, pp. 832-839.
7. Nagamine, K., M. Iwasaki, K. Shimomura, and K. Ishida. 1995. Method of probing inner-structure of geophysical substance with the horizontal cosmic-ray muons and possible application to volcanic eruption prediction, *Nuclear Instruments and Methods A*, Vol. 356, No. 2, pp. 585-595.
8. Lesparre, N., et al. 2010. Geophysical muon imaging: feasibility and limits, *Geophysical Journal International*, Vol. 183, pp. 1348-1361.
9. Olah, L., et al. 2013. Cosmic Muon Detection for Geophysical Applications, *Advances in High Energy Physics*, Vol. 2013 Article ID 560192.
10. C. Carloganu et al. 2013. (TOMUVOL Collaboration), Towards a Muon Radiography of the Puy de Dome, *Geoscientific Methods, Instrumentation and Data Systems*, vol. 2, no. 1, pp. 55-60, 2013.
11. Ambrosino, F., et al. 2014. The MU-RAY project: detector technology and first data from Mt. Vesuvius, *Journal of Instrumentation*, Vol. 9.
12. Schultz, L., et al. 2004. Image Reconstruction and Material Z Discrimination Via Cosmic-ray Muon Radiography, *Nuclear Instruments and Methods A*, Vol. 519, No. 3, pp. 687-694.
13. Borozdin, K., et al. 2003. Surveillance: Radiographic Imaging with Cosmic-ray Muons, *Nature*, Vol. 422, No. 277.
14. Priedhorsky, W., et al. 2003. Detection of High-Z Objects Using Multiple Scattering of Cosmic-ray Muons, *Revue of Scientific Instruments*, Vol. 74, No. 10.
15. Durham, J. M., et al. 2015. Tests of Cosmic Ray Radiography for Power Industry Applications, *AIP Advances*, Vol. 5 067111.
16. Sugita, T., et al. 2014. Cosmic-ray Muon Radiography of UO<sub>2</sub> Fuel Assembly, *Journal of Nuclear Science and Technology*, Vol. 51, No. 7-8, pp. 1024-1031.
17. Morris, C. L., et al. 2014. Analysis of Muon Radiography of the Toshiba Nuclear Critical Assembly Reactor, *Applied Physics Letters*, Vol. 104, 024110.
18. Perry, J. O., et al. 2013. Imaging a Nuclear Reactor Using Cosmic-ray Muons, *Journal of Applied Physics*, Vol. 113, 184909.
19. Borozdin, K., et al. 2012. Cosmic Ray Radiography of the Damaged Cores of the Fukushima Reactors, *Physical Review Letters*, Vol. 109, 152501.
20. Miyadera, H., et al. 2013. Imaging Fukushima Daiichi reactors with muon, *AIP Advances*, Vol. 3, 052133.
21. Guardincerri, E., et al. 2015 Detecting Special Nuclear Material Using Muon-induced Neutron Emission, *Nuclear Instruments and Methods A*, vol. 789, pp. 109-113.
22. Gustafsson, J. 2005. *Tomography of Canisters for Spent Nuclear Fuel Using Cosmic-ray Muons*, Uppsala, Sweden: Thesis, Uppsala University.
23. Osterland, M., et al. 2006. Tomography of Canisters for Spent Nuclear Fuel, in *Proceedings of the International Workshop on Fast Neutron Detectors and Applications*, Cape Town, South Africa.
24. Jonkmans, G., et al. 2013. Nuclear Waste Imaging and Spent Fuel Verification by Muon Tomography, *Annals of Nuclear Energy*, Vol. 53, pp. 267-273.
25. Ambrosino, F., et al. 2015. Assessing the Feasibility of Interrogating Nuclear Waste Storage Silos Using Cosmic-ray Muons, *Journal of Instrumentation*, vol. 10 T06005.
26. Clarkson, A., et al. 2014. The Design and Performance of a Scintillating-fibre Tracker for the Cosmic-ray Muon Tomography of Legacy Nuclear Waste Containers, *Nuclear Instruments and Methods A*, Vol. 745, pp. 138-149.
27. Chatzidakis, S., et al. 2015. Monte Carlo Simulations of Cosmic-ray Muons for Dry Cask Monitoring, *Transactions of the American Nuclear Society*, Vol. 112, No. 1, pp. 534-536.
28. Moliere, G. 1948. Theory of the scattering of fast charged particles, *Zeitschrift fur Naturforschung*, vol. 3a, p. 78.
29. H. A. Bethe. 1953. Moliere's Theory of Multiple Scattering, *Physical Review*, vol. 89, p. 1256.
30. Highland, V. L. 1975. Some Practical Remarks on Multiple Scattering, *Nuclear Instruments and Methods*, Vol. 192, No. 2, p. 497.
31. Lynch, G. R., and O. I. Dahl. 1991. Approximations to Multiple Coulomb Scattering, *Nuclear Instruments and Methods B*, Vol. 58, No. 1, p. 6.
32. Perry, J. O., et al., 2014. Analysis of the Multigroup Model for Muon Tomography, *Journal of Applied Physics*, Vol. 115, 064904.
33. McKinnon, M. A., et al. 1987. The MC-10 PWR Spent-Fuel Storage Cask: Testing and Analysis, Electric Power Research Institute Report NP-5268.



34. Agostinelli, S. ,et al. 2003. GEANT4 - A Simulation Toolkit, *Nuclear Instruments and Methods in Physics Research Section A*, Vol. 506, No. 3, pp. 250-303.



# Nuclear Materials Attribution for Reprocessed Uranium

*Christopher Grove, Connah Johnson, and Kevin Hesketh  
National Nuclear Laboratory Limited, Preston, Lancashire, UK*

## Abstract

This paper describes some research activities related to special nuclear materials attribution and proliferation resistance assessment carried out by the UK National Nuclear Laboratory (NNL). Given that the UK currently operates two reprocessing plants, it is important that UK should fully understand the characterization of the plutonium and reprocessed uranium (Rep U) that has been separated from nuclear fuel. NNL has previously studied plutonium attribution and has developed and implemented a methodology that is able to attribute a plutonium sample based on its measured plutonium isotopic composition. Attribution can be made to a particular type of reactor and the method also indicates the initial enrichment and discharge burnup of the fuel from which it originated. Plutonium was prioritized because of its sensitivities as a special nuclear material. Rep U is perhaps less sensitive, but the amount recovered from reprocessing is almost two orders of magnitude larger and it is no less important to be able to characterize it as fully as possible. The measured isotopic composition of a Rep U sample does not readily allow attribution in the same way as plutonium. This paper describes a simple procedure that was developed to allow Rep U attribution. It relies on a simple estimate of the initial U-235 content of the fuel from which the sample originates, based on the measured U-235 and U-236 contents. The initial enrichment estimate is then refined using a set of tabulations from the FISPIN (Fission Product Inventory) program and the measured U-236/U-235 ratio used to infer the discharge burnup. Finally, FISPIN tabulations of U-234 versus burnup can be used to infer the cooling time since reprocessing. The paper describes the approach and illustrates its application to some test samples.

## Introduction

Countries such as the UK consistently impose very stringent security requirements on facilities where special nuclear material (SNM) is handled. Combined with rigorous accounting procedures, SNM is very strongly safeguarded against theft or diversion. However, this does not apply everywhere and there

have been many instances of SNM being discovered outside of properly regulated control. The ability to reliably attribute SNM is very important in order to identify its likely source, but very often this is difficult to achieve, as illustrated by the Galaxy Serpent Tabletop Exercise that was recently carried out by the National Nuclear Forensics Library,<sup>1</sup> which illustrates how attribution is not a trivial task given the potential overlap between different reactor types.

UK National Nuclear Laboratory (NNL) has previously developed an attribution method for plutonium based on a multivariate plotting method<sup>2</sup> that, based on a combination of simulation and actual sample data, has been shown to give a reliable indication of the type of reactor in which a plutonium sample was produced. The method also provides an indication of the discharge irradiation of the fuel from which it was separated and the initial enrichment of the fuel. As part of its Signature Research Program (SRP), NNL has investigated whether the same type of approach would also work for reprocessed uranium (Rep U), meaning uranium that has been separated from irradiated fuel in a reprocessing plant. Although Rep U does not have the same sensitivities as plutonium it nevertheless is classed as SNM and also the mass of Rep U recovered from irradiated fuels is about 100 times greater than that of plutonium, so the inventories involved can potentially extend to many thousands of tons. Rep U attribution is not straightforward and requires an understanding of the evolution of the isotopes U-232, U-234, U-235 and U-236 with burnup which is provided in the following section. The emphasis is on uranium isotopic evolution in thermal reactors, because the existing commercial reprocessing plants are designed only to process thermal reactor fuels.

## Uranium Isotopic Evolution in Irradiated Thermal Reactor Fuel

Natural uranium ore has abundances of U-235 and U-238 of 0.72 and 99.3 weight percent (w/o) respectively, with approximately 55 ppm of U-234. The U-234 content is to some extent variable between different ore bodies and there is no consis-



tent standard to assume. U-234 is a neutron absorber and is produced from the U-238 decay chain (via an alpha decay to Th-234, followed by two beta decays to Pa-234 and U-234). In low-enriched uranium (LEU) fuel, as used in light water reactors (LWRs), the U-235 content is typically enriched to between 2 and 5 w/o and the U-234 abundance is also enhanced to typically between 200 and 500 ppm depending on the product U-235 enrichment and the tails U-235 assay.

During irradiation, the U-235 inventory decreases primarily because of fission events, but with about 15 percent being converted to U-236 by neutron captures. Figure 1 shows the U-235 inventory as a function of burnup for pressurized water reactor (PWR) and the advanced gas reactor (AGR). The data were generated using the FISPIN inventory code, which is very well validated and reliable for the main isotopes.<sup>3,4</sup> PWR and AGR are used here for illustration because these are the main reactor types currently in operation in the UK fleet and the approach is later extended to other reactor types. The U-235 inventory curves are shown for a representative range of initial enrichments and in each case the burnup is extended well beyond the point at which the fuel would normally be discharged just so that the dataset is not restricted in usage. Initially, the U-235 inventory decreases almost linearly with burnup, then levels off at high burnups. There is a tendency for PWR and AGR to diverge at high burnups, indicating some sensitivity to neutron spectrum that is attributable to the different resonance escape probabilities for the two reactor types. AGR has high resonance self-shielding and therefore a lower U-238 resonance capture rate and correspondingly lower Pu-239 production than PWR, which increases U-235 depletion. For a given initial enrichment, the ratio of U-235 inventories in PWR and AGR diverges with burnup as can be seen from the plots for initial enrichments of 2.1 w/o and 3.2 w/o in Figure 1. The PWR/AGR ratio for 2.1 w/o initial enrichment is 1.25 at 20 GWd/t, while for the 3.2 w/o initial enrichment the PWR/AGR ratio is 1.33 for 30 GWd/t (these points are highlighted inside the red ovals). At higher burnups the ratios increase further, but with limited practical relevance to normal reactor operations where the actual discharge burnup achievable depends on the initial enrichment. The highest enrichment case for AGR is 3.8 w/o, chosen because this bounds the enrichments that have been used in these reactors and because the highest enrichment specified for PWR is different, the upper two curves cannot be used for comparison purposes. The same applies to all the figures presented here.

**Figure 1.** U-235 inventory versus burnup and initial enrichment for PWR and AGR

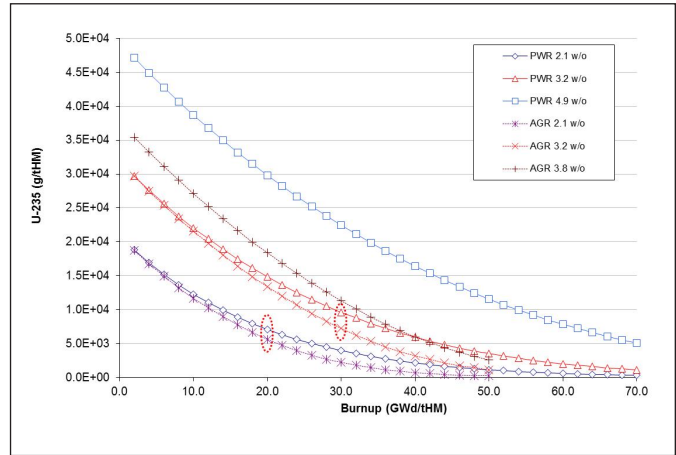


**Figure 2.** U-236 inventory versus burnup and initial enrichment for PWR and AGR

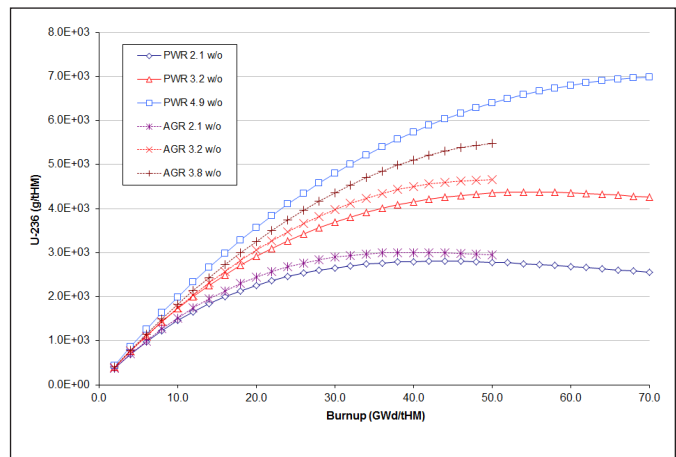
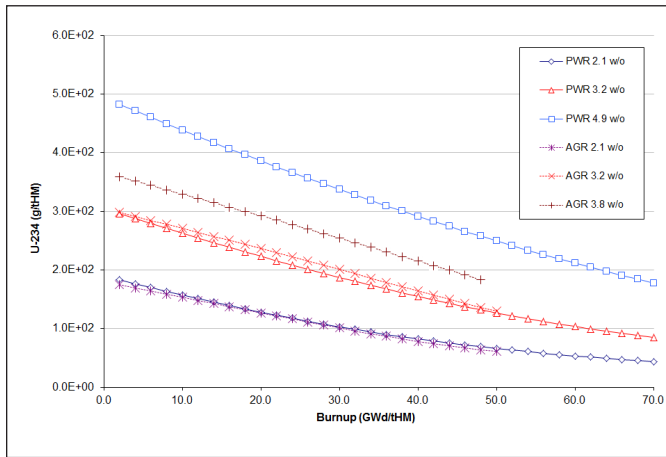


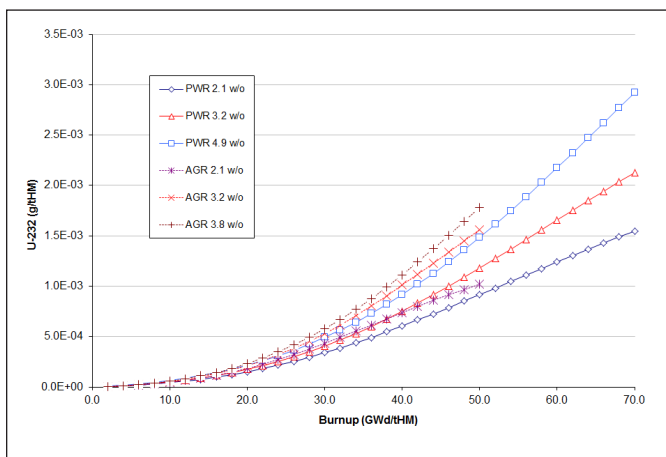
Figure 2 shows the corresponding plot for U-236, which builds up initially linearly and saturates at burnups relevant to commercial operation. The saturation mechanism occurs because the U-236 production rate decreases with burnup as the U-235 depletes and neutron captures remove the U-236 (by conversion to U-237/Np-237) at a rate that eventually matches the diminishing production rate. As is characteristic of graphite moderated systems, the neutron energy spectrum in AGR is more thermalized than PWR and there is a slight differentiation in U-236 evolution between the two reactor types (for a given initial enrichment AGR has a slightly higher U-236 inventory), but insufficient to give a useful signature.

The U-234 present in fresh fuel gradually depletes with burnup (see Figure 3), due to neutron captures dominating the various production methods. There is very little distinction be-

**Figure 3.** U-234 inventory versus burnup and initial enrichment for PWR and AGR



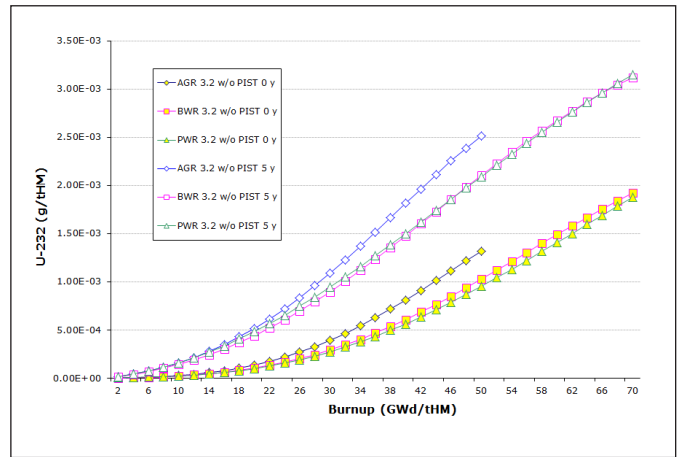
**Figure 4.** U-232 inventory versus burnup and initial enrichment for PWR and AGR at zero pre-irradiation storage time (PIST)



tween the two reactor types, indicating insensitivity to neutron spectrum (the graphite moderated AGR has a softer neutron spectrum than PWR).

Finally, irradiation produces trace quantities (ppb) of U-232 and U-233. There are also traces of U-237, but this is very short-lived and irrelevant here. The presence of U-232 at ppb levels is very important radiologically, because its decay chain is associated with a gamma decay from Tl-208. The U-232 is produced by several different routes, an important one of which is Pa-231 neutron capture (other routes include Pu-238  $\alpha$ -decay, U-233 (n,2n) and Th-232 neutron capture). Pa-231 is present in only very small quantities in freshly manufactured fuel, because it is left behind in the form of non-volatile fluorides in the UF<sub>6</sub> cylinders that supply the uranium to the fuel fabrication process. Subsequent to UF<sub>6</sub> volatilization, the Pa-231 builds up

**Figure 5.** U-232 inventory in PWR, BWR and AGR at pre-irradiation storage time (PIST) 0 and five years



linearly as a result of U-235 decay. The concentration of Pa-231 in fresh fuel therefore depends on the pre-irradiation storage time (PIST) between UF<sub>6</sub> volatilization and the start of irradiation and is the principal unknown affecting the U-232 abundance at discharge. Figure 4 shows the evolution of the U-232 inventory with burnup. There is some difference between AGR and PWR, indicating sensitivity to neutron spectrum, but the difference is too weak to be useful for attribution, especially when taking into account the large measurement and modelling uncertainties for such a weak production route and the compounding effect of the unknown PIST.

Figure 5 illustrates the strong effect of varying the PIST from zero to five years, and also includes boiling water reactor (BWR). There is a very close correspondence between PWR and BWR, so that differentiation between PWR and BWR is difficult.

A further complication is that both U-232 and U-234 are produced from decays of transuranics and continue to build up after the fuel has completed its irradiation. For U-234 the rate of build-up is slow and its concentration is only increased by about 20 percent after ten years cooling time after discharge. For U-232, the effect is much stronger, with its concentration increasing by more than a factor of two after cooling for ten years. If the fuel is reprocessed and Rep U separated out, both these production routes cease and there is no further build-up. Therefore, measurements of U-232 and U-234 in spent fuel are dependent on the unknown post-separation cooling time and they are also dependent on the unknown cooling time prior to separation.



The overall isotopic evolution of Rep U is quite complex and while there is some resolution of different reactor types, the resolution is not as strong as it is for plutonium and the effect of the unknown discharge burnup, PIST and pre-separation and post-separation cooling times severely complicate any attempt at attribution. This is exacerbated further by the observation that the U-235 discharge inventory for today's reactor types are all typically in the range 0.7 to 1.0 w/o, irrespective of the initial U-235 enrichment, coinciding with the end of the useful life of the fuel (where it can no longer contribute sufficiently to core reactivity and power output). The fact that the U-235 discharge inventory ranges of the different reactor types overlap make the U-235 virtually useless as a differentiator between reactor types and initial enrichments. Efforts to resolve Rep U isotopics using the same multi-variate approach used for plutonium confirmed that U-235 is largely a confounding factor that needs to be excluded. Overall, the multi-variate approach was not successful and failed to provide any useful discriminating power.

## Rep U Attribution Approach

An attempt to develop a multi-attribute method for Rep U analogous to the existing method for plutonium was not successful because there is insufficient differentiation between the different types of reactor. In particular, the FISPIN results show that there is virtually zero attribution information in the measured U-234 and that the U-232 varies widely depending on the pre-irradiation storage time. Another difficulty with the multi-attribute approach is that the measured U-235 is difficult to make use of because it depends on the unknown initial enrichment and the unknown burnup and doesn't correlate with reactor type (because all reactors deplete U-235 down to the same range in spent fuel, between 0.7 to 1.0 w/o).

However, examination of the FISPIN calculations carried out in the initial feasibility work, has indicated a simple approach that does appear to be promising. The approach starts with the observation that the measured U-236 assay of the sample contains implicit information relating to how much U-235 has been removed by fission and neutron capture events (to produce the U-236). The thermal capture/absorption ratio

$$R = \frac{S_c}{S_f + S_c} \text{ of}$$

U-235 is approximately 0.14. This suggests that for every capture event in U-235, about 7 U-235 atoms will have been lost to

the combination of fissions and captures. Taking, as a first step, the capture/absorption ratio to be constant (which amounts to neglecting neutron captures by U-236 and neutron spectrum variation with burnup), this observation can be used to estimate the initial U-235 enrichment given the measured U-235 and U-236 in the sample. Knowing the initial U-235 is much more useful than the U-235 at discharge and is promising. Examination of the FISPIN tabulations for the different reactor types suggests a more representative initial guess for R in the range 0.16 to 0.17. This is the starting point for the attribution analysis. Though this approach is very crude, it is acceptable, because at this stage we are only seeking an estimate of the initial enrichment that will be refined later.

Having found a first estimate of the initial enrichment, the next step is to refine it using one of the FISPIN tabulations that correspond to the same initial enrichment or a nearby tabulation. This gives an improved value of R, which gives a second estimate of the initial enrichment. The next step is to plot the U-236/U-235 ratio from the sample measurement and compare it against plots of the U-236/U-235 ratio versus burnup pre-calculated by FISPIN. This gives a good indication of the discharge burnup of the sample. At this stage the minimum expectation is that the initial U-235 enrichment of the sample and burnup at which it was discharged will have been estimated. This provides a possible indication of the reactor type.

The final step in the attribution comes from the observation that the U-236/U-235 versus burnup curves are slightly divergent for the different reactor types and for different initial enrichments. Depending on which reactor type the FISPIN tabulation corresponds to, the indicated burnup will vary to some extent. The end-point is a number of possible initial enrichment/discharge burnup combinations corresponding to different reactor types.

Figures 6, 7, and 8 show some sample U236/U-235 mass ratio plots for PWR, BWR, and AGR respectively and it is these plots that are proposed as the basis of the attribution method. They all have the same horizontal and vertical axes to facilitate comparison and specifying a logarithmic scale for the vertical axis helps distinguish the curves at low burnup. Note that apart from the PWR 4.9 w/o case, all the curves extend well beyond the practically relevant burnups. There is overlap for PWR and BWR as expected, while AGR is separated from them. Interestingly, MAGNOX is very distinct from the other cases and will be easy to distinguish. At its nominal discharge burnup, spent fuel typically has a U-235 content in the range 0.7 to 1.0





**Figure 6.** U236/U235 mass ratio versus burnup - PWR

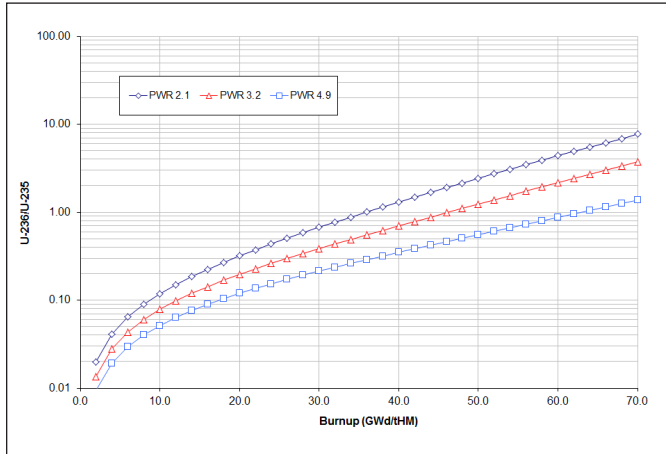


**Figure 7.** U236/U235 mass ratio versus burnup - BWR

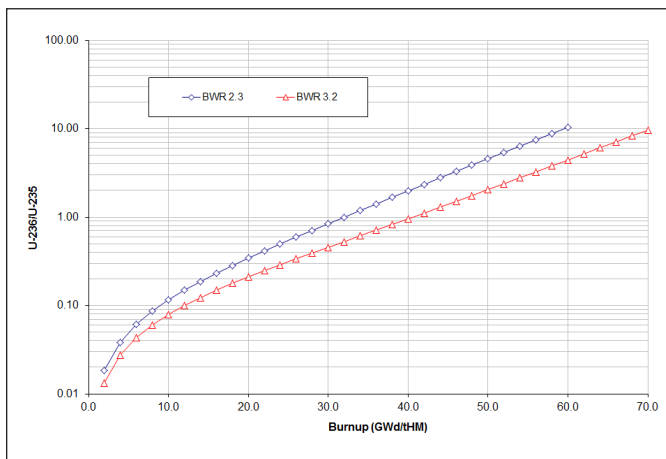
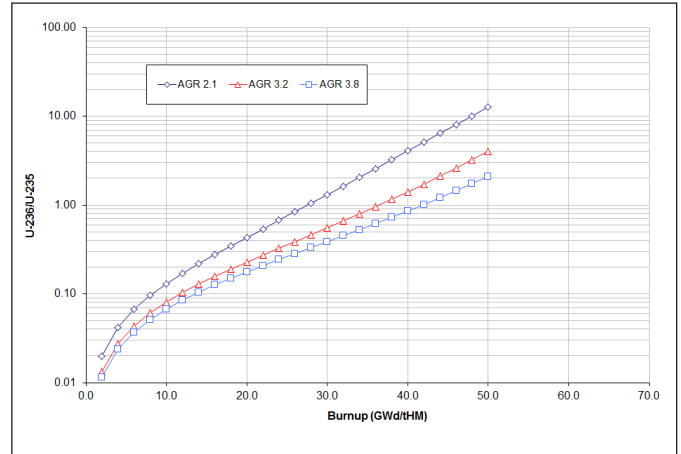


**Figure 8.** U236/U235 mass ratio versus burnup - AGR



ing the attribution is minimal, because these two isotopes are known from validation tests against experimental data to be well predicted and with small measurement uncertainties. The same also applies to U-234, but not to U-232, for which both the calculation and measurements uncertainties are likely to be much larger.

### Testing the Attribution Approach

This section illustrates the potential of the proposed attribution method by applying it to some specific examples. The first example is that of a sample of  $UO_3$  for which the measured isotopic assay is available. The sample is known to have originated from reprocessing of PWR fuel and to have been separated late 1996 and sampled in 1997. The measured uranium isotopic composition of the sample is shown in Table 1:

**Table 1.** Isotopic composition of  $UO_3$  sample (PWR fuel, 1996/97)

| U-232              | U-234        | U-235     | U-236             | U-238          |
|--------------------|--------------|-----------|-------------------|----------------|
| 2 ppb <sub>1</sub> | 220 ± 10 ppm | 0.851 w/o | 0.400 ± 0.003 w/o | 98.8 ± 0.4 w/o |

<sup>1</sup> Uncertainty estimate not available

w/o, with lower inventories of U-236 so that the U-236/U-235 ratio is typically no more than 0.4. The 0.4 U-236/U-235 ratio is evident from Figures 6, 7, and 8 for each of the reactor types, if the discharge burnups are matched to the initial enrichments. For PWR, for example, (Figure 6) a U-236/U-235 ratio of 0.4 is obtained at discharge burnups of approximately 23, 32 and 46 GWd/tHM burnup for initial enrichments of 2.1, 3.2, and 4.9 w/o respectively. These burnups coincide with the natural discharge burnup of fuel assemblies with this enrichment. The same analysis also applies to BWR (Figure 7) and AGR (Figure 8). At burnups that are beyond the design discharge burnup, the U-235 inventory is depleted to very low levels and the U-236/U-235 ratio diverges and values in excess of 0.4 implies fuel that has been irradiated beyond its natural discharge burnup.

Since this approach relies on U-235 and U-236, the potential for uncertainties on the FISPIN inventory calculations bias-

Applying the proposed methodology to this sample results in an estimated initial enrichment of  $3.21 \pm 0.02$  w/o (using the quoted measurement uncertainty on U-236). This estimate is obtained by dividing the measured U-236 assay by an initial estimate of the capture/absorption ratio R of 0.1695 obtained from a FISPIN tabulation for PWR fuel with an initial enrichment of 3.2 w/o. This gives the amount by which the initial U-235 has been depleted:  $\Delta 235 = 0.4/0.1695 = 2.35$  w/o. Adding this to the measured U-235 assay gives an estimate for the



initial U-235 enrichment of 3.21 w/o. This estimate is insensitive to which reactor type the capture/fission ratio R is taken from. With this initial enrichment, the measured U-236/U-235 ratio of 0.47 is used to estimate the discharge burnup from the 3.2 w/o curves of Figures 6 to 8 and gives the results indicated in Table 2:

**Table 2.** Discharge burnup estimates

| Tabulation | Attributed discharge burnup (GWd/tHM) |
|------------|---------------------------------------|
| PWR 3.2    | 33 ± 2                                |
| BWR 3.2    | 30 ± 2                                |
| AGR 3.2    | 28 ± 2                                |

This indicates three possible matches to PWR, BWR, and AGR with different burnups matching each. This is useful information that might be used to corroborate other attributions. In this case, it is possible to rule out AGR as the reactor type using the sample date of 1997 (at which time the initial enrichments were lower). This implies a discharge date prior to 1990, at which point AGR mean discharge burnups were considerably lower than 28 GWd/t. The final attribution is therefore either a PWR at ~33 GWd/t or a BWR at ~30 GWd/t. Both these attributions are plausible because the initial enrichments and discharge burnups both fit well with PWR and BWR spent fuel characteristics available at that time.

A sensitivity analysis for this specific case results in a change in attributed discharge burnup estimated at approximately ±1.5 GWd/t for a ±10 percent change in the capture/absorption ratio R. Within the context of this application, this is an acceptably small uncertainty, especially considering that R could reasonably be expected to have a smaller uncertainty with suitably fine tabulation intervals. Assuming that the unknown uncertainty on the sample U-235 measurement is small, the main contributor to the uncertainty estimates in Table 2 are the calculation uncertainties on U-235 and U-236 from FISPIN estimated at 5 percent and 10 percent respectively, which in turn implies an uncertainty of ± 2 GWd/tHM on the discharge.

It is possible to gain additional information from the measured U-234 concentration for this sample. Figure 3 indicates from the PWR 3.2 curve that a reasonable estimate for the initial U-234 concentration would be approximately 300 ± 10 ppm (the actual value depends to a small extent on the unknown tails enrichment and does not depend on reactor type). At the attributed burnup of 33 GWd/t, this would have depleted to approximately 180 ppm. The measured value of 219 ppm

indicates an enhancement of about 20 percent, presumably due to build-up during the cooling period between discharge and separation. A 20 percent enhancement equates to approximately ten years' cooling. So the sample would correspond to fuel that was cooled for ten years before separation. Though the actual cooling time for the sample is unknown, ten years nevertheless is a very reasonable guess. A value significantly longer than ten years would not be reasonable, because PWR discharge burnups as high as 33 GWd/t were only routinely attained in the mid-1980s.

The second example is a set of four spent fuel sample measurements from the Galaxy Serpent international benchmark exercise in which the UK recently participated, with NNL supplying one of the three attribution assessments from the UK based on the measured plutonium isotopic abundances.<sup>1</sup> The four measured samples are designated ERATO-1 to ERATO-4 and include measurements of the U-235 and U-236 concentrations. Table 3 shows the measured U-235 and U-236 concentrations for the four ERATO samples. The methodology leads to an initial enrichment estimate for all four samples of 3.4 w/o (assuming that the samples come from a PWR, as indicated by all three attribution methods used by the UK in Galaxy Serpent, gives the burnups indicated in the sixth column). As an illustration of the approach, the calculation for ERATO-1 used an estimate for the capture/absorption ratio R of 0.168 obtained from FISPIN tabulations for 3.2 w/o initial enrichment. Using the measured U-236 assay of 0.382 w/o gives an estimate of the amount by which U-235 has been depleted  $\Delta^{235} = 0.382/0.168 = 2.274$  w/o. Added to the measured U-235 assay of 1.125 w/o this indicates an initial enrichment of 3.4 w/o. These attributed initial enrichments and discharge burnups correlate very well with NNL's attribution based on the plutonium isotopics (Table 4) and applying the two attribution methods provides valuable independent corroboration. The attributed burnups also correlate closely with the burnup inferred from Nd-148 measurements.<sup>5</sup>

In this instance, there is prior evidence pointing to the samples originating from a PWR. Table 5 shows the effect on the estimated discharge burnups of not making this assumption and postulating BWR or AGR as alternative sources. The spread of burnups is small, especially if AGR can be omitted, which is certainly the case for the ERATO samples, but the data could equally be fitted to BWR or VVER reactors, so that there is no definitive attribution to a specific reactor type.

**Table 3.** Attribution of ERATO samples based on U-235 and U-236 measurements

|         | Measured U-235 (w/o) | Measured U-236 (w/o) | U-236/U-235   | Estimated initial U-235 enrichment (w/o) | Attributed discharge burnup (GWd/t) | Nd-148 burnup measurement (GWd/t) |
|---------|----------------------|----------------------|---------------|--|-------------------------------------|-----------------------------------|
| ERATO-1 | 1.125 ± 0.003        | 0.382 ± 0.001        | 0.340 ± 0.001 | 3.4 ± 0.1                                | 28                                  | 27.05 ± 0.81                      |
| ERATO-2 | 2.030 ± 0.005        | 0.236 ± 0.001        | 0.116 ± 0.001 | 3.4 ± 0.1                                | 14                                  | 11.72 ± 0.35                      |
| ERATO-3 | 1.383 ± 0.004        | 0.332 ± 0.001        | 0.240 ± 0.001 | 3.4 ± 0.1                                | 23                                  | 22.65 ± 0.68                      |
| ERATO-4 | 1.727 ± 0.004        | 0.275 ± 0.001        | 0.159 ± 0.001 | 3.4 ± 0.1                                | 17                                  | 15.27 ± 0.46                      |

**Table 4.** Attribution of ERATO samples based on measured plutonium isotopic abundances

| ERATO sample | Most probable reactor type | Years between discharge and analysis | Estimated initial U-235 enrichment (w/o) | Attributed sample discharge burnup (GWd/t) |
|--------------|----------------------------|--------------------------------------|--|--|
| ERATO-1      | PWR                        | 1.5                                  | 3.5                                      | 27.9 ± 1.0                                 |
| ERATO-2      | PWR                        | 3.5                                  | 3.5                                      | 12.2 ± 0.5                                 |
| ERATO-3      | PWR                        | 1.5                                  | 4.0                                      | 25.7 ± 0.8                                 |
| ERATO-4      | PWR                        | 1.0                                  | 4.0                                      | 19.0 ± 0.7                                 |

**Table 5.** Dependence of discharge burnup on reactor type

|         | Attributed discharge burnup (GWd/t) |     |     |
|---------|-------------------------------------|-----|-----|
|         | PWR                                 | BWR | AGR |
| ERATO-1 | 28                                  | 26  | 25  |
| ERATO-2 | 14                                  | 13  | 13  |
| ERATO-3 | 23                                  | 22  | 21  |
| ERATO-4 | 17                                  | 17  | 16  |

## Conclusions

An approach has been developed that is able to use the measured isotopic composition of a Rep U sample to attribute the sample to a reactor type, the initial enrichment of the fuel, its burnup, and the cooling time since reprocessing. Though the measured isotopic characterization cannot be expected to allow a completely reliable attribution, some useful attribution is nevertheless possible. As with plutonium attribution, the application of other constraints, such as knowledge of the historic operating characteristics of different reactor types, can be helpful at reducing the number of potential attributions that can reasonably be assigned.

The approach has been developed and tested for Rep U from commercial reactor fuel reprocessing. However, the approach is also likely to be valid for Rep U originating from reprocessing low-enriched uranium (LEU) or highly enriched uranium (HEU) research reactor fuels, because the neutron spectra of thermal spectrum commercial and research reactors overlap and the capture/fission ratio R is similar. Broadening the FISPIN tabulations to cover LEU and HEU research reactors would be an obvious extension of this work.

## References

- Borgardt, J. D., and F. M. G. Wong. 2014. Galaxy Serpent: A Web-based Tabletop Exercise Using the Concept of National Nuclear Forensics Libraries, *Journal of Nuclear Materials Management*, Volume 42, No. 4.
- Heydon, A. J., C. A. Christopher, P. Thompson, P. G. Turner, R. Gregg, K. W. Hesketh, A. E. Jones, and J. Y. Goulermas. 2014. The UK's Contribution to the Galaxy Serpent Tabletop Exercise, *Journal of Nuclear Materials Management*, Volume 42, No. 4.
- Burstall, R. F. 1979. FISPIN – A Computer Code for Nuclide Inventory Calculations, PND-R-328(R), UK Atomic Energy Authority.
- Parker, D. R., and R. W. Mills. 1972. FISPIN10 Validation Review, RAT 1972 Issue 02, RAWG/P(01)04, March 2002, OECD-NEA, <https://www.oecd-nea.org/science/wpncs/ADSNF/reports/.../FISPIN.pdf>.
2012. Standard Test Method for Atom Percent Fission in Uranium and Plutonium Fuel (Neodymium-148 Method) ASTM E321 96.



# Np/Pu Seeding of U in the Breeder Regions in an ASTRID-type Sodium Fast Reactor to Avoid Production of Very High-quality Fissile Material

Christopher Grove and Kevin Hesketh  
National Nuclear Laboratory Limited, Preston, Lancashire, UK

## Abstract

The UK has been investigating scenarios in which fast reactors are deployed in a breeding cycle that is not dependent on external uranium supply. Although it is not certain whether there will ever be a driver for strategic independence in the UK, it is nevertheless important that all the options are examined and their implications understood. An ASTRID-type Sodium Fast Reactor (SFR) with an iso-breeder core (overall breeding ratio marginally above 1.0) would be a plausible option in such a scenario and has been assumed in some of the reference scenarios. However, there is a theoretical vulnerability to a proliferation scenario in which the axial breeder regions are sheared separately in the head end of a reprocessing plant and used to recover very high isotopic quality plutonium. This paper describes an assessment of the effectiveness of Np-237 and plutonium seeding of the breeder blankets in order to avoid the production of such high isotopic quality fissile materials. The study was initially intended to focus on Np-237 seeding, but it was found that plutonium seeding would be more practicable. The purpose of the study was not to demonstrate that an ASTRID iso-breeder could be operated with a high degree of intrinsic proliferation resistance, but rather to investigate whether seeding the breeding blankets could avoid the production of virtually pure Pu-239 that otherwise is produced in the breeder region. The study demonstrates that seeding the breeder regions is effective to a limited extent by ensuring that pure Pu-239 production is avoided. Unseeded breeder regions produce plutonium which is in the weapons grade category and could be regarded as incompatible with the IAEA INPRO guideline that: *"the attractiveness of nuclear material and nuclear technology in an Innovative Nuclear System for a nuclear weapons program should be low."*

## Introduction

Sodium voiding is an important consideration in sodium fast reactors (SFR). Any mechanism that voids sodium in the core

causes the neutron energy spectrum to become more energetic and has the potential to inject significant reactivity. A positive sodium void coefficient can be managed if other feedback mechanisms such as fuel temperature (Doppler) are sufficiently strong, but it could be argued that a better approach is to design the core to make the void coefficient less positive or even negative. This can be achieved by using a core configuration in which leakage of neutrons increases in the event of sodium voiding and this is the approach that has been adopted for the ASTRID SFR prototype which France is designing. ASTRID (see Figure 1) uses a core with a large diameter and small height, which combined with internal and external axial breeder regions does not have a large positive sodium void reactivity (this is the CFV core design).

As part of its Nuclear Road Map,<sup>1</sup> the UK has been investigating scenarios in which fast reactors are deployed in a breeding cycle that is not dependent on external uranium supply. Although it is not certain whether there will ever be a driver for strategic independence in the UK, it is nevertheless important that all the options are examined and their implications understood. An ASTRID-type SFR with an iso-breeder core (overall breeding ratio marginally above 1.0) would be a plausible option in such a scenario. However, there is a theoretical vulnerability to a proliferation scenario in which the axial breeder regions are sheared separately in the head end of a reprocessing plant and used to recover high-fissile-quality plutonium. This paper describes an assessment of the effectiveness of Np-237 and plutonium seeding in order to avoid the production of plutonium of such high isotopic quality. The study was initially intended to focus on Np-237 seeding, but it was found that plutonium seeding was more effective and more practicable. The purpose of the study was not to demonstrate that an ASTRID iso-breeder could be operated with a high degree of intrinsic proliferation resistance, but rather to investigate whether seeding the breeding blankets could avoid the production of virtually pure Pu-239 that otherwise is produced in the breeder region.

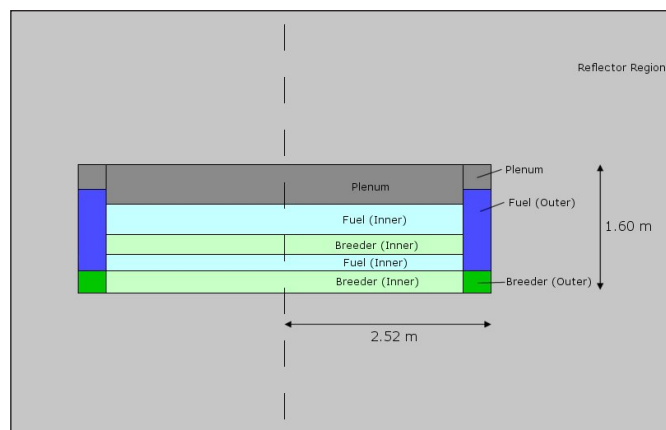
The motivation is guided by the International Atomic Energy Agency (IAEA) INPRO<sup>2</sup> and Gen IV<sup>3</sup> international collaborations, where it is accepted that best practice should minimize the attractiveness of fissile material generated in the system. The UK would very likely seek to implement best practice wherever possible and follow the INPRO guidelines and the context of the study was to investigate what could practically be achieved in this respect. The ERANOS fast reactor code package<sup>4</sup> was used to model an ASTRID-type core configuration in which the axial breeder regions are seeded with Np-237 or reactor-grade plutonium in an attempt to avoid the production of high-fissile-quality plutonium.

### SFR Core Model

The ERANOS fast reactor code suite<sup>4</sup> was used to model the ASTRID CFV core, rated at 600 MWe (1500 MWth). The CFV core (Figure 1) consists of an inner fuel region in which the fuel rods vary axially between regions of breeder and fuel material with a large sodium plenum above.<sup>5</sup> The fuel is UO<sub>2</sub>-PuO<sub>2</sub> (mixed-oxide: MOX) with a high Pu content of 16 weight percent (w/o). The breeder region of the standard design core consists of depleted UO<sub>2</sub>. The fuel clad is stainless steel. The outer fuel region (the blue region in Figure 1) has an increased axial height compared with the inner region, which is an additional positive coolant void coefficient mitigation measure. The core was modelled with ERANOS using the R-Z geometry option in 33 neutron energy groups, with the key resonance elements (U, Pu, Th, Zr, C) modelled in 1968 energy groups in the ECCO cell calculations, prior to condensation to thirty-three groups.

As modelled, the reactor operates on a single batch scheme (mainly due to necessary simplification of the modelled reprocessing scheme when using ERANOS). The reactor operates for 5 x 400 days (2,000 days in total) before all fuel is removed. The assumption is made that the breeder material is extracted after the first cycle (400 days) of operation. Removing breeder material at 400 days represents a hypothetical proliferator's first opportunity to remove material from the core without recourse to an unusual reactor operating regime. Although in this core design the fuel and breeder are integral to individual fuel rods, it is assumed that a determined proliferator would utilize mechanical chopping of the fuel rods in order to separate fuel from breeder.

**Figure 1.** ASTRID CFV core schematic diagram



### Breeder Region Seed Compositions

Three distinct seed types are used in this study: Np-237, plutonium obtained from PWR reprocessing in equilibrium, and plutonium recycled from SFR in equilibrium. The plutonium isotopic compositions are shown in Table 1:

**Table 1.** SFR & PWR plutonium isotopic composition

| Source     | Weight percentage (w/o) |        |        |        |        |        |
|------------|-------------------------|--------|--------|--------|--------|--------|
|            | Pu-238                  | Pu-239 | Pu-240 | Pu-241 | Pu-242 | Am-241 |
| <b>PWR</b> | 4.0                     | 50.0   | 23.0   | 12.0   | 9.5    | 1.5    |
| <b>SFR</b> | 2.7                     | 45.8   | 33.4   | 6.2    | 10.7   | 1.2    |

When seeding the breeder with Np-237, three individual runs were performed using Np loading of 0.017 w/o, 1 w/o and 5 w/o (in relation to the total breeder mass). The material added to the breeder is pure Np-237. The 0.017 w/o, figure is determined by the amount of Np-237 that can be generated from an unseeded SFR operating for a full term of 2,000 days. Thus, it represents — as a first approximation — the amount of Np-237 that could be obtained from recycle of Np after extraction from spent fuel from the core. Seeding the breeder material with 1 w/o or 5 w/o Np-237 would require an external source of neptunium in order to provide the necessary quantity.

Plutonium is added to the breeder in proportions of 1, 5, and 10 w/o for ex-PWR Pu. SFR plutonium is added in proportions of 1, 5, and 11.9 w/o. The 11.9 w/o value represents the total amount of plutonium that could be obtained from recycle of Pu after extraction from spent fuel that has undergone 2000 days of irradiation in the core. The remaining breeder material consists of depleted uranium: 99.7 w/o U-238, 0.3 w/o U-235.



## Np-237 Seeding — Results

Figure 2 shows the plutonium isotopic composition for plutonium bred in the SFR inner breeder seeded with Np-237. Np-237 initial seed concentrations are (from left to right) 0.017 w/o, 1.0 w/o, and 5 w/o respectively. The results are plotted for irradiation times between 400 days (which is the earliest time at which the breeder material would be accessible) and full-term irradiation at 2,000 days. With no seeding of the breeder region, the plutonium isotopic quality at 400 days corresponds to weapons grade material and even after 2,000 days' irradiation the Pu-239 content remains in excess of 90 w/o. Seeding with Np-237 at 0.017 w/o has no discernible impact and is completely ineffective. With 1.0 w/o Np-237 seeding the Pu-239 fraction remains high at 400 days at approximately 92.5 w/o, but ingrowth of Pu-238 at 400 days is such that the Pu-238 amounts to 5.9 w/o of the total plutonium content. With 5.0 w/o Np-237 seeding the Pu-238 at 400 days accounts for 23.6 w/o of the total plutonium inventory and the Pu-239 fraction is 75.3 w/o.

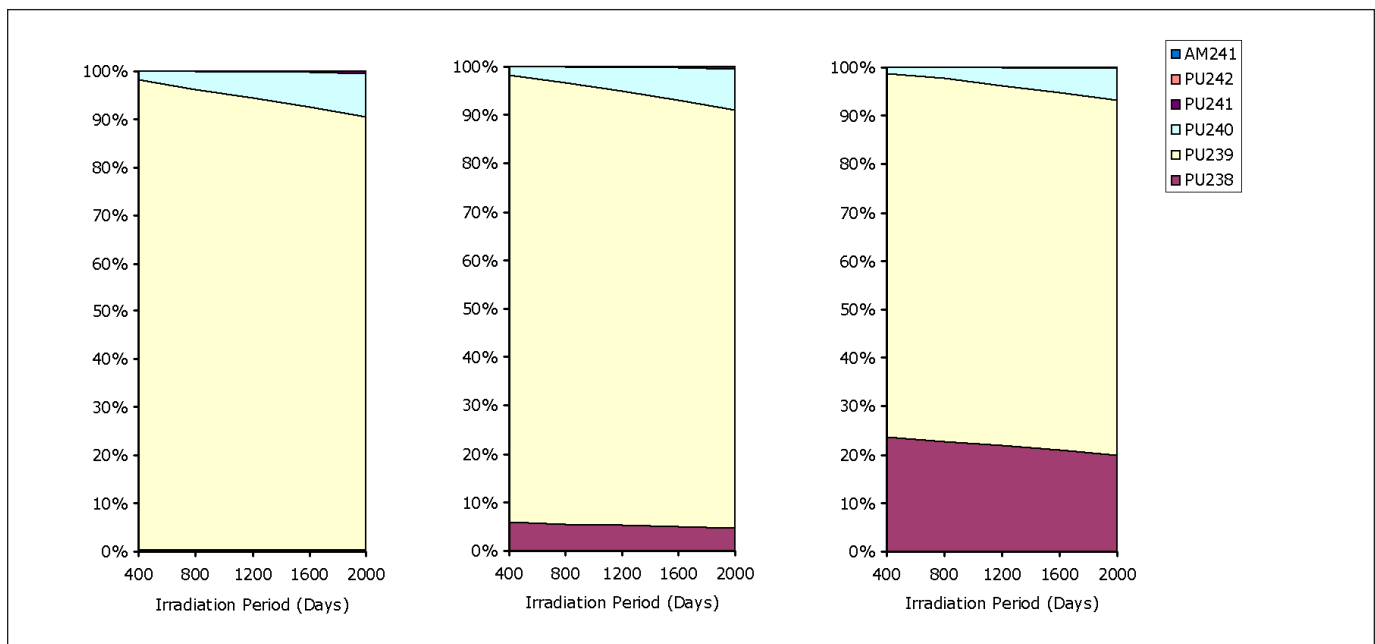
Seeding the breeder regions with 1.0 w/o and 5.0 w/o Np-237 is effective in avoiding the production of pure Pu-239, which satisfies one of the objectives of this study. It is difficult to comment on the materials attractiveness of plutonium containing 5.9 w/o or 23.6 w/o Pu-238 except to say that the heat output is likely to significantly complicate its utilisation in a

nuclear explosive device compared with pure Pu-239. It is notable that even the higher Pu-238 content is significantly below the threshold of 80 percent at which plutonium is exempted from the IAEA nuclear material categorization<sup>6</sup> and therefore the full requirements of nuclear security and safeguards would still be applicable.

## Pu Seeding — Results

Figure 3 shows the evolution of the plutonium isotopic composition for breeder plutonium for low, medium and high plutonium seed levels (corresponding to 1.0, 5.0 and 10.0 w/o), using plutonium derived from PWR reprocessing. Figure 4 shows the corresponding plots for seeding with plutonium derived from SFR reprocessing (in this specific case the low medium and high seed levels correspond to 1.0, 5.0 and 11.9 w/o respectively). These figures show the fissile fraction defined as  $(Pu239+Pu241)/Total\ Pu$ , which is used as a measure of isotopic quality, as a function of irradiation time. At long irradiation times the two datasets appear to be heading toward the same equilibrium asymptotes, with the isotopic quality of the plutonium increasing with irradiation time such that the limiting irradiation time is now 1,200 days or more and not the 400 days that applies with Np-237 seeding.

**Figure 2.** Evolution of Pu isotopics with irradiation time in breeder region with Np-237 initial seed concentrations are (from left to right) of 0.017 w/o, 1.0 w/o and 5 w/o respectively







The medium and high seed cases were run largely to provide an upper bound. With the high Pu seed concentration, the 239+241 fraction builds towards equilibrium at around 65 percent, which coincides with reactor grade plutonium. With the medium Pu seeding the fissile quality reaches equilibrium at between 70 and 75 w/o, which equates to that of low burnup commercial reactor spent fuel. Neither case could conceivably be claimed to be anything other than weapons usable so that as for Np-237 seeding even these limiting cases cannot be claimed to be proliferation proof. In practice, seeding the breeder zones with medium or high Pu seeding would largely remove the distinction between the driver fuel regions and the breeder regions and might adversely affect positive void coefficient mitigation. With 1.0 w/o Pu seeding the void mitigation effect of the breeder zones could reasonably be expected to be preserved, but the 239+241 fraction builds up to an equilibrium close to 86 percent. Although such material would most certainly be weapons usable, it still would represent a considerable improvement on an unseeded breeder where the 239+241 fraction is in excess of 90 percent at 2,000 days. At 400 days' irradiation, 1.0 w/o Pu seeding yields between 75

and 80 percent 239+241 fraction, compared with >95 percent for the unseeded breeder.

Seeding the breeder zones with 1.0 w/o Pu would incur a fuel fabrication cost penalty, but not as significant as Np-237 seeding, since all the fabrication operations could be accommodated within a MOX production facility. Operator doses could also be expected to be close to those of fabricating fuel with an unseeded breeder. Therefore, seeding the breeder regions with a low concentration of Pu appears to offer a significant step forward in terms of avoiding the production of very high-fissile-quality plutonium, with minimum technological risk and economic penalty. With an unseeded breeder the worst case indicated is of a proliferator having access to plutonium with 98 percent 239+241 fraction after 400 days' irradiation. With 1.0 w/o Pu seeding, the worst case equates to about 86 percent 239+241 fraction. However, it is emphasized that although this is an improvement on the unseeded case, the isotopics quality in the breeder remains in the upper range of current commercial reactor fuels and cannot conceivably be claimed to be proliferation proof.

**Figure 3.** Evolution of plutonium isotopic quality with irradiation time – PWR sourced plutonium

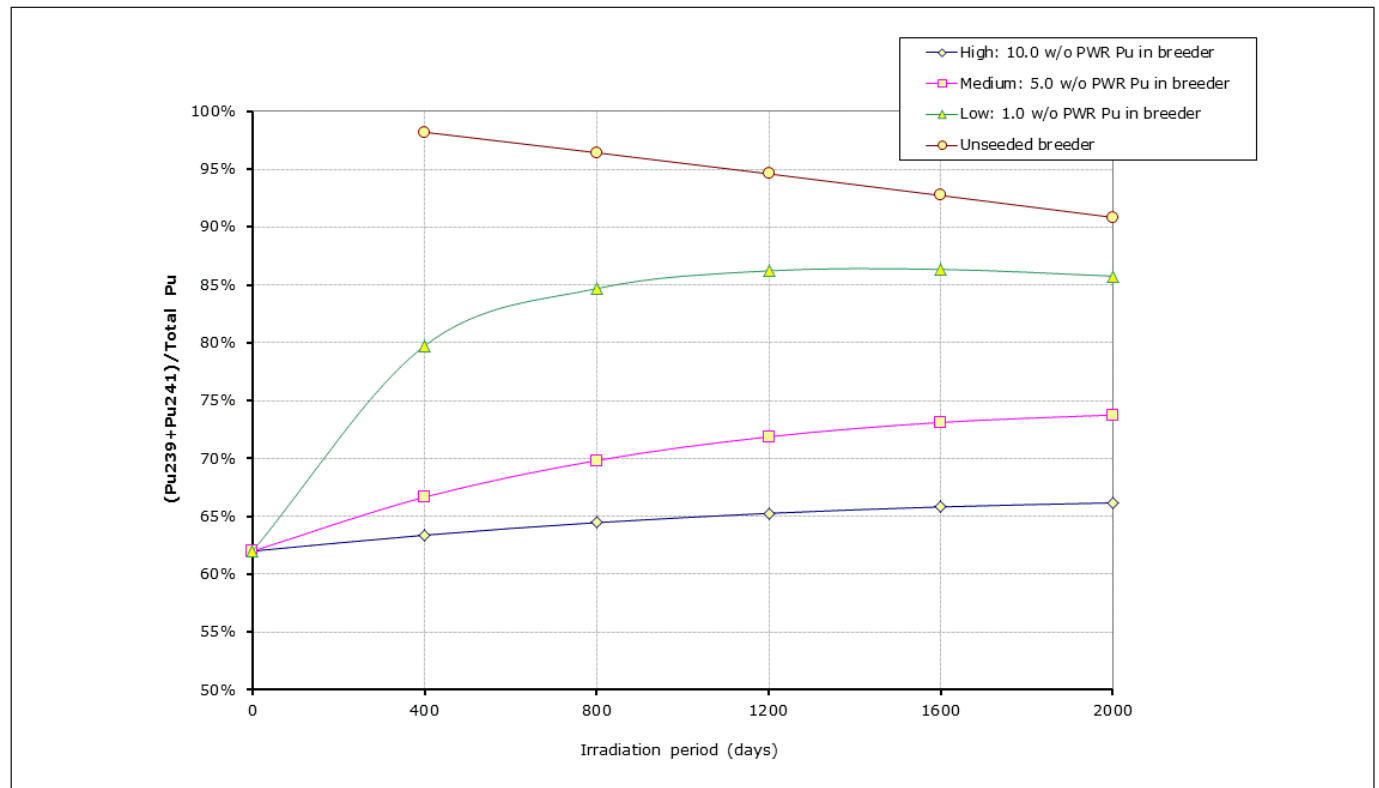
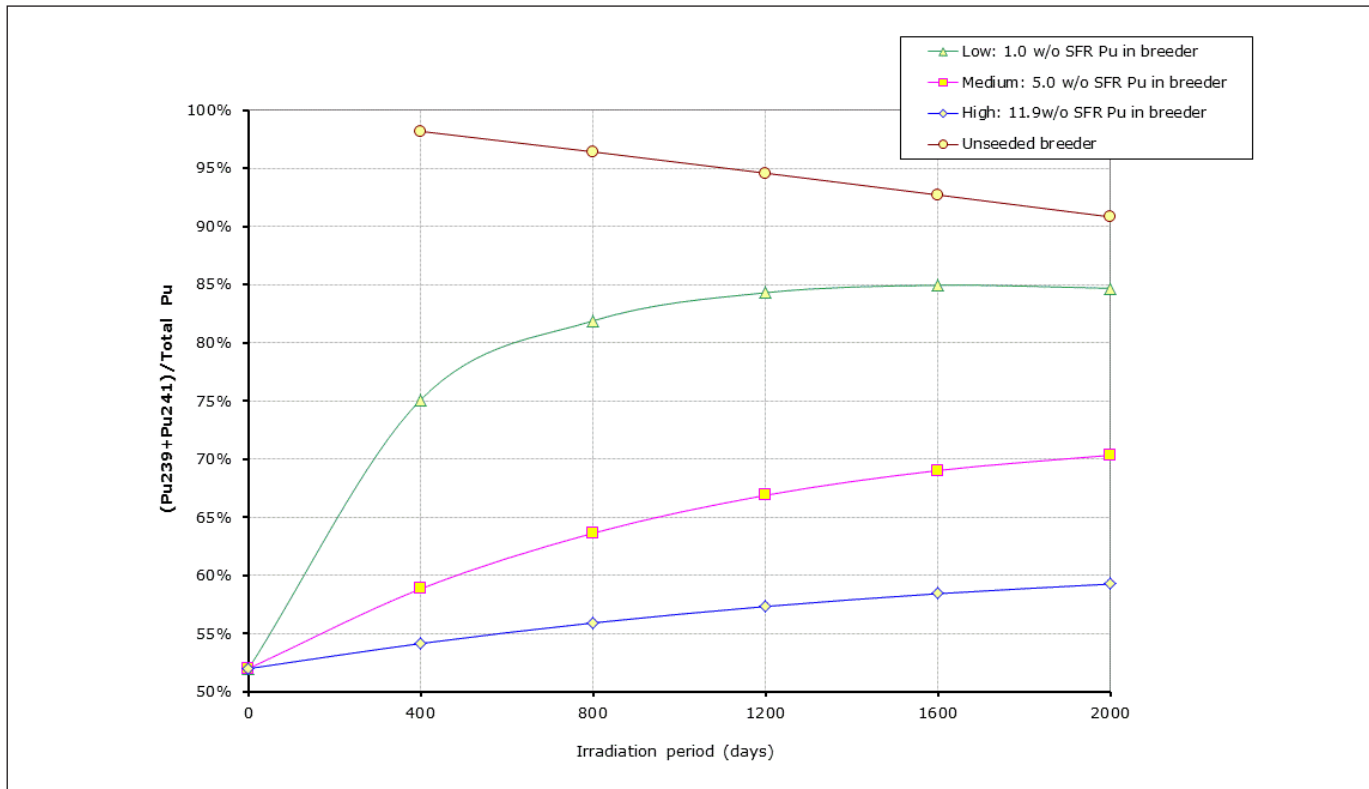




**Figure 4.** Evolution of plutonium isotopic quality with irradiation time – SFR-sourced plutonium



## Logistics of Seeding with Np-237

The 1.0 and 5.0 w/o Np-237 seed concentrations considered here were chosen arbitrarily and further consideration needs to be given to the logistics of sourcing Np-237 and whether these seed concentrations are sensible. There are two broad scenarios that need to be considered:

1. The initial core and early cycles for an ASTRID iso-breeder in which the fissile material is obtained from recycled spent LWR fuel.
2. Equilibrium cycle in ASTRID iso-breeder core.

These two scenarios are significantly different. In LWR spent fuel the Np-237 inventory is typically in the range 600-700 g/tHM, compared with the plutonium inventory of 11,000-12,000 g/tHM. In the ASTRID core the total heavy metal masses of the driver and breeder regions are 81 tHM and 59 tHM respectively. The initial plutonium inventory of 13 tPu needed for the driver regions at a nominal 16 w/o total plutonium concentration could be obtained by reprocessing approximately 1100 tHM of spent LWR fuel. With Np-237 partitioning, the same LWR fuel mass would yield in the region of 700 kg of Np-237,

which would allow the breeder regions to be seeded with just over 1 w/o of Np-237, fortuitously coinciding with one of the data points analysed here.

The equilibrium Np-237 inventory in the ASTRID core is approximately an order of magnitude smaller than that of LWR spent fuel and in the equilibrium cycle there is only sufficient Np-237 available to seed the breeder regions at around 0.1 w/o. This is because of the more favourable fission/capture ratio of Np-237 in the fast neutron spectrum that allows fast spectrum systems to burn Np-237 and other transuranics. During the transition from the initial cycle to the equilibrium cycles, the Np-237 inventory would gradually decline during the transition to equilibrium and a 1.0 w/o Np-237 seed strategy could not be maintained beyond the initial transition cycles. There is therefore a considerable logistical difficulty with seeding the breeder regions with 1.0 w/o Np-237 in a sustainable way and 5.0 w/o seed is definitely ruled out even in the initial cycles. Moreover, extracting Np-237 from LWR spent fuel reprocessing and its subsequent incorporation in the breeder regions of ASTRID fuel sub-assemblies would incur significant cost penalties that further diminish its attractiveness.

The practicality of manufacturing breeder pellets containing 5.0 w/o Np-237 would likely demand remote fabrication methods and combined with the need to source the Np-237 would make fuel fabrication very complex and expensive. With 1.0 w/o Np-237 seeding, fuel fabrication is likely to be simplified, but nevertheless still penalised economically. It is concluded that seeding with Np-237 at about 1.0 w/o might appear to strike a reasonable compromise between maximising Pu-238 content and manufacturing feasibility, subject to availability of Np-237 and demonstration that the fuel fabrication cost penalty is tolerable.

The driver for this study was to determine whether seeding the breeder regions with Np-237 or Pu would be effective at decreasing the proliferation risk posed by high-fissile-quality plutonium generated in the breeder regions. Seeding with Np-237 seems to produce the least attractive fissile material because of the very large heat source from the Pu-238, but also would be more expensive, would present major logistical difficulties, and not be sustainable beyond the early transition cycles. A further consideration is that the separation of Np-237 poses a proliferation risk because Np-237 is itself a fissionable material. For these reasons, seeding the breeder regions of ASTRID with plutonium is considered more favourable, even though its proliferation resistance performance is not quite as good.

## Proliferation Vulnerability Assessment

The intended operational mode of the ASTRID CFV core is that after irradiation for 2,000 days the fuel sub-assemblies would be discharged from the core and stored for a period of a few years to allow the decay heat output to decline. Following this cooling period the fuel would be sheared and dissolved as the first step in reprocessing. During the fuel shear step the inner sub-assemblies would be sheared as a whole, with fuel pellets from both driver regions and the breeder regions both subject to dissolution in the same batch without any attempt to partition them. Such co-dissolution would result in the high-fissile-quality plutonium in the breeder regions being mixed with the much larger mass of plutonium from the driver regions. The overall isotopic composition of the plutonium would be dominated by the contribution from the driver region and would be categorised as reactor grade. Therefore, the system operated as intended would not generate weapons grade fissile material.

However, there is a vulnerability in that a relatively minor modification in head-end operations could be conceived that could be effective at partitioning the breeder regions and which

could be used to produce dissolution batches containing very high-fissile-quality plutonium. The only protection against this would be safeguards and verification measures. The worst case scenario, with partitioning of breeder regions from fuel sub-assemblies discharged after 400 days' irradiation, would yield plutonium with a Pu-239 content estimated in the region of 98 percent. This is inconsistent with the Basic Principle for proliferation resistance as advocated by IAEA INPRO:<sup>7</sup> *"The attractiveness of nuclear material (NM) and nuclear technology in an Innovative Nuclear System for a nuclear weapons program should be low. This includes the attractiveness of undeclared nuclear material that could credibly be produced or processed in the INS."* As a minimum, compliance with this INPRO basic principle requires that the plutonium that could credibly be produced should be categorised as posing a risk no higher than reactor grade. Seeding the breeder zones with 1.0 w/o Np-237 or 1.0 w/o Pu would be sufficient to ensure this is the case.

The INPRO basic principle for proliferation resistance is prefaced by the statement: *"Proliferation resistance intrinsic features and extrinsic measures shall be implemented throughout the full life cycle for innovative nuclear energy systems to help ensure that Innovative Nuclear Systems will continue to be an unattractive means to acquire fissile material for a nuclear weapons program. Both intrinsic features and extrinsic measures are essential, and neither shall be considered sufficient by itself."* Seeding the breeder regions with 1 w/o Np-237 or 1.0 w/o Pu would count as intrinsic features under this principle, but would not in any way affect the need for extrinsic measures, such as safeguards and security.

## Conclusions

The fuel for the ASTRID CFV core, which has axial breeder zones in the fuel pins, introduces a potential proliferation pathway. Selective cropping of fuel assemblies to isolate the breeder zones from the driver zones in dissolution, could in theory be used for a proliferator to extract weapons grade plutonium. This is not consistent with the IAEA INPRO Basic Principle of avoiding the production of fissile material of high attractiveness. This study has demonstrated that seeding the axial breeder zones with >1 w/o of Np-237 is in theory an approach that could be used to degrade the attractiveness of the fissile material that could potentially be isolated. However, Np-237 seeding will adversely affect fuel fabrication costs and the logistics of obtaining the required inventory of Np-237 also poses potential difficulties. If a fleet of ASTRID CFV reactors



was operated in a synergistic cycle with LWRs, there would be enough Np-237 produced in the LWRs to meet the inventory needed for seeding. However, in a fleet composed entirely of ASTRID CFV reactors, production of Np-237 is much lower and there would be insufficient inventory available. Seeding with plutonium seems more practicable, with a much smaller penalty of the cost of fuel fabrication and ensures that the plutonium produced in the breeder zones falls into the reactor-grade category. This goes some way towards satisfying the INPRO Basic Principle, but it should be emphasized that while this is a step in the right direction, it is not possible to claim that the system can be made in any sense proliferation proof. The best that can be claimed that seeding the breeder zones with 1 w/o plutonium reduces the theoretical proliferation risk to be more comparable with existing reactor types.

## References

1. 2013. Nuclear Energy Research and Development Roadmap: Future Pathways, <https://www.gov.uk/>.
2. 2014. Options to Enhance Proliferation Resistance of Innovative Small and Medium Sized Reactors IAEA Nuclear Energy Series Technical Reports Guides No. NP-T-1.11.
3. 2014. Technology Roadmap Update for Generation IV Nuclear Energy Systems, January 2014, Issued by the OECD Nuclear Energy Agency for the Generation IV International Forum, <https://www.gen-4.org/>.
4. Rimpault, G., et al. 2002. The ERANOS Code and Data System for Fast Reactor Neutronic Analyses, *Proceedings of the International Conference on Physics of Reactors, Seoul, Korea*.
5. Fontaine, B., et al. 2011. The French R&D on SFR core design and ASTRID Project, *Proceedings of GLOBAL 2011*, Makuhari, Japan.
6. 2008. Nuclear Security Recommendations on Physical Protection of Nuclear Material and Nuclear Facilities (INFCIRC/225/Revision 5).
7. Guidance for the Application of an Assessment Methodology for Innovative Nuclear Energy Systems INPRO Manual — Overview of the Methodology, IAEA-TEC-DOC-1575 Rev. 1, Nov 2008, ISBN 978-92-0-111110-4, ISSN 1816-9317.



# Modeling and Analysis Methods for an On-Line Enrichment Monitor

*L. Eric Smith, Kenneth D. Jarman, Richard S. Wittman, and Mital A. Zalavadia  
Pacific Northwest National Laboratory, Richland, Washington USA*

*José March-Leuba  
Oak Ridge National Laboratory, Oak Ridge, Tennessee USA*

---

## Abstract

The International Atomic Energy Agency (IAEA) has developed an On-Line Enrichment Monitor (OLEM) as one possible component in a new generation of safeguards measures for uranium enrichment plants. The OLEM measures  $^{235}\text{U}$  emissions from the  $\text{UF}_6$  gas flowing through a unit header pipe using NaI(Tl) spectrometers, and corrects for gas density changes using pressure and temperature sensors in order to determine the enrichment of the gas as a function of time. In parallel with the OLEM instrument development, a Virtual OLEM (VOLEM) software tool has been developed that is capable of producing synthetic gamma-ray, pressure, and temperature data representative of a wide range of enrichment plant operating conditions. VOLEM complements instrument development activities and allows the study of OLEM for scenarios that will be difficult or impossible to evaluate empirically. Uses of VOLEM include: uncertainty budget analysis and performance prediction for typical and atypical operational scenarios; inter-comparison of candidate gamma-ray spectral analysis and enrichment estimation algorithms; and testing of the OLEM analysis and reporting software. This paper describes the technical foundations of VOLEM and illustrates how it can be used. An overview of the nominal instrument design and deployment scenario for OLEM is provided, with emphasis on the key online-assay measurement challenge: accurately determining the portion of the total  $^{235}\text{U}$  signal that comes from a background that includes solid uranium deposits on the piping walls. Monte Carlo modeling tools, data analysis algorithms and uncertainty quantification methods are described. VOLEM is then used to quantitatively explore the statistical uncertainty budgets and predicted instrument performance for a plausible range of typical plant operating parameters, and one set of candidate analysis algorithms. Additionally, a series of VOLEM case studies illustrates how an online enrichment monitor might respond in scenarios ex-

pected to be atypical, for example weak pressure transients or significant changes in background levels.

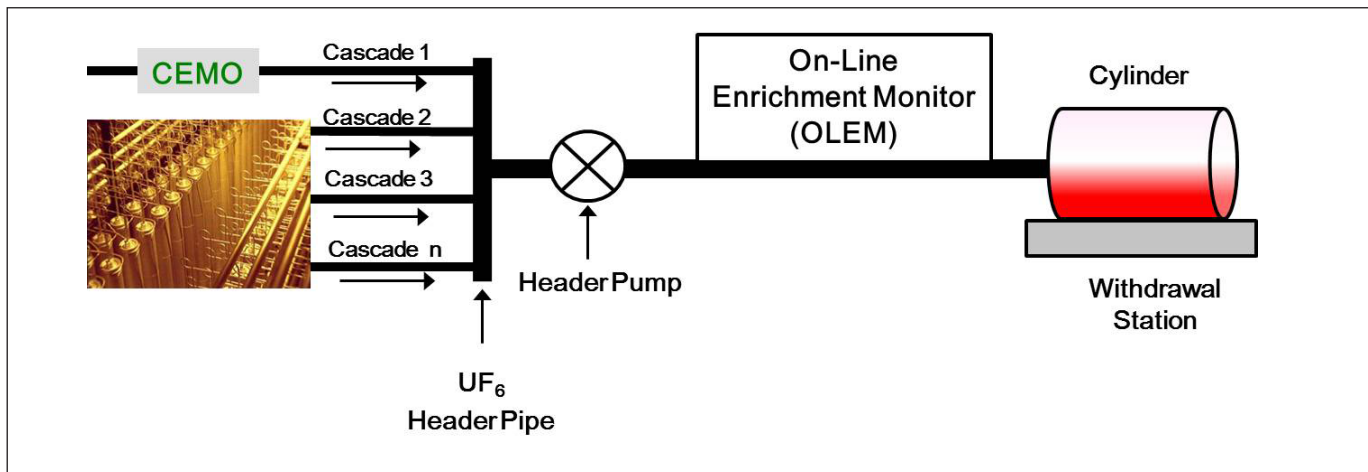
## Introduction

As global uranium enrichment capacity under international safeguards expands, the International Atomic Energy Agency (IAEA) is challenged to develop next-generation safeguards approaches at gaseous centrifuge enrichment plants (GCEPs) while working within budgetary constraints. The IAEA's safeguards approach for GCEPs is intended to provide timely detection of a) diversion, b) excess production beyond declared amounts, and c) the production of enrichment levels higher than declared.<sup>1</sup> The IAEA continues to pursue innovative techniques and an integrated suite of safeguards measures to address the verification challenges posed by advanced centrifuge technologies and the growth in separative work unit capacity at modern centrifuge enrichment plants.<sup>1-3</sup> The ability to continuously and independently monitor not only the uranium mass balance but also the  $^{235}\text{U}$  mass balance in the facility would support all three verification objectives described above. Continuous, unattended monitoring of enrichment levels of in-process  $\text{UF}_6$  gas would be a key enabler for monitoring the  $^{235}\text{U}$  mass balance.

On-line enrichment monitors are not a new concept in the safeguards community; the IAEA can draw on experience gained with a device called a Continuous Enrichment Monitor Online (CEMO).<sup>4-7</sup> CEMO had a relatively limited objective: provide indication of whether the enrichment of the gas flowing in the pipe was greater than 20 percent  $^{235}\text{U}$ . This earlier instrument was located on the output of each cascade where gas pressure is low but relatively stable. The device required a radioactive source for determination of gas density (using transmission measurements); source replacement presented maintenance challenges.



**Figure 1.** Example OLEM deployment scenario in which the device assays the output flow (product or tail material) from the multiple cascades comprising an enrichment unit, and at a location on the high-pressure side of the unit header pump. Also shown are the locations where the IAEA's previous generation of online monitors (i.e., CEMO) were deployed (on each cascade pipe).



For the IAEA's next generation of online enrichment monitor, considerably more is being asked. The IAEA sees two primary measurement objectives for the On-Line Enrichment Monitor (OLEM): 1) continuous monitoring of all declared gas flow to detect production of higher-than-declared enrichment, and 2) high-accuracy quantification of gas enrichment as a function of time,  $E(t)$ , to support verification of the cylinder's average enrichment, and in conjunction with data from subsequent cylinder mass measurements,  $^{235}\text{U}$  mass.<sup>3</sup>

The OLEM device was designed to be compatible with large modern centrifuge enrichment plants with a capacity of several thousand tons SWU/year. Such a facility might have several units (e.g., 6-10), each consisting of multiple (e.g., 10) cascades. It is impractical to monitor the outputs of each cascade, as was done with CEMO, due to the large number of locations. Further, the CEMO location is unattractive for high-accuracy, quantitative gas monitoring because of the low gas pressure at those locations. The unit header pipes are advantageous locations for OLEM (Figure 1) because there the gas flow from multiple cascades is combined and in most modern plants, a unit header pump increases the gas pressure to a few tens of Torr on product and tails header pipes, thereby producing a relatively strong gas signal compared to the background presented by, for example, wall deposits or nearby cylinders. In addition, this location affords the opportunity for the IAEA to directly monitor the gas pressure, since there are generally fewer proprietary concerns from operators, compared to the low-pressure portions of the plant. Other challenges arise at this location, however, including gas-pressure transients during

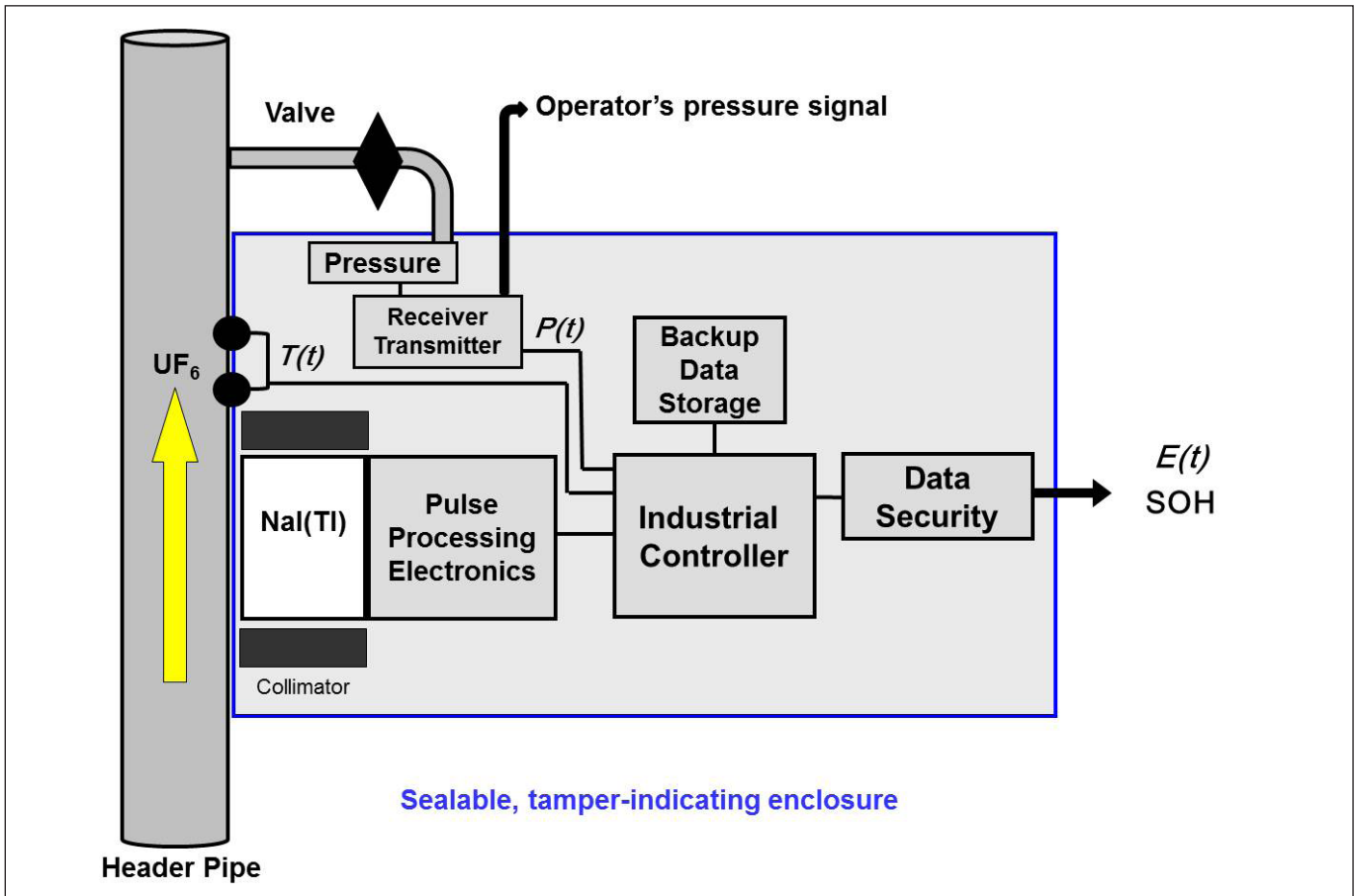
cylinder filling and evacuation processes. The OLEM Collection Nodes are to be mounted externally on a unit header pipe, making it possible to use the OLEM at both new and existing enrichment plants.

The IAEA, under the auspices of the United States' Support Program to the IAEA, began the development of OLEM prototypes in 2011. A nominal OLEM Collection Node design is shown in Figure 2 and uses NaI(Tl) gamma-ray spectrometers to collect the net signal specific to  $^{235}\text{U}$  (e.g., the emission at 186 keV) in the uranium hexafluoride ( $\text{UF}_6$ ) gas flowing past the device. Options for measuring the  $\text{UF}_6$  gas pressure,  $P(t)$  include a signal-sharing device installed on one of the operator's pressure gauges (as in Figure 2), or a dedicated IAEA pressure sensor. Temperature of the  $\text{UF}_6$  gas inside the pipe,  $T(t)$ , is inferred using temperature sensors (i.e. resistance temperature detectors) attached to the outside of the header pipe. The OLEM Collection Node is housed in a tamper indicating enclosure that can be attached to unit header pipes of various diameters. The OLEM design utilizes modular, commercial components with plug-and-play extensibility in mind and is intended to meet the IAEA's guidelines and requirements for unattended and remotely monitored safeguards systems. The OLEM can be deployed incrementally to support phased deployment and plant expansion, and is intended to meet the IAEA's guidelines and requirements for unattended and remotely monitored safeguards systems.

Based on IAEA modeling<sup>10</sup> and proof-of-principle field measurements by Los Alamos National Laboratory at a commercial enrichment plant,<sup>11</sup> IAEA provided OLEM performance targets specified in terms of total (statistical and systematic) relative



**Figure 2.** Schematic of an OLEM Collection Node that combines gamma-ray spectrometry using a NaI(Tl) detector with gas pressure and temperature data to calculate the relative enrichment of the gas as a function of time,  $E(t)$ . Data security methods support off-node transmission of  $E(t)$  and state of health (SOH) data.



uncertainties for  $E(t)$ :  $\sigma_p = 1$  percent,  $\sigma_F = 2$  percent and  $\sigma_T = 3$  percent for product, feed and tails gas streams, respectively. Oak Ridge National Laboratory (ORNL) is the lead developer in the OLEM project.<sup>9</sup> The IAEA has recently completed a field trial of OLEM instruments in an operational enrichment plant.<sup>22</sup>

As a part of the OLEM development project, a Virtual OLEM (VOLEM) has been developed. The VOLEM is intended to emulate, to a high degree of fidelity, how OLEM Collection Nodes will function in the IAEA safeguards verification scenarios at enrichment facilities. VOLEM complements the prototype development activities and allows the study of OLEM for scenarios that will be difficult or impossible to evaluate empirically. Uses of VOLEM include: uncertainty budget analysis and performance prediction for typical and atypical operational scenarios; inter-comparison of candidate gamma-ray spectral analysis and enrichment estimation algorithms; and testing of the OLEM analysis and reporting software.

In this paper, an overview of the OLEM measurement scenario is provided with focus on the pressure transients that can occur on the high-pressure side of the header pump, and how those transients might be used to meet a key challenge in online enrichment monitoring: the quasi-continuous calibration of the static background, which is typically dominated by wall deposits in the pipe. The methods for producing synthetic gamma-ray spectra, pressure and temperature data are described. Data analysis methods, including uncertainty budget analysis and candidate gamma-ray spectral analysis methods are then discussed. Results of performance prediction studies based on the statistical contributions to total uncertainty, under steady-state operational conditions, are presented. Case studies for atypical scenarios, including transient plant conditions, indicate where systematic uncertainties in reported enrichment values might arise.



## OLEM Measurement Scenario

For the calculation of the relative enrichment of the  $UF_6$  gas flowing through the OLEM's field of view (see Figure 2),  $S$  is defined as the total signal associated with  $^{235}U$ , summed over a measurement interval of live time  $t$ .  $S$  is composed of counts from  $^{235}U$  in the gas and from "background"  $^{235}U$ . This background,  $W$ , is typically dominated by solid uranium compounds that have deposited on the walls of the piping (see next section for more discussion). Also included in  $W$  could be  $^{235}U$  in adjacent piping or nearby cylinders within the collimator's field of view. In this paper, the wall deposits and ambient background are presumed to be static. Note that  $S$  and  $W$  correspond to a given spectral region of interest and spectral analysis algorithm, and are assumed to have a Poisson distribution.

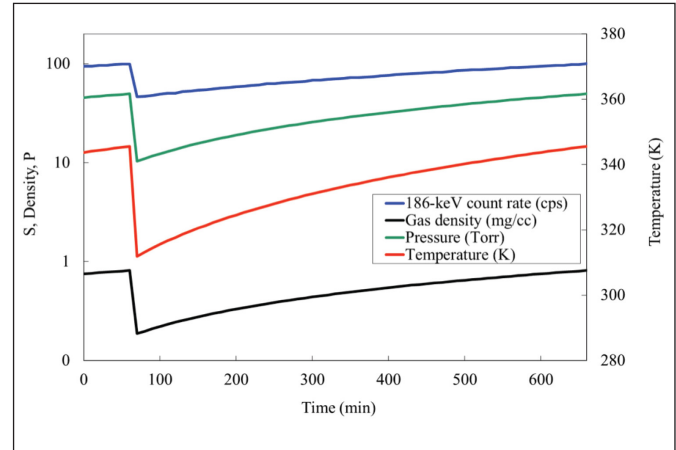
The  $UF_6$  density  $\rho_{gas} = \rho_{gas}(P, T)$  may be estimated from measurements of pressure  $P$  (Torr) and temperature  $T$  (Kelvin). Under these assumptions, the signal over time  $t$  from gas at relative enrichment  $E$  (weight percent  $^{235}U$ ) is proportional to  $E\rho_{gas}t$ . Therefore, given an estimate of  $W$  and measurements of  $S$  and  $\rho_{gas}$ , the relative enrichment of the  $UF_6$  gas passing in front of the OLEM sensor during time  $t$  can be estimated by

$$E = K_G \rho_{gas}^{-1} (S - W) / t, \quad (1)$$

where  $K_G$  ( $mg^{235}UF_6 / cm^3 \cdot cps$ ) is a calibration constant relating the 186-keV count rate collected from the gas to the density of  $^{235}U$  hexafluoride in the OLEM's field of view. This calibration constant can be determined from Monte Carlo radiation transport simulations or from well-calibrated laboratory or field measurements.

Equation 1 is relatively straightforward to use for the deployment scenario where gas pressure and temperature, as well as ambient background, are constant. This is not the case, however, for the unit header pipe locations envisioned for OLEM. In many modern gaseous centrifuge enrichment plants, transients are created by the connection of a cold, empty cylinder at the withdrawal stations, in the header pipe of facilities with withdrawal stations utilizing direct desublimation. Typically, the transient consists of a sharp drop in gas pressure and temperature followed by a gradual increase in pressure and temperature as the cylinder is filled. Figure 3 provides a quantitative example in which synthetic pressure and temperature transients have been defined for approximately ten hours after the connection of an empty, cold cylinder. Gas enrichment is assumed constant during this time period. The behavior of  $S$ ,

**Figure 3.** Example behavior of gas pressure, temperature and density, and the total  $^{235}U$  signal as a function of time before and after the attachment of a cold, empty cylinder to a product withdrawal station



$P$ ,  $T$ , and gas density (here according to the Weinstock equation of state<sup>12</sup>) are shown. The pressure, in this synthetic scenario, climbs from 10 to 50 Torr, and the gas temperature increases as well. The magnitude of that temperature changes will depend on several factors, including the location of the OLEM relative to the header pump and cylinders. In this study, a temperature increase of approximately 30 degrees Kelvin. Note that the absolute values of pressure and temperature during the transient were chosen to be representative of enrichment plant operations, not actual conditions at a specific facility.

In the nominal OLEM measurement scenario used in this paper, each gamma-ray spectrum is acquired over a user-defined time interval  $t_{gamma}$  (ten minutes in this paper). The pressure and temperature vectors are collected at user-defined time intervals  $t_{press}$  and  $t_{temp}$  (both one minute in this paper). In the analysis algorithms used in this paper, multiple gamma-ray spectra are summed over a reporting time interval  $t_{report}$ , nominally two hours in this work, but ultimately to be negotiated with facility operators.

## Virtual OLEM

The VOLEM software package is capable of producing synthetic data streams over a wide range of enrichment plant operating conditions that include: the enrichment, pressure, and temperature of the gas; the shape and magnitude of the pressure transients that can occur in unit header pipes during cylinder product and tail cylinder filling; the enrichment and areal density of the deposits; the spectral shape and amplitude of other ambient background source terms. The VOLEM user

provides these parameters as input to the software, along with variables that define the time-segmentation of the data acquisition, analysis and reporting. The VOLEM then writes the synthetic raw data streams to the standard file formats produced by the actual OLEM Collection Node, and executes the analysis algorithms and reports results using the same software package installed on the microcontroller of the OLEM Collection Node.

## Monte Carlo Modeling and Validation

The radiation transport simulations performed in support of VOLEM were performed using Monte Carlo N-Particle (MCNP) version 5.<sup>13</sup> The model uses a 100-cm length of 10.23-cm (inner diameter) Schedule 40 aluminum pipe typical of modern enrichment plants. The UF<sub>6</sub> gas in the pipe is modeled as pure UF<sub>6</sub> at 25 Torr and 293 K ( $4.82 \times 10^{-4}$  g/cm<sup>3</sup> under ideal-gas assumptions). The uranium isotopes in the gas, only <sup>235</sup>U and <sup>238</sup>U are modeled here, are considered to be freshly separated (“young”) with negligible daughter grow-in, based on two assumptions: 1) the withdrawal process from the feed cylinders removes any contaminant fluoride compounds involving uranium daughters, and 2) the dwell time for UF<sub>6</sub> in a modern GCEP cascade is typically less than a few hours.<sup>14</sup>

The wall deposit is modeled as a uniform layer of UO<sub>2</sub>F<sub>2</sub> with an areal density of 900 μg/cm<sup>2</sup> (see next section for more discussion of wall deposits). The uranium isotopes in the deposit are assumed to be at least ninety days old so that the daughters important to gamma-ray spectroscopy are in equilibrium: <sup>231</sup>Th (half-life of 1.1 days) with <sup>235</sup>U, <sup>234</sup>Th (half-life of 24.1 days) with <sup>238</sup>U, and <sup>234m</sup>Pa (half-life of 1.2 days) with <sup>234</sup>Th. Emission energies and intensities for all gas and deposit source terms were based on data from Reference 15.

To allow flexibility in modeling a range of plant operating conditions (e.g., pressure, enrichment, and wall-deposit thickness), some simplifying assumptions were adopted. First, attenuation in the deposit, both of the deposit emissions and the gas emissions, is assumed negligible. Second, self-attenuation in the gas is taken to be negligible. These effects can be reasonably ignored in this analysis, since the initial focus is quantifying statistical, not systematic, uncertainties. For example, even a relatively heavy deposit of 1000 μg/cm<sup>2</sup> attenuates the 186-keV signature by less than 0.2 percent. Similarly, even for the portion of the 186-keV gamma emissions coming from the far side of a pipe (i.e., 10 cm from the detector) filled with gas at a high pressure of 50 Torr, self-attenuation would be less

than 2 percent. Note that these attenuation factors must be addressed in field implementation, as they represent potential sources of systematic bias.

Under these assumptions, a “basis spectra” approach was developed in which the significant gamma-ray source terms were modeled separately: a) young <sup>235</sup>U in gas, b) old <sup>235</sup>U in deposit, and c) old <sup>238</sup>U in deposit. Each basis spectrum is linearly scaled according to the corresponding operating conditions, for example gas density or deposit thickness. The individual basis spectra are then summed to create the simulated OLEM spectrometer response for those specific plant conditions.

The NaI(Tl) gamma-ray spectrometer was modeled as a 7.62-cm diameter by 1.27-cm thick crystal surrounded by a 0.5-mm aluminum can, with a low-density (1.0 g/cm<sup>3</sup>) aluminum volume behind the crystal to approximate the photomultiplier and tube base. Energy resolution, in relative full-width-half-maximum, was defined to be 7.0 percent at 662 keV with an energy dependence typical of NaI(Tl).

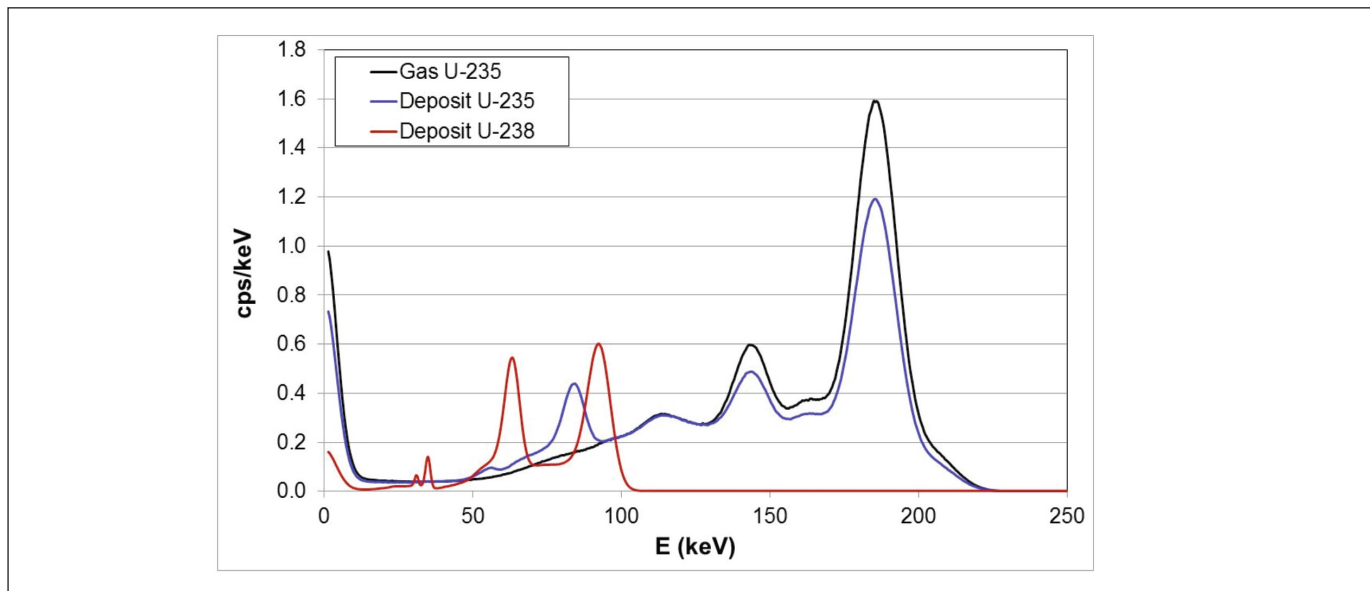
A cylindrical collimator is 1.0-cm thick tungsten lined with 0.5 cm of iron. The purpose of the iron layer is to attenuate tungsten X-rays and thereby allow the measurement of lower-energy emissions from uranium and its daughters, particularly the 63.3-keV emission from <sup>234</sup>Th. Note that in actual OLEM instruments, alternative X-ray attenuation layers (e.g., copper and tin) may be used. Also, additional collimation and shielding may be necessary to reduce the effect of ambient background in field deployments. For example, gas and deposits in nearby pipes could produce direct and scattered gamma rays at the detector, and nearby cylinders will increase the gamma-ray and neutron background.

The primary effect of the ambient background in the spectra recorded by OLEM will be an increase in the continuum underlying the peak regions of interest (e.g., 186 keV). One of the basis-spectra source terms is intended to approximate these continuum effects from scatter created by far-field sources, but no comprehensive analysis of ambient background effects was performed in this study. Characterizing the effects of ambient background under real plant conditions is best performed in field testing at an operating facility; the OLEM deployment locations will be chosen with consideration toward minimizing the background intensity and variability.

Examples of basis-spectra for the collimated NaI(Tl) spectrometer are shown in Figure 4 (excluding the ambient background source term described above). Examples of VOLEM



**Figure 4.** Examples of “basis spectra” corresponding to each of the major online-monitoring source terms as recorded in a nominal instrument design, assuming the following plant conditions: gas pressure of 25 Torr, gas and deposit at 5.0 percent  $^{235}\text{U}$ , and wall deposit of  $900\text{ mg/cm}^2$ . The deposit source terms assume that daughters are in equilibrium.



spectra for various plant conditions ranging from high-pressure, high-enrichment product to low-pressure tails streams are shown in Figure 5.

Empirical data collected with a prototype OLEM device on a  $\text{UF}_6$  flowing test loop at ORNL was used for validation of VOLEM-simulated gamma-ray spectra.<sup>25</sup> The NaI(Tl) spectrometer measured  $7.54 \times 1.27\text{ cm}$  and had a collimated field of view consistent with that described previously for the MCNP-based synthetic spectra. As in the MCNP simulations, the OLEM instrumentation was mounted on Schedule 40 aluminum pipe with an inner diameter of  $10.23\text{ cm}$ . The pipe length in the flowing test loop was  $50\text{ cm}$ , as compared to  $100\text{ cm}$  in the simulations.

For these experiments, the pressure, temperatures, and enrichment of the gas were measured precisely and there were no appreciable wall deposits. Data were collected at three gas enrichment levels (0.2 percent, 0.71 percent, and 6.0 percent) and the pressure was varied stepwise over a range that is representative of the high-pressure side of header pumps. At each pressure value, steady-state spectral data was collected for at least two hours so that statistical uncertainties in the recorded spectra were negligible.<sup>25</sup>

Figure 6 shows a comparison of the measured and simulated responses at a gas enrichment of 6.0 percent and pressure of 41 Torr, with negligible wall deposits. The spectral

shapes compare favorably with the exception of the uranium X-ray region. The departures here are likely caused by the lack of beta-induced photon production in the MCNP modeling (a significant source of X-rays in this type of geometry) and very different surroundings in the simulation and measurement (test loop inside a fume hood). There is good agreement in the 186-keV energy region—the region of most interest for online enrichment monitoring. For an energy window spanning 140 to 220 keV, the simulated count rate is 89.2 cps and the measured rate is 94.1 cps, a relative difference of approximately 5 percent.

A comparison of simulated and measured count rates in the 140-220 keV region, for low and high gas pressures at three different enrichment levels, is provided in Table 1. The relative difference in count rates for the 0.71 percent and 6.0 percent gas enrichments are less than 7 percent, with the simulated values being consistently low. The negative bias for the simulated OLEM response is approximately 30 percent for the 0.2 percent enrichment. The relatively limited information available from the flow-loop tests precluded resolution of the discrepancy, but the authors believe that imperfect background correction in the measured data, and small differences between the simulation and measurement configurations, are likely explanations. These effects are not significant at higher gas enrichments, but for the very weak gas signal at 0.2 percent



**Figure 5.** Example VOLEM pulse-height spectra for three different combinations of plant operating parameters: gas and deposit enrichment, gas pressure, and deposit thickness. These example spectra assume very long acquisition times in order to clearly illustrate low-intensity features.

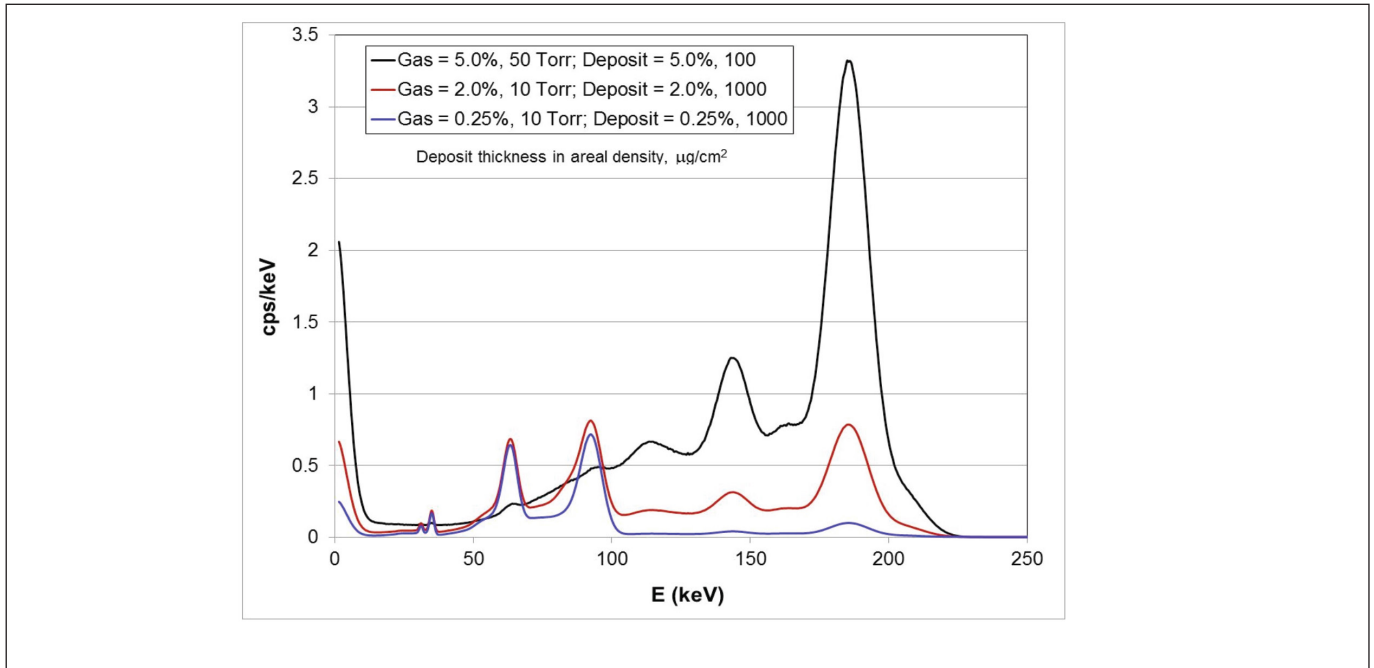
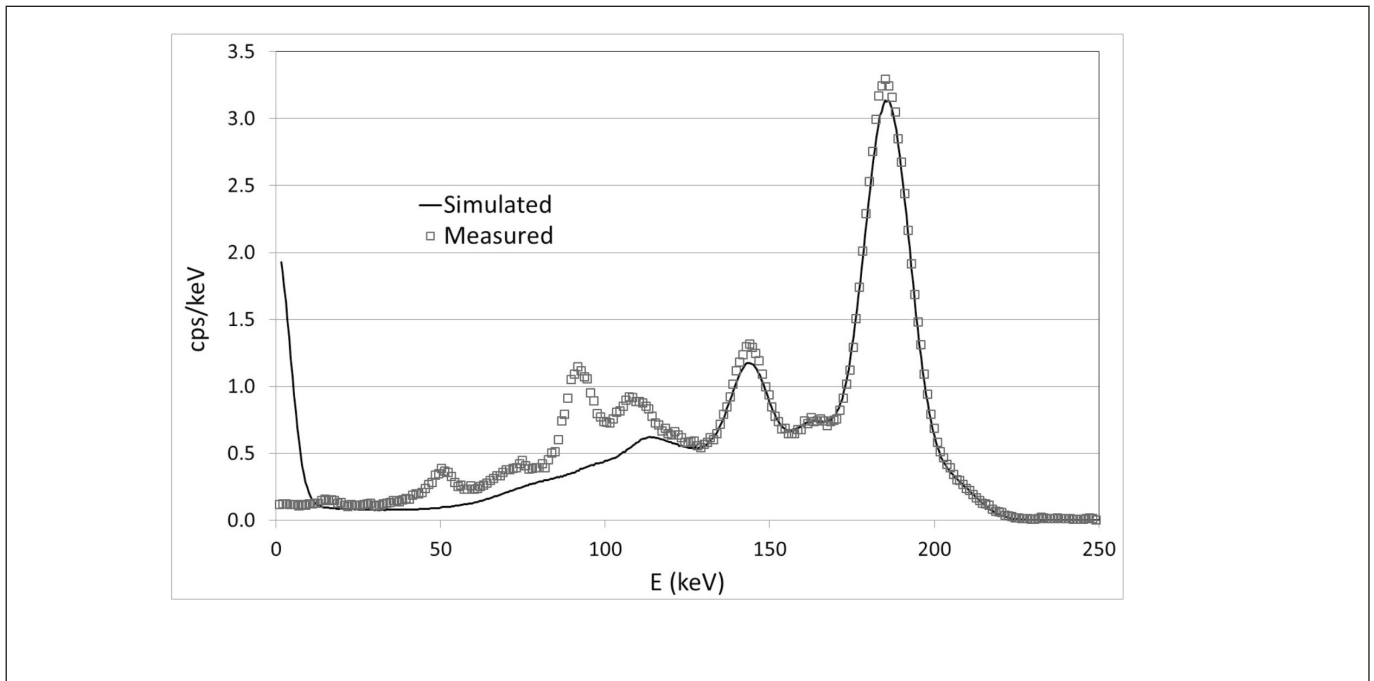


**Figure 6.** Comparison of measured (test loop) and simulated (VOLEM) gas signal for enrichment of 6.0 percent and pressure of 41 Torr.



enrichment, become appreciable. The general conclusion from the benchmarking results presented here is that VOLEM's basis-vector modeling approach is sufficiently accurate to support

the kind of OLEM performance estimation studies presented in this paper.



**Table 1.** Comparison of measured (test loop) and simulated (VOLEM) count rates in an energy window spanning 140-220 keV, for three gas enrichments at low and high gas pressures.

| Enrichment (wt percent) | Pressure (Torr) | Measured (cps) | Simulated (cps) | Relative difference (percent) |
|-------------------------|-----------------|----------------|-----------------|-------------------------------|
| 0.20                    | 14.4            | 1.5            | 1.0             | -32                           |
| 0.20                    | 35.7            | 3.6            | 2.6             | -28                           |
| 0.71                    | 10.6            | 2.9            | 2.7             | -6.9                          |
| 0.71                    | 42.2            | 11.5           | 10.9            | -5.2                          |
| 6.0                     | 12.5            | 28.9           | 27.1            | -6.2                          |
| 6.0                     | 41.0            | 94.1           | 89.2            | -5.2                          |

## Analysis Methods

### Background Determination

The key challenge in the practical implementation of online enrichment monitoring is the development of a self-contained, quasi-continuous method for determining the  $^{235}\text{U}$  background,  $W$ , which is typically dominated by uranium deposits on the piping wall. Previous studies provide helpful descriptions of the mechanisms of uranium deposition on uranium pipes in enrichment plant conditions.<sup>16-20</sup> These studies indicate that there are two main sources of wall deposits, with the dominant mechanism being reactions that involve the oxides and hydroxides of aluminum (from the pipe), adsorbed water molecules (from air in-leakage) and perhaps elemental impurities in the aluminum. The solid products that remain on the wall are typically  $\text{UO}_2\text{F}_2$  and  $\text{AlF}_3$ , but light gases such as HF are also produced.<sup>18</sup> This sort of deposit formation is expected to occur most prominently near valves, collars, and bends where air penetration into the piping is more likely. The second source of wall-deposit material is the direct deposition of thorium due to the alpha decay of uranium nuclei as the  $\text{UF}_6$  gas passes through the plant.<sup>18</sup> This effect is ignored in this study for two reasons. First, prior work has indicated that the role of direct-thorium deposition is a relatively small contributor to the total wall-deposit mass. Second, though the directly deposited thorium emits gamma rays and X-rays, it is not expected to significantly contribute to the 186-keV region emphasized in this study.

The uranium deposition rate on the pipe walls depends on plant design, cleanliness and operating conditions. Packer et al. performed a study of the deposits in the header pipes of an operational centrifuge enrichment plant.<sup>18</sup> These header pipes had been in operation for periods up to approximately seven years. Deposition rates were found to vary by a factor of two

or more in different header pipes; the average growth rate was somewhat higher in the first months of operation ( $\sim 90 \mu\text{g}/\text{cm}^2/\text{year}$ ) than during later time periods ( $\sim 50 \mu\text{g}/\text{cm}^2/\text{year}$ ). The maximum deposits were measured to be approximately  $650 \mu\text{g}/\text{cm}^2$ . Based on this prior work, this study defines the "typical" range of wall-deposit thicknesses to be  $100 \mu\text{g}/\text{cm}^2$  to  $1000 \mu\text{g}/\text{cm}^2$ . The lower values are intended to represent header pipes that have been in operation less than a year or two, while the top of the range represents relatively long periods of operation, perhaps fifteen years or more. Wall deposits significantly higher (or lower) than this range are considered "atypical" in this study.

To set the scale of how important the wall-deposit effect can be, consider the following scenario: gas at 3.0 percent  $^{235}\text{U}$  and pressure of 40 Torr; deposit at 3.0 percent  $^{235}\text{U}$  and areal density of  $1000 \mu\text{g}/\text{cm}^2$ . In this case, the total simulated count rate in the 186-keV peak is approximately 35 cps, with approximately 10 cps ( $\sim 30$  percent) coming from the wall deposit. Further, the sometimes-sporadic nature of deposit growth (e.g., due to air in-leakage during maintenance activities) makes it desirable to monitor the deposit contribution at least frequently, if not continuously.

Based on previous studies by others and ongoing analysis by the authors, there are several candidate methods for determining the contributions from the wall deposit to the  $^{235}\text{U}$  signal. The process for identifying promising methods for the online monitoring scenario considered several criteria: degree of independence (i.e., minimizing the need for operator-declared information), ability to provide quasi-continuous recalibration to minimize systematic uncertainties, simplicity and robustness, applicability for various plant designs (e.g., different takeoff station designs), and the uncertainty contribution to the calculation of gas enrichment. In the context of these criteria, each of the candidate methods is described briefly here.

Perhaps the most straightforward correction method is the use of operator declarations of enrichment based on mass spectrometer analysis of gas samples. These samples, typically taken by the operator for process control, could also be used to recalibrate deposit corrections. Such an approach is not ideal for routine wall-deposit calibration because it depends heavily on operator-declared information, would require frequent analysis effort from the IAEA for the modification of the calibration parameters, and would be difficult to implement in a quasi-continuous fashion. However, the infrequent use of operator mass spectrometer data could prove useful for periodic (e.g.,



once per year) absolute calibration checks on more continuous methods, or in the case where other methods are not viable (e.g., no pressure transients).

Contrast in geometric field of view for specific collimator designs can also be used to determine wall-deposit contributions, as with the portable CHEM instrument.<sup>16,21</sup> A slit collimator that provides significantly different collection efficiencies for the gas and deposit via 90 degrees of rotation, can be used to calculate the relative contributions of gas and deposit. This collimator configuration, however, would add significant weight and complexity to the OLEM, would reduce the collection efficiency for the gas signal, would require manual intervention by IAEA staff, and would not support near-continuous recalibration of the wall-deposit correction.

Another possible wall-deposit correction is the use of the 63.3-keV gamma-ray from <sup>234</sup>Th to monitor the evolution of the deposit. This method would directly monitor the growth of the <sup>238</sup>U daughter in the OLEM field of view, but would require inferring the concentration of <sup>235</sup>U in the deposit. Such an approach would require an initial calibration of the <sup>235</sup>U in the wall deposit using another method (e.g., operator mass spectrometry on the gas). Subsequently, relative increases in <sup>235</sup>U concentration could be inferred by time-correlating <sup>234</sup>Th signal increases to gas enrichment results. Careful collimator design is necessary to ensure that tungsten X-rays do not obscure the 63.3-keV signature in a NaI(Tl) spectrum. The indirect nature of this wall-deposit correction approach makes it less attractive, but it could prove a useful complement to other correction methods.

Prominent among the candidate wall-deposit correction methods for the online monitoring is the pressure-transient approach that was initially explored through IAEA modeling<sup>10</sup> and proof-of-principle field measurements by Los Alamos National Laboratory,<sup>11</sup> and more recently in field trials of OLEM prototypes by the IAEA and ORNL.<sup>22</sup> The enabling principle of this deposit calibration method is that the pressure transients induce changes in the gas signal, but the wall-deposit signal stays constant, allowing the isolation of the <sup>235</sup>U source term coming from the deposit. This approach is most straightforward if the gas enrichment remains constant during the calibration period, a condition which is assumed in the analysis presented in this paper.

The pressure-transient method appears particularly promising for OLEM for several reasons. First, it is compatible with plants that utilize header withdrawal stations based on direct

desublimation of the gas into a chilled cylinder—the type of withdrawal station common to modern plants. In addition, the pressure-transient method requires no additional data or hardware beyond that already envisaged for OLEM. Finally, it would support quasi-continuous re-calibration (every few days at a minimum) of the wall-deposit correction.

An example estimation of  $W$  based on the pressure-transient behavior is illustrated in Figure 7. Time-segmented gamma-ray spectra during the gradual climb in pressure and concurrent increase in gas density (assuming constant  $E$  during that time period) can be used to empirically determine a relationship for  $S(\rho_{gas})$ . In this example, the gas and deposit enrichment are both assumed to be 0.2 percent, the wall deposit is 1000  $\mu\text{g}/\text{cm}^2$ , and the pressure and temperature transients are taken from a portion of the curves in Figure 3. Ten-minute ( $t_{gamma}$ ) spectra integration intervals and one-minute pressure and temperature collection intervals ( $t_{press}$  and  $t_{temp}$ ) are assumed. It is assumed that pressure and temperature are then averaged over the ten-minute spectral measurement period. The gas density in VOLEM is estimated using the Weinstock equation of state:

$$\rho_{gas} = \frac{K_{PT} P}{1 - B_W P/T^3 T}, \quad (2)$$

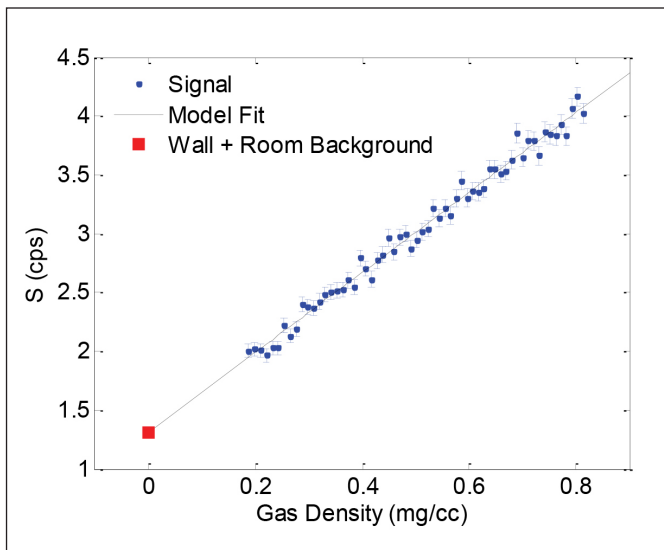
where  $K_{PT}$  is a calibration constant ( $\text{mg UF}_6 \cdot \text{K} / \text{cm}^3 \cdot \text{Torr}$ ) equal to the molar mass of the  $\text{UF}_6$  gas divided by the ideal gas constant and  $B_W$  ( $\text{K}^3/\text{Torr}$ ) is an additional calibration constant for the Weinstock equation. Note that the ideal gas law, used in the estimate of enrichment error, is an excellent approximation to Equation 2 in realistic OLEM applications for the temperatures and pressures considered here. A linear least-squares fit to the  $S(\rho_{gas})$  data provides an empirical estimate of  $W$ . Specifically, the ordinary least-squares estimate is given by:

$$\hat{W} = \frac{\overline{\rho^2 S} - \overline{\rho S} \overline{\rho}}{\overline{\rho^2} - \overline{\rho}^2}, \quad (3)$$

where the overbar represents an average over the measurements used in the estimate, here a total of  $N = 60$  values (10 hours) of density and total 186-keV counts.<sup>23</sup> The estimate of  $W$  in the example is a constant 1.31 cps. Note that the slope of the least-squares fit to  $S(\rho_{gas})$  can be used for empirical determination, and periodic confirmation, of the calibration constant  $K_G$  in Equation 1. In Figure 7, the gas accounts for approximately 3.40 cps/(mg/cc).



**Figure 7.** Example how a series of total  $^{235}\text{U}$  signal data points,  $S$  (cps), collected during a pressure transient can be used to estimate the static background,  $W$  (wall deposit plus ambient room background). The VOLEM-generated data assumed a ten-minute spectrum integration interval, gas and deposit enrichment of 0.2 percent  $^{235}\text{U}$ , and deposit of  $1000 \mu\text{g}/\text{cm}^2$ .



The fitting process described above for the 186-keV ROI can also be applied on a bin-wise basis to the full-range energy spectra collected by the OLEM. That bin-wise static background spectrum can then be utilized in various ways. For example, spectral analysis algorithms based on specific energy windows can sum the background spectrum over that energy window to produce a single scalar value for the background in that energy window, during a specific measurement time interval. This process is described in the next section for two example spectral analysis algorithms. The bin-wise background, however, could also be utilized for other purposes that include the monitoring of the wall-deposit characteristics and to detect potential spoofing scenarios. In the former, the 63.3-keV emission from  $^{234}\text{Th}$  could be monitored to ensure that if it is changing, that it is changing slowly and in a predictable fashion. In the case of the latter, sources placed near an OLEM to blind or perturb the instrument in some way, could be quickly detected based on elevated total background levels, or the appearance of specific peaks (e.g., 662 keV from  $^{137}\text{Cs}$ ).

### Spectral Analysis for Net Gas Signal

Once a background-subtracted gamma-ray spectrum is generated for a given measurement interval, there are a number of different spectral analysis methods that could be employed to extract the net gas signal (i.e.,  $S - W$ ) data needed for enrich-

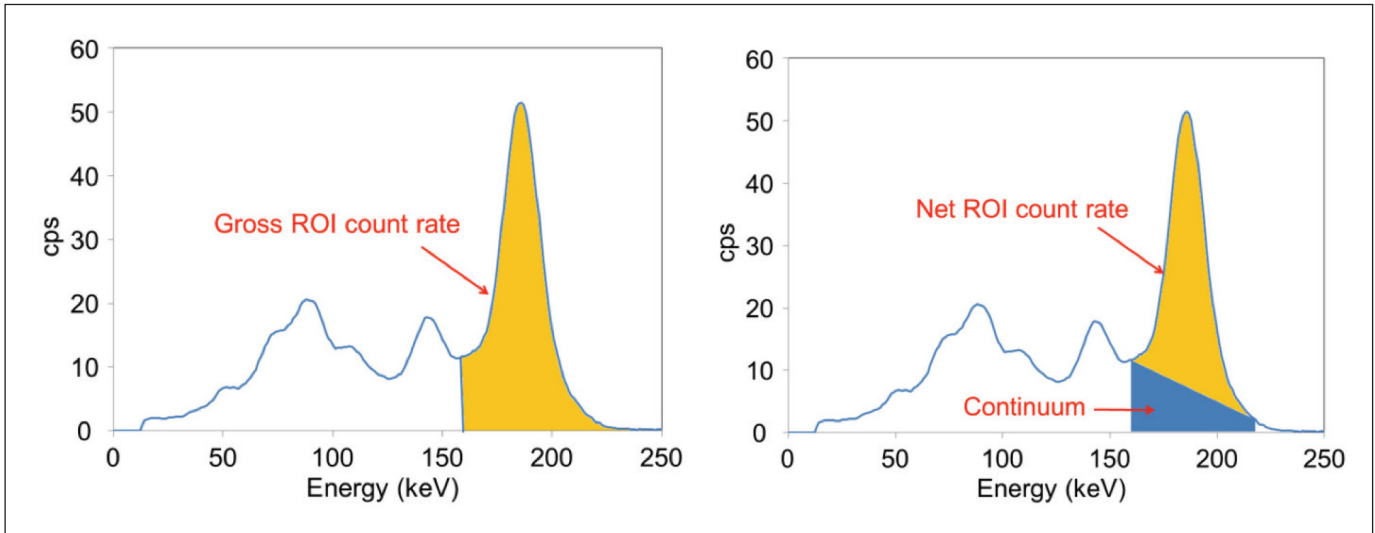
ment calculations. Two candidate methods are described and tested in this paper, and depicted in Figure 8.

The “ROI summation” method leverages the fact that in principle, the pressure-transient background calculation method described above will remove all source terms uncorrelated to the gas  $^{235}\text{U}$  signal. This means that the background-subtracted spectrum should have little or no contribution from higher-energy source terms that create the continuum underneath the peak. Therefore, it should be unnecessary to remove the continuum counts under the  $^{235}\text{U}$  peaks since those counts also derive from the gas itself. The net  $^{235}\text{U}$  gas signal can be defined as a simple summation of all counts in an ROI specific to  $^{235}\text{U}$ . Such an ROI can be defined to be quite narrow so that it encompasses only the 186-keV peak or more broadly (e.g., from 140 to 220 keV) to include more of the  $^{235}\text{U}$  gamma-ray emissions (see left pane of Figure 8). It is expected that the X-ray region ( $\sim 70$  to 120 keV) should be avoided since the intensity of this region is likely not linearly proportional to  $^{235}\text{U}$  concentration in the gas, due to the nature of X-ray production in the OLEM scenario. It is expected that field experience will help to further inform ROI boundaries that minimize overall enrichment uncertainty.

The traditional “trapezoidal” peak analysis method (right pane of Figure 8) can also be used to analyze online enrichment monitor data. This method is expected to be most useful when the separation of non-gas contributions using the ROI summation method described above is difficult or not viable at all. This could be the case, for example, when there are no pressure transients on which to base a static-background calculation, or the transients are too weak to do so accurately. Also, a highly variable ambient background, for example the frequent movement of nearby cylinders that could perturb the ambient background and the underlying continuum in a transient way, could preclude the effective use of the ROI summation method. In the trapezoidal method, a peak ROI is defined (e.g.,  $\pm 1.5 \sigma$  about the 186-keV peak centroid), anchor points at those ROI boundaries are determined, and an estimate of the continuum underlying the peak (typically trapezoidal in shape), is calculated and subtracted from the total counts in the ROI region.<sup>24</sup> Because this method subtracts only continuum, accurate removal of the deposit’s contribution to the 186-keV peak count rate is possible only if that deposit contribution can be estimated via other means (e.g., calibration measurements at very low gas pressures).

In theory, the ROI summation method should be superior

**Figure 8.** Illustration of the “ROI summation” (left) and “trapezoidal” (right) spectral analysis methods.



to traditional peak-fitting algorithms in terms of simplicity and total uncertainty since it directly removes the static contributions from the wall deposit, and has the advantage of not adding statistical fluctuations caused by the selection of anchor points for continuum subtraction or fitting of a nominal peak shape (e.g., Gaussian). In the performance prediction and uncertainty budget analysis that follows, the ROI summation method is used.

### Uncertainty Quantification

One of the primary uses of VOLEM is to aid the quantification and understanding of the uncertainty in the OLEM enrichment estimates. Uncertainty quantification is important from several perspectives, including the identification of primary contributing factors (here referred to as an uncertainty budget), prediction of expected total uncertainty under different plant conditions, and provision of confidence bounds associated with individual real-time enrichment estimates. Analytical formulas as well as sample-based or Monte Carlo ensemble statistics may be used for uncertainty quantification, and both are exercised in this paper (for statistical uncertainty analysis only).

In Reference 10, the following propagation-of-error formula was derived from Equation 1 under the ideal gas law  $\rho_{gas} = K_{PT} P/T$ , for point values of  $P$ ,  $T$ ,  $W$ , and  $S$ :

$$\sigma_E^2 \approx \left( \frac{K_G}{t_{gamma} K_{PT}} \right)^2 \left[ \left( \frac{T(S-W)}{P^2} \right)^2 \sigma_P^2 + \left( \frac{S-W}{P} \right)^2 \sigma_T^2 + \left( \frac{T}{P} \right)^2 \sigma_W^2 + \left( \frac{T}{P} \right)^2 \sigma_S^2 \right], \quad (4)$$

where  $K_{PT}$  is a calibration constant ( $\text{mg UF}_6 \cdot \text{K} / \text{cm}^3 \cdot \text{Torr}$ ) equal to the molar mass of the  $\text{UF}_6$  gas divided by the ideal gas constant, and  $\sigma_P$ ,  $\sigma_T$ ,  $\sigma_W$ , and  $\sigma_S$  represent measures of (statistical) uncertainty on the values of  $P$ ,  $T$ ,  $W$ , and  $S$  used in this calculation. Formally, the (true) mean values of  $P$ ,  $T$ ,  $W$ , and  $S$  are to be used in this formula, and approach taken in Reference 10 using simulated data. In this work, a similar procedure was adopted using VOLEM data. Furthermore,  $S$  is assumed to be Poisson so that its variance is given by its mean value. This formula can then be used to quantify the impact of error in each component value used in Equation 1.

In the case studies described in the next section,  $W$  is estimated using simulated or measured  $S$ ,  $P$ , and  $T$  values over multiple previous two-hour reporting periods, and the  $S$ ,  $P$ , and  $T$  values obtained in the current reporting period are used along with the previous estimate of  $W$  to estimate enrichment from Equation 1. For example, the two-hour averages (reporting period) of ten-minute measurements of  $S$ ,  $P$ , and  $T$  may be used in the equation:

$$\hat{E} = K_G (\langle S \rangle - \hat{W}) / (\langle \rho_{gas} \rangle t_{gamma}) \quad (5)$$

where  $\langle S \rangle$  and  $\langle \rho_{gas} \rangle$  are average values in each reporting period,  $n = t_{gamma} / t_{report} = 12$  is the number of measurements during the reporting period, and  $\hat{W}$  is the estimated background. The bracket notation is used here for averaging rather than the overbar as in Equation 3, to distinguish the first as an average over  $n$  “new” measurements and the second



as an average over  $N$  previous measurements. Now extending Equation 4 to account for the statistical uncertainty in the averaged values rather than point values, propagation of error produces the following:

$$\sigma_E^2 \approx \left( \frac{K_G}{f_{\text{gamma}} \langle \rho_{\text{gas}} \rangle} \right)^2 \left[ \left( \frac{\langle (S-\hat{W}) \rangle^2}{\langle \rho_{\text{gas}} \rangle^2} \right) \left( \frac{\langle \rho_{\text{gas}} \rangle}{P^2} \right) \frac{\sigma_P^2}{n} + \left( \frac{\langle \bar{S}-\hat{W} \rangle^2}{\langle \rho_{\text{gas}} \rangle^2} \right) \left( \frac{\langle \rho_{\text{gas}} \rangle}{T^2} \right) \frac{\sigma_T^2}{n} + \hat{\sigma}_W^2 + \frac{\sigma_S^2}{n} \right], \quad (6)$$

where  $\langle P \rangle$  and  $\langle T \rangle$  are average values in each reporting period,  $\hat{\sigma}_W$  is an estimate of standard deviation in  $\hat{W}$ , and  $\hat{\sigma}_W^2$  represents the variance in  $S$ . Again, the formula is strictly valid as a linear approximation when the true mean values of  $S$ ,  $P$ ,  $T$ , and  $W$  are used in the averages. Notice that in this formula for  $\sigma_E^2$ , the individual contributions of statistical uncertainty in each measured or estimated variable can be identified. The estimate of  $\hat{\sigma}_W^2$  used here is based on a similar propagation of error on the ordinary least-squares estimate given in Equation 3:

$$\hat{\sigma}_W^2 \approx \frac{\overline{\rho^2} \bar{S} - 2\overline{\rho^2} \bar{\rho} \bar{S} + \overline{\rho^2} \bar{\rho}^2 \bar{S}}{N(\overline{\rho^2} - \bar{\rho}^2)} + \sum_{j=1}^N \left( \frac{\partial \hat{W}}{\partial \rho_j} \right)^2 \left[ \left( \frac{\rho_j}{T_j} \right)^2 \sigma_T^2 + \left( \frac{\rho_j}{P_j} \right)^2 \sigma_P^2 \right] \quad (7)$$

where

$$\frac{\partial \hat{W}}{\partial \rho_j} = \frac{2(\bar{S} - \hat{W}) \rho_j + 2\hat{W} \bar{\rho} - \bar{\rho} S_j - \bar{\rho} \bar{S}}{N(\overline{\rho^2} - \bar{\rho}^2)} \quad (8)$$

and  $j$  indexes the measurement number  $1, 2, \dots, N$  and here again,  $N = 60$ . (Note that in Reference 10, a different estimator was used for  $\hat{\sigma}_W^2$ , based on weighted, rather than ordinary, least squares.) A benefit of the analytical calculation presented here is that it can be obtained without developing full simulation and/or analysis capability for OLEM, and it relies on simple model calculations, thereby serving as a rough viability analysis prior to further investment (cf. Reference 10).

As a complement to analytical methods, ensemble (Monte Carlo or sample) statistics can be used to estimate uncertainty. Simulation or measurement over multiple experiments (e.g., time periods spanning the filling of multiple product cylinders) under identical conditions enables straightforward averaging, thereby providing overall OLEM statistical uncertainty estimates from sample standard deviation of enrichment estimates calculated from Equation 5.

The two uncertainty-budget analysis methods have been exercised and compared in this study. For the Monte Carlo results, multiple simulations of the same cylinder fill were

generated for each case study and the standard deviation of enrichment estimates were computed to estimate statistical uncertainty in enrichment,  $\sigma_E$ . For a given case study representing a choice of true enrichment and wall-deposit level, 3,000 replicate cylinders under the same measurement conditions were simulated, and the ROI summation method described above was used to estimate enrichment at each two-hour reporting period for each cylinder. This produced 3,000 replicate estimates of enrichment at five reporting periods each. Ensemble statistical uncertainty was then calculated at each reporting period as the standard deviation of the replicate enrichment estimates. This process was repeated for eight total combinations of four enrichment levels and two wall deposit levels.

Note that several other potential sources of systematic uncertainty, for example inaccuracies in the physical model of the gas density behavior with pressure and temperature, self-attenuation in the gas and deposit, and instrument drift, are not included in the analysis scenarios discussed below.

## Results and Discussion

Unless otherwise noted, the results presented in this section are based on the assumptions described here. The header-pipe inner diameter is 10.23 cm, typical of product header pipes. The enrichment facility utilizes takeoff stations for product and tails that are based on direct desublimation of gas into a chilled cylinder. Feed stations are assumed to have similar pressure transients, but this may not be the case in practice. Enrichment in the header pipes is modeled as 0.70 percent for feed material, 0.20 percent for tails material, and between 2.0 percent and 5.0 percent for product material. Wall deposits are assumed to be  $\text{UO}_2\text{F}_2$  uniformly deposited over the surface of the pipe in the OLEM field of view, with an areal density as high as  $1000 \mu\text{g}/\text{cm}^2$ .

Gas pressure and temperature vary according to the nominal pressure transients described in Figure 3;  $P$  ranges from 10 Torr to 50 Torr and  $T$  ranges from 312 K to 346 K over the course of each ten-hour cylinder filling period. The calibration constant relating gas density to pressure and temperature is  $K_{PT} = 5.65 \text{ mg UF}_6 \cdot \text{K} / \text{cm}^3 \cdot \text{Torr}$ , and  $B_W = 1.81 \times 10^3 \text{ K}^3/\text{Torr}$ . For the pressure and temperature gauges, nominal statistical uncertainty values of  $\sigma_P = 0.25 \text{ Torr}$  and  $\sigma_T = 0.5 \text{ K}$  were adopted based on the conservative estimates of the data provided by the instrument manufacturer. For example, the accuracy of the pressure sensor is  $\pm 0.5$  percent of the measured value; how-

ever, a constant value of 0.25 Torr for  $\sigma_p$  was adopted for all values between 10 and 50 Torr. Similarly, the accuracy of the temperature sensor (RTD) is better than 0.1 K, but a value of 0.5 K was assumed for  $\sigma_T$ .

Estimation of  $W$  assumes a rolling ten-hour window of ten-minute measurements, beginning with the first cylinder transient which lasts for 10 hours (as indicated in Figure 3). Wall-deposit growth is assumed to be sufficiently slow that the deposit can be considered constant during the filling of a single cylinder.

The enrichment of the gas flowing past the OLEM is constant during the analysis period. The absolute efficiency calibration constant for the collection of 186-keV counts from the gas is  $K_G = 8.152 \times 10^{-4} \text{ mg } ^{235}\text{UF}_6 / \text{cm}^3 \cdot \text{cps}$  for the ROI summation analysis based on MCNP simulation and an ROI defined to be  $\pm 1.5 \sigma$  about the 186-keV peak centroid.

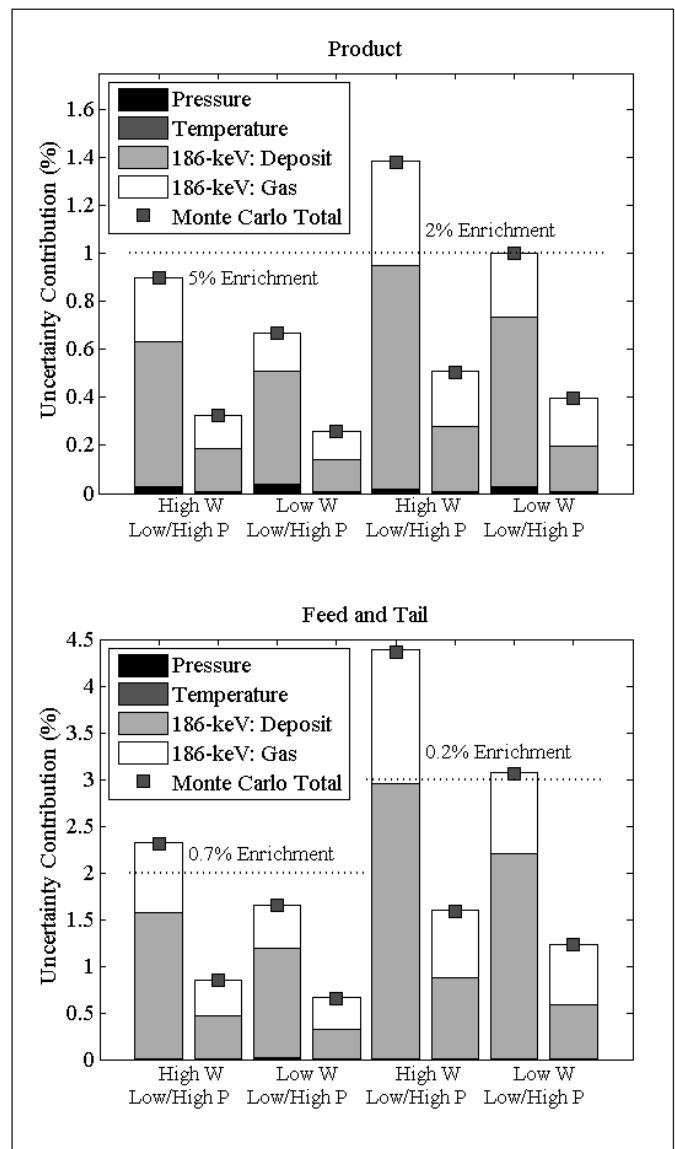
In the following sections, uncertainty quantification methods are used to understand and predict OLEM performance under plant conditions expected to be typical, and under a selection of conditions that might be considered atypical.

### Typical Scenarios: Performance Prediction

The baseline OLEM case studies assume steady-state operation (i.e., no startup effects), gas and deposit enrichment at 5 percent, 2 percent, 0.7 percent, and 0.2 percent, and deposits at 100 or 1000  $\mu\text{g}/\text{cm}^2$ . Statistical uncertainty budget estimates using the analytical methods described previously are shown in Figure 9. The fractional contribution of each component of uncertainty to the aggregate statistical uncertainty  $\sigma_E$  is approximated by the fraction of that component in the bracketed sum of squares in Equation 6, and the values in the figures are relative uncertainties (e.g.,  $\sigma_E / Ex100\%$ ). Note that these performance-prediction analyses address only the statistical components of uncertainty for typical, steady-state plant operation. Sources of systematic error, for example poor instrument calibration or instrument drift, as well as other possible systematic errors previously discussed, are not addressed.

The broad ranges of pressure and wall-deposit thickness on the high-pressure side of the header pump lead to a range of behavior in the uncertainty budgets and in the predictions for aggregate uncertainty. For scenarios with high gas pressure (approximately 50 Torr) and low wall-deposit levels (100  $\mu\text{g}/\text{cm}^2$ ), the deposit and gas uncertainty contributions are comparable in magnitude, and in all cases those contributions are larger than the uncertainties associated with the measurement

**Figure 9.** Analytical predictions for OLEM statistical uncertainty budgets for various combinations of enrichment, pressure (Torr) and wall-deposit thickness (areal density,  $\mu\text{g}/\text{cm}^2$ ). Top: product at 5.0 and 2 percent. Bottom: feed (0.7 percent) and tails (0.2 percent). Monte Carlo estimates for aggregate statistical uncertainty under the same conditions are shown as solid black squares. OLEM performance targets for  $\sigma_E$  at 1 percent for product, 2 percent for feed and 3 percent for tails, are shown in dashed lines for comparison. High and Low  $W$  refer to high (1000  $\mu\text{g}/\text{cm}^2$ ) and low (100  $\mu\text{g}/\text{cm}^2$ ) wall deposits, respectively, and High and Low  $P$  refer to high (46 Torr) and low (14 Torr) gas pressure, respectively.



of pressure and temperature. On the other extreme are the scenarios with low pressure (approximately 10 Torr) and high wall-deposit levels (1000  $\mu\text{g}/\text{cm}^2$ ). The deposit uncertainty, which must be extrapolated from the pressure-transient data, dominates the statistical uncertainty budget in these scenarios.



Monte Carlo-based estimates for aggregate statistical uncertainty are also shown in the figure for comparison. With the analytical propagation-of-error formulas used here, the analytical and Monte Carlo estimates, although computed entirely independently, are essentially identical. This is to be expected when the component uncertainties are relatively small, as the analytical formula simply provides a linear approximation to the full contribution of those components to the aggregate. Monte Carlo estimates incorporate the fully nonlinear effects of pressure, temperature, deposit, and signal ( $S$ ) statistical uncertainty on enrichment uncertainty, and will therefore only deviate from the analytical formula when those effects are large. Here, they provide a useful check on the analytical results.

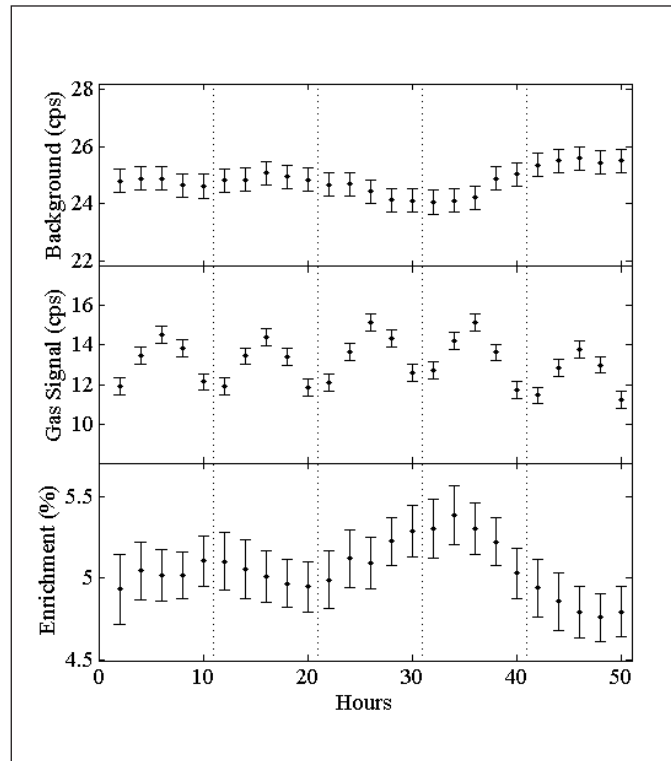
### Atypical Scenarios: Performance Prediction

In this section, the effects of atypical plant conditions are explored using the VOLEM. There are two primary components to the total uncertainties presented here: statistical uncertainties (as discussed in the previous section, represented by the error bars) and the systematic biases that arise under transient plant conditions.

#### Weak Pressure Transients

Some OLEM deployment locations may exhibit limited variation in pressure due to the design of the withdrawal stations or other factors. In these cases, the efficacy of the wall-deposit calibration approach described in this report may be significantly degraded. To explore the impact of weak pressure transients, this scenario assumes a sinusoidal pressure variation with period ten hours (1 cylinder) and a pressure range of just 2.5 Torr (10.3 to 12.8 Torr). As in one of the typical scenarios analyzed earlier, gas and deposit enrichment are 5 percent  $^{235}\text{U}$ , and the deposit areal density is  $1,000 \mu\text{g}/\text{cm}^2$ . Estimates of background, net gas signal, and enrichment over time in this scenario are shown in Figure 10. Note that the true (simulated) background is constant, so the apparent cyclic behavior in its estimate represents a systematic error in the calculated enrichment, caused by the temporal variation in pressure. Confidence bounds ( $\pm \sigma$ ) in all following figures were estimated using the analytical formulas in Equations 3 through 6 and assuming Poisson noise on the total signal (background plus gas signal), and approximating the true mean  $S$ ,  $P$ ,  $T$ , and  $W$  by their measured or estimated values.

**Figure 10.** OLEM estimates of background, net gas signal, and enrichment, assuming weak, sinusoidally varying pressure transients ranging from 10.3 to 12.8 Torr. Gas and deposit enrichments are 5 percent  $^{235}\text{U}$ ; deposit areal density is  $1,000 \mu\text{g}/\text{cm}^2$ .



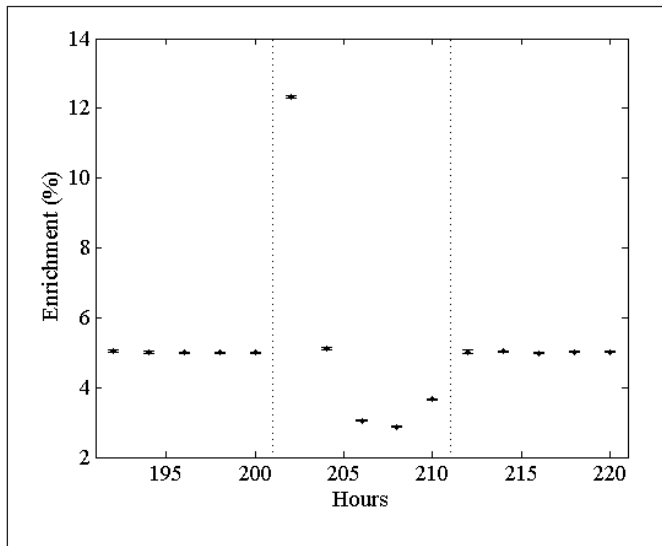
#### Large Background Changes

To explore the effects of a large, rapid, temporary change in the background, such as may occur when one or more cylinders come in close proximity to the OLEM, the areal density of the deposit was abruptly increased from  $100$  to  $1,000 \mu\text{g}/\text{cm}^2$  at the beginning of a two-hour reporting period. That higher level of deposit was maintained for the rest of the case study duration, leaving gas and deposit enrichment fixed throughout. This approximation assumes that gamma-ray source terms presented by ambient background (e.g., nearby cylinders) can be reasonably represented by the source term assumed for the deposit (i.e., “old uranium” where uranium daughters are in equilibrium). In practice, that may not be the case and future work will consider more variability in the source terms assumed for ambient background.

Figure 11 shows how the enrichment algorithms used in this study produce erroneous gas enrichment values for approximately eight to ten hours (approximately the length of time to measure a full cylinder) until an accurate estimate of



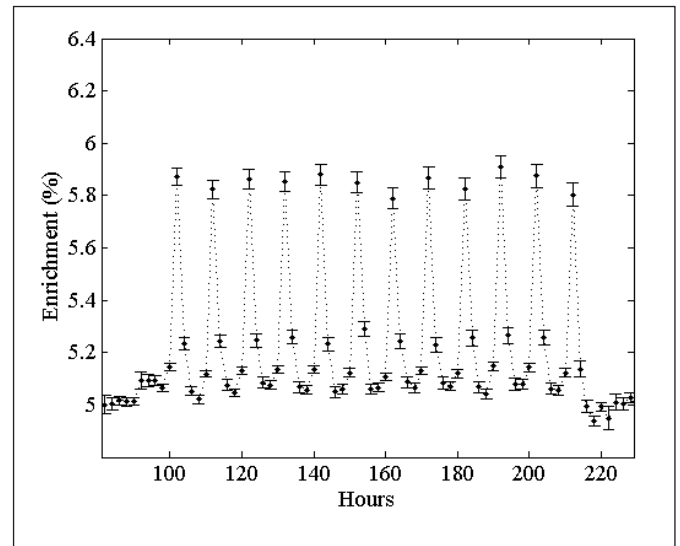
**Figure 11.** OLEM performance predictions for a scenario in which the ambient background is abruptly and temporarily (for a period extending beyond the timeframe shown, beginning immediately after  $t = 200$  hours) increased by a factor of ten while gas enrichment remains constant. Gas and deposit are 5 percent  $^{235}\text{U}$ ; the background change is simulated by changing deposit areal density from  $100 \mu\text{g}/\text{cm}^2$  to  $1,000 \mu\text{g}/\text{cm}^2$ .



background is realized. In this example, the first reporting period after the abrupt background change occurs at the beginning of a new cylinder fill, corresponding to the low end of the pressure transient (and thus low gas 186-keV signal). The delayed enrichment estimate, using the previous too-low background estimate, produces an erroneously high enrichment value, then slowly adjusts, briefly producing erroneously low values at the higher end of the pressure transient. The enrichment estimate then adjusts smoothly to the correct value after several reporting periods.

A large, gradual change in background, such as may occur when wall deposits grow substantially, was also studied. In this case study, the wall-deposit contribution to background increased linearly by a factor of 10 over a time period of 120 hours. The results are shown in Figure 12, where erroneous jumps in the calculated gas enrichment arise with a periodicity reflecting the ten-hour cylinder filling period. This effect is caused by the fact that the pressure ramp grows to 50 Torr every ten hours and then resets to 10 Torr. But the enrichment is evaluated every two hours. There is a systematic error in the determination of the background because it varies with time in a manner that happens to be correlated with the pressure increase during cylinder filling. The impact of the background error is larger for the two-hour enrichment period when the

**Figure 12.** OLEM performance predictions for a scenario in which the ambient background is gradually increased by a factor of ten over a period of 120 hours (beginning at  $t = 100$  hours) while gas enrichment remains constant. Gas and deposit are 5 percent  $^{235}\text{U}$ ; the background change is simulated by changing deposit areal density from  $100 \mu\text{g}/\text{cm}^2$  to  $1,000 \mu\text{g}/\text{cm}^2$ .



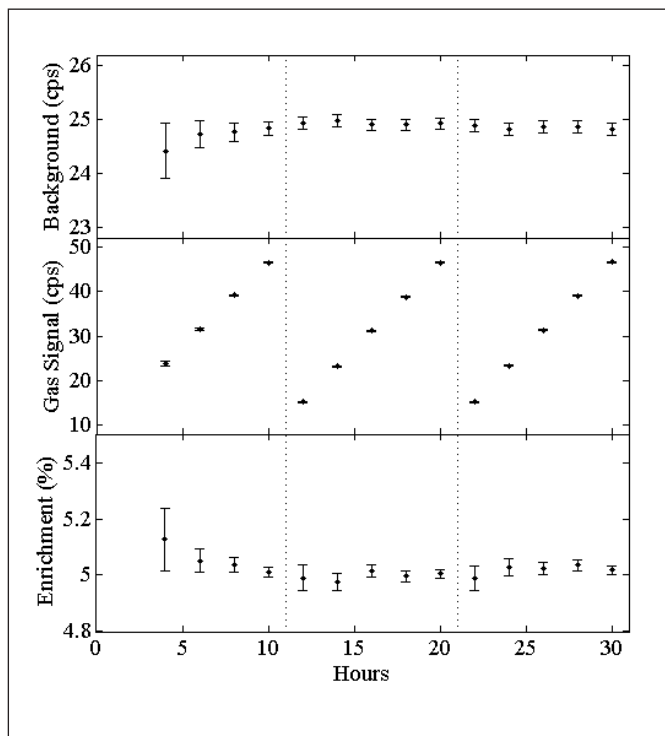
pressure is lowest, and this causes the ten-hour periodicity on the results. At the end of each ten-hour period, the impact of the compounding increase in measured 186-keV signal due to the wall deposits results in an erroneously very low estimate of that wall deposit, leading to an erroneously high enrichment estimate. As measurements from the next ten-hour period begin (low pressure), the wall deposit estimate is gradually corrected until the measurements from the end of the pressure transient again cause a jump.

### Startup Effects

Figure 13 illustrates the process of estimating the wall-deposit and net (gas)  $^{235}\text{U}$  contributions to signal, and enrichment, during each two-hour reporting time and over a sequence of several cylinders after the initial startup of the OLEM instrument. Confidence bounds are larger at the beginning, where less than the full ten hours of measurements on the first cylinder's data is available for the wall-deposit estimate. Enrichment confidence bounds cycle over each cylinder filling period, increasing at the beginning of the cylinder, primarily due to the reduced gas signal (due to lower gas pressures) at the beginning of each new pressure transient.



**Figure 13.** Example estimates of wall-deposit (top), gas (middle), and enrichment (bottom) during OLEM instrument startup. Vertical dashed lines indicate the division between successive cylinders. Gas and deposit enrichment are 5 percent  $^{235}\text{U}$ ; deposit areal density is  $1,000 \mu\text{g}/\text{cm}^2$ .



## Conclusions

A basis-spectra method for predicting on-line monitoring signatures has been developed and validated using measured data. VOLEM data streams for pressure, temperature, and gamma-ray spectrometer response were generated over a representative range of plant conditions: enrichment, pressure and wall-deposit thickness. The simulated signatures were then coupled to analytical error-propagation methods and Monte Carlo sampling to predict the components of the statistical uncertainty budget for a nominal instrument design and enrichment analysis approach.

A central challenge to OLEM viability is minimizing the statistical and systematic uncertainties associated with wall-deposit calibration, particularly for header pipes with relatively high deposit levels. Successful development of a wall-deposit correction method that is accurate, independent (does not require information from the operator) and quasi-continuous is a key technical enabler for a robust online enrichment monitor. The pressure-transient wall-deposit correction method proposed by others and quantitatively exercised in this paper holds

promise for plants using takeoff stations based on desublimation into chilled cylinders, assuming that gas enrichment levels are stable during the time periods used for deposit calibration.

Total statistical uncertainties for the various scenarios analyzed here can be compared to the OLEM performance targets (statistical plus systematic):  $\sigma_p = 1$  percent,  $\sigma_F = 2$  percent and  $\sigma_T = 3$  percent for product, feed and tails gas streams, respectively. For typical, steady-state plant operating conditions and high wall-deposit levels, it may be difficult to achieve performance targets during low-pressure periods of the cylinder filling process, especially for feed and tail cylinders. For relatively new or clean plants (i.e., with low deposit levels) and during periods of higher-pressure operation, OLEM statistical uncertainties are expected to be well below the target total uncertainties. Whether systematic uncertainties such as instrument drift or calibration errors (not addressed in this work) push the total field uncertainties higher than the IAEA targets is a question to be addressed via field trials.

Atypical scenarios (e.g., transient plant conditions) present challenges that will need to be addressed with appropriate analysis algorithms. For the preliminary analysis algorithms employed in this study, weak header-pipe transients had a significant negative effect on the precision of the wall-deposit calibration. Large and rapid changes in the background, such as may occur when one or more cylinders come in close proximity to the on-line instrument, can produce large biases in enrichment estimates until the wall-deposit calibration approach accurately captures the change. Similarly, biases in enrichment estimates were seen during the course of large, gradual changes in background, such as may occur when wall deposits change substantially. Further study of analysis algorithms and representative transients is needed in order to understand how systematic uncertainties produced by atypical plant conditions can be minimized.

It should be noted that the focus of the analyses presented in this paper was on the uncertainty of enrichment values reported from a single two-hour "snapshot," and those results were taken to be representative of the uncertainty associated with the average enrichment of a full cylinder. In practice, however, multiple  $E$  values would be calculated during the cylinder filling process and averaging of those values should reduce the statistical uncertainty of the enrichment value for the entire contents of the cylinder.

It is also important to note that the performance results presented in this paper were based on simulated VOLEM data

streams and a nominal online enrichment monitor design. Therefore, these results should not be taken as equivalent to those that would be realized with the actual OLEM instruments installed in operational plants, using the IAEA's suite of analysis algorithms.

## Acknowledgments

Funding for this work was provided by the U.S. Support Program to the IAEA. The authors are appreciative to Jae Joe of Brookhaven National Laboratory for management of the OLEM project on behalf of the U.S. Support Program, including VOLEM-related tasks. For technical guidance in the early stages of the VOLEM modeling, and invaluable operational and practical insights about online enrichment monitors and their application for international safeguards, the authors thank Alain Lebrun of the IAEA Department of Safeguards. Kiril Ianakiev of Los Alamos National Laboratory, through the sharing of his online measurement experience in an operating enrichment plant, contributed greatly in the formative stages of the IAEA's OLEM concept and consequently, to the VOLEM modeling and analysis presented here.

## References

1. Cooley, J. N. 2007. Model Safeguards Approach and Innovative Techniques Implemented by the IAEA at Gas Centrifuge Enrichment Plants, *Proceedings of the 48<sup>th</sup> INMM Annual Meeting*.
2. Lebrun, A. R., et al. 2009. Improved Verification Methods for Safeguards Verifications at Enrichment Plants, *Proceedings of the ANIMMA Conference*.
3. Smith, L.E., A.R. Lebrun, and R. Labella. 2013. Potential Roles of Unattended Safeguards Instrumentation at Centrifuge Enrichment Plants. *Journal of Nuclear Materials Management*.
4. Reilly, T. D., E. R. Martin, J. L. Parker, L. G. Speir, and R. B. Walton. 1974. Continuous In-Line Monitor for UF<sub>6</sub> Enrichment. *Nuclear Technology* (23).
5. Close, D. A., J. C. Pratt, and H. F. Atwater. 1985. Development of an Enrichment Measurement Technique and its Application to Enrichment Verification of Gaseous UF<sub>6</sub>, *Nuclear Instruments and Methods. A* (240).
6. Packer, T. W., and E. W. Lees. 1984. Measurement of the Enrichment of Uranium in the Pipework of a Gas Centrifuge Plant, *Proceedings of the 6th ESARDA Symposium*.
7. Packer, T. W., and E. W. Lees. 1985. Measurement of the Enrichment of UF<sub>6</sub> Gas in the Pipework of a Gas Centrifuge Plant, *Proceedings of the ESARDA Symposium*.
8. International Atomic Energy Agency. 2012. User Requirements: On-line Enrichment Monitor, IAEA SG-EQ-OLEM-UR-0001, IAEA Department of Safeguards.
9. Younkin, J. R., J. R. Garner, N. C. Rowe, and L. E. Smith. 2012. A Robust and Flexible Design for Gas Centrifuge Enrichment Plant Unattended Online Enrichment Monitoring, *9th International Conference on Facility Operations-Safeguards Interface*.
10. Smith, L. E., and A. R. Lebrun. 2011. Design, Modeling and Viability Analysis of an Online Uranium Enrichment Monitor, *IEEE Nuclear Science Symposium Proceedings*.
11. Ianakiev, K. D., et al. 2012. Field Trial of LANL On-Line Advanced Enrichment Monitor for UF<sub>6</sub> GCEP, *Proceedings of the 53<sup>rd</sup> INMM Annual Meeting*.
12. Weinstock, B., E. Weaver, and J. Malm. 1959. Vapor pressures of NpF<sub>6</sub> and PuF<sub>6</sub>; Thermodynamic Calculations with UF<sub>6</sub>, NpF<sub>6</sub> and PuF<sub>6</sub>. *Journal of Inorganic and Nuclear Chemistry*, vol. 11(2).
13. X-5 Monte Carlo Team. 2003. MCNP – A General N-Particle Transport Code, Version 5 – Volume I: Overview and Theory. LA-UR-03-1987, Los Alamos National Laboratory, Los Alamos, New Mexico.
14. Whitaker, J. M. 2005. Uranium Enrichment Plant Characteristics, a Training Manual for the IAEA. ORNL/TM-2005/43, Oak Ridge National Laboratory.
15. Brown, E., and R. B. Firestone. 1986. *Table of Radioactive Isotopes*, Lawrence Berkeley National Laboratory, University of California: Wiley-Interscience, John Wiley and Sons, Inc.
16. Close, D. A., J. C. Pratt, and H. F. Atwater. 1985. Development of an Enrichment Measurement Technique and its Application to Enrichment Verification of Gaseous UF<sub>6</sub>. *Nuclear Instruments and Methods A*, (240).
17. Hughes, M. R., and T. A. Nolan. 1984. Uranium Deposition Study on Aluminum: Results of Early Tests. K/PS-819, Martin Marietta Energy Systems.
18. Packer, T. W., and E. W. Lees. 1984. Measurement of the Enrichment of Uranium in the Pipework of a Gas Centrifuge Plant. *Proceedings of the ESARDA Symposium*.
19. Packer, T.W., and E.W. Lees. 1985. Measurement of the Enrichment of UF<sub>6</sub> Gas in the Pipework of a Gas Centrifuge Plant. *Proceedings of the ESARDA Symposium*.



20. Aaldijk, J. K., P. A. C. de Betue, and R. J. S. Harry. 1987. The Problem of Deposits in Enrichment Verification on  $UF_6$  Gas in Pipes. *Proceedings of the ESARDA Symposium*.
21. Close, D. A., M. A. Nelson. 2005. Cascade Header Enrichment Monitor (CHEM) Operating Procedures: IAEA Software for the Rokkasho Enrichment Plant. LA-UR 02-7388, Los Alamos National Laboratory, Los Alamos, New Mexico.
22. Ely, J., et al. 2014. On-Line Enrichment Monitor (OLEM) Supporting Safeguards at Enrichment Facilities. *IAEA Safeguards Symposium, 2014*.
23. Draper, N. R. and Smith, H. 1998. *Applied Regression Analysis*. Wiley & Sons, 3<sup>rd</sup> ed.
24. Knoll, G. F. 2000. *Radiation Detection and Measurement*, Wiley & Sons, 3<sup>rd</sup> ed.
25. March-Leuba, J., L. D. Trowbridge, D. W. Simmons, H. Jennings. On Line Enrichment Monitor (OLEM)  $UF_6$  Tests. Oak Ridge National Laboratory, ORNL/PTS-56557, June 20



# Comparison of an Exact to an Approximate Sample Size Calculation for Attribute Testing

Thomas Krieger and Tom L. Burr

International Atomic Energy Agency, Department of Safeguards, Division of Information Management, Vienna, Austria

## Abstract

To calculate the number of inspector samples to verify declared operator items, the performance measure used by the International Atomic Energy Agency (IAEA) is the probability of finding at least one defective item when the number of defects is at least enough to acquire a significant quantity of nuclear material. The “IAEA formula” that defines the sample size  $n_{IAEA}$  is based on approximating the exact formula for the probability to select one or more defects among the  $n_{IAEA}$  samples. One task that emerged from the IAEA’s reviewing and updating activities of its statistical methodologies was to evaluate the accuracy of  $n_{IAEA}$ . Therefore, this paper shows that an alternative sample size calculation that is based on the exact formula for the non-selection probability leads to a value  $n_{IAEA}$  within the set  $\{n_{IAEA} - 3, n_{IAEA} - 2, n_{IAEA} - 1, n_{IAEA}\}$  for all safeguards-relevant cases. The new sample size calculation is slightly more complicated to calculate, but it should not present significant implementation issues; and, in situations where samples are expensive it is appealing, because it requires the same or less inspector samples than  $n_{IAEA}$  derived by the IAEA formula.

## Introduction to the International Atomic Energy Agency (IAEA) Formula

The formula to calculate the number of samples  $n_{IAEA}$  to be selected for attribute sampling by the inspector in a stratum is given by

$$n_{IAEA} = \lceil N (1 - \beta^{1/[M/\bar{x}]}) \rceil \quad (\geq 1) \tag{1}$$

where  $N$  is the number of items in the stratum,  $\beta$  is the specified non-detection probability,  $M$  is the goal amount (generally, one significant quantity) and  $\bar{x}$  is the average nuclear material weight of an item in the stratum, see Reference 1. The ceiling  $\lceil a \rceil$ ,  $a \in \mathbb{R}$ , is the smallest integer not less than  $a$ . Attribute

sampling occurs when the nuclear material is in items, and measurement errors can be neglected, see Reference 1 or 2. The IAEA uses “zero-acceptance” sampling, which means that the sample “fails” if the inspector detects one or more defective items (the only “acceptable sample” is one with zero-defects, and hence the term “zero-acceptance” sampling). Therefore, by assumption and definition, an inspector’s sample can only lead to the wrong conclusion if there is at least one significant quantity missing, but no defective item is in the inspector’s sample. If measurement errors cannot be neglected, then a more complicated calculation is required, which is beyond the scope of this paper, but see References 3 and 4. Also, if there is significant variation in the item nuclear masses, then the stratum is not homogeneous, so an alternate framework is needed, which is also beyond the scope of this paper.

Let  $r \in \{1, \dots, N\}$  be the number of falsified items in the stratum and let  $n$  be the inspector’s sample size in sampling without replacement. In the context of attribute sampling schemes, the event of non-detection occurs if and only if no defective item is in the sample. Therefore, the non-detection probability as a function of  $n$  and  $r$  is calculated using probabilities computed from the hypergeometric distribution, see, e.g., References 5, 6, and 7.

$$\beta(n, r) = \mathbb{P}(\{\text{having no defects in the sample}\}) = \frac{\binom{r}{0} \binom{N-r}{n-0}}{\binom{N}{n}} = \prod_{j=0}^{r-1} \left(1 - \frac{n}{N-j}\right). \tag{2}$$

The basis for the IAEA formula is the following: Because each item in the stratum has the average item content  $\bar{x}$ , the operator would have to falsify  $\lceil M/\bar{x} \rceil (\geq 1)$  items in order to acquire a significant quantity of nuclear material. Therefore, we obtain with Equation 2:



$$\beta(n, [M/\bar{x}]) = \prod_{j=0}^{[M/\bar{x}]-1} \left(1 - \frac{n}{N-j}\right) \leq \prod_{j=0}^{[M/\bar{x}]-1} \left(1 - \frac{n}{N}\right) = \left(1 - \frac{n}{N}\right)^{[M/\bar{x}]} \quad (3)$$

The IAEA stratum sample size  $n_{IAEA}$  is determined by equating the right hand side of Equation 3 to the specified non-detection probability  $\beta$ . This leads to the IAEA formula Equation 1, where the outer ceiling is needed, so that the sample size is an integer.

## A New Inspection Sample Size Calculation

The IAEA is reviewing and updating its statistical methodologies for safeguards, and in doing so, a question arose whether the sample size determined by solving the “exact” problem, i.e., by finding  $n_{IAEA} = n_{IAEA}(\beta, N, M/\bar{x})$  with

$$n_{exact} = \min \left\{ n \in \{1, \dots, N\} : \prod_{j=0}^{[M/\bar{x}]-1} \left(1 - \frac{n}{N-j}\right) \leq \beta \right\} \quad (4)$$

could lead to a considerably smaller sample size compared to  $n_{IAEA}$ . Note that this “exact” calculation in Equation 4 uses the exact formula for the non-detection probability as given by Equation 2, but  $n_{exact}$  is not truly exact due to the inherent discreteness of the solution space. Also note, that because  $\beta(n, [M/\bar{x}])$  is a monotone decreasing function of  $n$  with  $\beta(0, [M/\bar{x}]) = 1$  and  $\beta(n, [M/\bar{x}]) = 0$  for all  $n > N - [M/\bar{x}]$ , the existence of  $n_{exact}$  is guaranteed.

An explicit expression of  $n_{exact}$  as a function of  $\beta, N$  and  $[M/\bar{x}]$  does not exist because Equation 4 is a non-trivial polynomial function of degree  $[M/\bar{x}]$ . Therefore, the new sample size given by Equation 4 is slightly more complicated to calculate, but should not present significant implementation issues.

Comparisons of  $n_{exact}$  to  $n_{IAEA}$  made in the past for specific values of  $\beta, N$  and  $[M/\bar{x}]$  have indicated good agreement. This paper proves the good agreement for all safeguards-relevant cases  $\beta \in (0.05, 1)$ , any  $N$  and any  $[M/\bar{x}]$ .

It is clear by construction that  $n_{exact} \leq n_{IAEA}$ , so it is important from an effort consideration viewpoint to quantify the difference between  $n_{IAEA}$  and  $n_{exact}$ , i.e.,

$$n_{IAEA} - n_{exact} = [N(1 - \beta^{1/[M/\bar{x}]})] - n_{exact}(\beta, N, M/\bar{x}).$$

The main result of this paper is given in our

**Theorem:** For any  $\beta \in (0, 1)$ , any  $N$  and any  $[M/\bar{x}]$  we have

$$[N(1 - \beta^{1/[M/\bar{x}]})] - n_{exact}(\beta, N, M/\bar{x}) < -\ln(\beta) + 1. \quad (5)$$

For all safeguards-relevant cases, i.e.,  $\beta \in (0.05, 1)$ , we get

$$[N(1 - \beta^{1/[M/\bar{x}]})] - n_{exact}(\beta, N, M/\bar{x}) \leq 3. \quad (6)$$

**Proof:** Let  $\beta \in (0, 1)$  be fixed for the proof of Equation 5. We first show that for any  $r=1, 2, \dots$  the inequality

$$\ln(\beta) < r(\beta^{1/r} - 1) \quad (7)$$

holds. This can be seen from the generalized mean value theorem, see, e.g., Reference 8, p. 222: Let  $f$  and  $g$  be two differentiable functions on an open interval  $(a, b)$ ,  $a < b$ , and continuous on  $[a, b]$ , then there exist at least one  $c \in (a, b)$  with

$$g'(c)(f(b) - f(a)) = f'(c)(g(b) - g(a)). \quad (8)$$

We apply this theorem to a  $\beta \in (0, 1)$ ,  $b := 1$ ,  $f(x) = x^{1/r}$  and  $g(x) = \ln(x)$ . Because  $g'(x) = 1/x > 0$  we get with Equation 8 and  $c^{1/r} < 1$

$$\frac{1 - \beta^{1/r}}{-\ln(\beta)} = \frac{1}{r} c^{1/r} < \frac{1}{r},$$

i.e., inequality 7. In order to prove statement 5 we note that

$$\left(1 - \frac{n}{N - ([M/\bar{x}] - 1)}\right)^{[M/\bar{x}]} \leq \prod_{j=0}^{[M/\bar{x}]-1} \left(1 - \frac{n}{N-j}\right).$$

Putting the left hand side equal to  $\beta$  leads to a lower bound of  $n_{exact}$  namely

$$n_{lower} = (N - [M/\bar{x}] + 1)(1 - \beta^{1/[M/\bar{x}]}) \quad (9)$$

Because  $[N(1 - \beta^{1/[M/\bar{x}]})] = N(1 - \beta^{1/[M/\bar{x}]}) + \delta$  with  $\delta \in [0, 1)$ , we get with Equation 9 and inequality 7 for  $r = [M/\bar{x}]$ ,

$$\begin{aligned} [N(1 - \beta^{1/[M/\bar{x}]})] - n_{exact}(\beta, N, M/\bar{x}) &< N(1 - \beta^{1/[M/\bar{x}]}) + \delta - n_{lower} \\ &= ([M/\bar{x}] - 1)(1 - \beta^{1/[M/\bar{x}]}) + \delta \\ &< -\ln(\beta) + 1, \end{aligned} \quad (10)$$

which proves inequality 5. For the safeguards-relevant cases, i.e.,  $\beta \in (0.05, 1)$  we have  $-\ln(\beta) \leq -\ln(0.05) \approx 2.99573 < 3$  and get with (10)

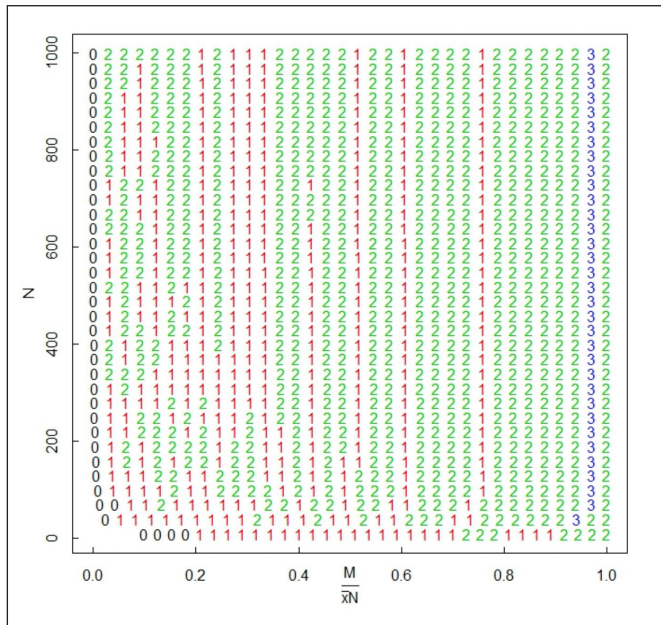
$$[N(1 - \beta^{1/[M/\bar{x}]})] - n_{exact}(\beta, N, M/\bar{x}) < 4. \quad (11)$$

Since  $[N(1 - \beta^{1/[M/\bar{x}]})]$  as well as  $n_{exact}(\beta, N, M/\bar{x})$  are integers, their difference is also an integer and we finally obtain inequality 6 for all  $\beta \in (0.05, 1)$ , which completes the proof.





**Figure 1.** Graphical representation of the absolute differences  $n_{IAEA} - n_{exact}$



Now we will comment on the result of our Theorem. First, although inequalities are used in steps of the proof, it turns out that the bound of 3 is actually achieved. For example, let  $\beta = 0.05, N = 100$  and  $[M/\bar{x}] = 95$ . Then we have  $n_{exact} = 1$ , while  $n_{IAEA} = 4$ . Or, let  $\beta = 0.05, N = 377$ , and  $[M/\bar{x}] = 150$ . Then we get  $n_{exact} = 6$ , while  $n_{IAEA} = 8$ .

Second, Figure 1 plots the absolute differences  $n_{IAEA} - n_{exact}$  for  $\beta = 0.05$  and various values of  $N$  and  $M/\bar{x}$ . In Figure 1, the values of the ratio are distributed equally between the two extremes, i.e.,  $M = \bar{x}$  (one item is falsified) and  $M = N\bar{x}$  (all items are falsified):

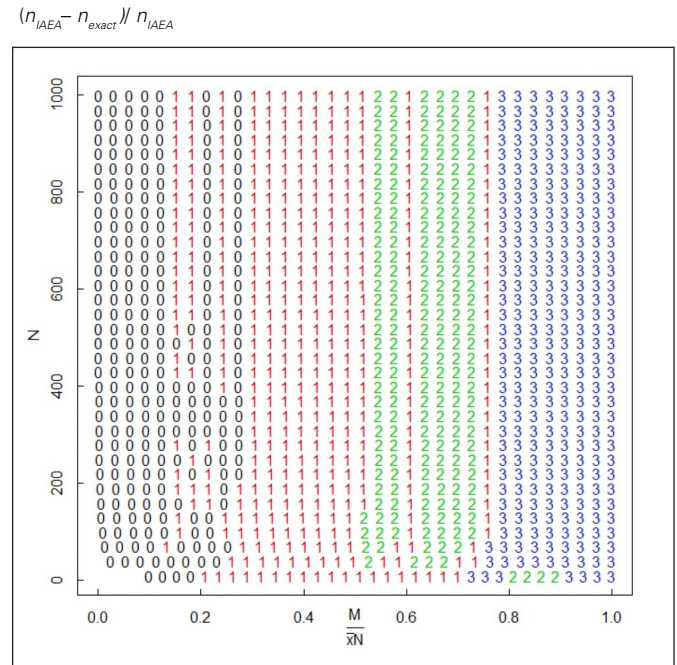
$$\frac{M}{\bar{x}} = 1 + (N - 1) \frac{i}{size} \quad \text{with } N = 10 + 30j \text{ for } i, j = 0, \dots, size, \quad (12)$$

where we chose  $size = 33$  for effective plotting. Because the ratio  $M/\bar{x}$  in Eq. (12) has the upper limit of  $N$ , we instead plot  $M/(\bar{x}N)$  given by

$$\frac{M}{\bar{x}N} = \frac{1}{N} + \left(1 - \frac{1}{N}\right) \frac{i}{33} \in \left[\frac{1}{N}, 1\right] \quad \text{with } N = 10 + 30j \text{ for } i, j = 0, \dots, 33.$$

From Figure 1 we see that the condition  $M/(\bar{x}N) \rightarrow 1$  is a necessary but not sufficient for  $n_{IAEA} - n_{exact} = 3$  (see also the example in the last paragraph). The unexpected 2s in the last column can be justified as follows:  $M/(\bar{x}N) = 1$  implies that the full content of each item has to be diverted, which leads to an exact sample size equal to 1. In contrast, the IAEA formula gives us, using Equations 1 and 7,  $n_{IAEA} = \lceil N(1 - 0.05^{1/N}) \rceil < \lceil -\ln(0.05) \rceil = 3$ , i.e.,  $n_{IAEA} - n_{exact} = 2$ .

**Figure 2.** Graphical representation of the relative differences  $(n_{IAEA} - n_{exact}) / n_{IAEA}$



Finally, because the IAEA formula 1 reflects current practice, we can also consider the relative difference  $(n_{IAEA} - n_{exact}) / n_{IAEA}$  as a performance measure. Because

$$0 \leq \frac{n_{IAEA} - n_{exact}}{n_{IAEA}} \leq 1 - \frac{1}{n_{IAEA}},$$

for plotting purposes, we code the case  $0 \leq (n_{IAEA} - n_{exact}) / n_{IAEA} < 0.1$  with 0s,  $0.1 \leq (n_{IAEA} - n_{exact}) / n_{IAEA} < 0.3$  with 1s,  $0.3 \leq (n_{IAEA} - n_{exact}) / n_{IAEA} < 0.5$  with 2s, and  $0.5 \leq (n_{IAEA} - n_{exact}) / n_{IAEA} < 1$  with 3s. Figure 2 plots the relative differences  $(n_{IAEA} - n_{exact}) / n_{IAEA}$  for  $\beta = 0.05$  and various values of  $N$  and  $M/\bar{x}$  in the same way as explained for Figure 1.

For example, the 3s in Figure 2 mean that  $n_{exact}$  is at least 50 percent smaller than  $n_{IAEA}$ . Note that it can be shown that the maximum of  $(n_{IAEA} - n_{exact}) / n_{IAEA}$  is 75 percent.

## Discussion and Further Work

We regard the IAEA's sample size based on the approximate calculation as being highly accurate in the sense that it is within of the sample size based on the exact calculation. We leave it to the reader to decide if a maximum discrepancy of 3 is sufficiently accurate for intended applications. If users prefer the exact calculation because it leads to a small reduction in the number of required samples, then certainly the exact calculation is recommended. The new exact sample size calculation is slightly more complicated, but should not present significant



implementation issues, and it requires the same or less inspector samples than  $n_{IAEA}$  derived by the IAEA formula. For qualitative gross defect measurements (i.e., for measurement situations in which measurement errors can be ignored), the exact calculation could be applied, and potentially reduce the number of required measurements by up to .

We mentioned in the Introduction that the “IAEA formula” assumes that there is no measurement error. When measurement errors must be considered, one might also consider allowing for false alarms, so alternate sampling schemes that allow for finding a few apparent defects could be considered. Also, a key assumption for both  $n_{IAEA}$  and  $n_{exact}$  calculations is that the items in the stratum have the same nuclear material mass. In any stratum for which there is non-negligible variation in the true nuclear material mass among items, an alternate sample size calculation is needed, and we anticipate that the required sample size will be larger than both  $n_{IAEA}$  and  $n_{exact}$  as calculated in this paper.

## Acknowledgement

The authors thank Jan Wüster (IAEA, Department of Safeguards, Division of Information Management) for valuable discussions and the suggestion to add the two figures.

## References

1. IAEA. 2002. IAEA Safeguards Glossary, 2001 Edition (IAEA International Nuclear Verification Series No. 3), Vienna: IAEA.
2. Thyregod, P. 1988. Sampling Plans, in *Encyclopedia of Statistics* (Kotz, S.; Johnson, L., eds), New York, Wiley, pp. 246-254.
3. Franklin, M. 1989. Non-Detection Probabilities of Attribute Mode Sampling Plans, *Proceedings of the 11th ESARDA Symposium*.
4. Burr, T. L., F. W. Spencer, D. R. Weier, and R. L. Weitz. 2008. Statistical Algorithm for Sampling from a Growing Population, *Journal of Nuclear Materials Management*, Vol. 36, No. 3.
5. Avenhaus, R., and M. J. Canty. 1996. *Compliance Quantified—An Introduction to Data Verification*, Cambridge, UK: Cambridge University Press.
6. IAEA. 1999. IAEA Safeguards Statistical Concepts and Techniques (Fifth Edition), Vienna: IAEA.
7. Jaech, J. L. 1973. *Statistical Methods in Nuclear Material Control*, Oak Ridge, Tennessee: Technical Information Center, U.S. Atomic Energy Commission.
8. Ross, K. A. 1980. *Elementary Analysis: The Theory of Calculus*, New York: Springer-Verlag.

*Thomas Krieger received a Doctorate in mathematics in 2003. After a post-doc position at the Universität der Bundeswehr München, Germany, where his research activities were focused on topics in applied mathematics and game theoretical analysis of safeguards systems, he joined the IAEA in 2012. Together with his co-author Tom L. Burr, Thomas is responsible for the reviewing and updating activities of the IAEA's statistical methodologies for safeguards.*

*Tom L. Burr received a PhD in statistical science in 1992 when he joined Los Alamos National Laboratory working on statistical aspects of non-proliferation. Tom has been at the IAEA since 2014 when he joined his co-author Thomas Krieger in reviewing and updating the IAEA's statistical methodologies for safeguards.*

**Keywords:** Attribute testing, IAEA formula, Sampling plans



# Simulation Study for Detection of Pin Diversion with the Differential Die-away Instrument Using Fresh Nuclear Fuel

*Alison V. Goodsell*

*Los Alamos National Laboratory, Los Alamos, New Mexico USA, and Nuclear Security Science and Policy Institute, Texas A&M University, College Station, Texas USA*

*Vladimir Henzl, Martyn T. Swinhoe*

*Los Alamos National Laboratory, Los Alamos, New Mexico USA*

*William S. Charlton*

*Nuclear Security Science and Policy Institute, Texas A&M University, College Station, Texas USA, and National Strategic Research Institute at the University of Nebraska, Omaha, Nebraska USA*

---

## Abstract

The Differential Die-away (DDA) technique is currently being investigated at Los Alamos National Laboratory to better understand the development and deployment challenges for its use as a non-destructive, active interrogation method for assay of nuclear fuel assemblies. Inspired by the successful application for nuclear waste assay, this application of the DDA technique is based on the active interrogation by a pulsed DT neutron generator of a fuel assembly submerged in water. Induced fission neutrons from the fuel assembly are detected by surrounding  $^3\text{He}$  detectors, which provide information on the time of detection (list-mode data) of individual neutrons with respect to the time of the interrogating neutron pulse. The magnitude and dynamic evolution of the neutron population recorded by surrounding thermal neutron detectors reflects the fuel assembly characteristics and composition. In this paper, we report on results from a simulation study using MCNPX focusing on how random pin diversion scenarios (or partial defects) influence the dynamic evolution of the signal observed by individual  $^3\text{He}$  detectors. We use a combination of fresh low-enriched, natural, depleted uranium dioxide ( $\text{UO}_2$ ) fuel rods, and stainless steel rods to create perturbations in PWR-like fuel pin matrices mimicking removal or substitution of ten (10) pins to quantitatively determine the impact on the DDA signal, including signal magnitude, die-away time, and, importantly, individual detector sensitivity to diversion position in the fuel assembly. Analysis of the trends in the results calculated for the fresh fuel diversion cases provides insight into observable effects caused by similar types of diversion scenarios in spent fuel. This supports

the conclusion that the DDA technique can provide a wealth of information about the assayed item and is suitable for spent fuel measurements.

## Introduction

The primary role of the International Atomic Energy Agency's (IAEA) safeguards mission is to deter the proliferation of nuclear weapons through the timely detection of the misuse or diversion of a significant quantity of special nuclear material.<sup>1</sup> Currently, the international nuclear safeguards community is investigating a variety of advanced non-destructive assay (NDA) techniques for the characterization and verification of spent nuclear fuel assemblies. An area of particular interest is the ability to identify illicit diversion of nuclear fuel pins masked by substitution of pins with lower grade or non-nuclear material.

One technique being intensively researched is based on the differential die-away (DDA) method, which is an active NDA method using an external high-energy neutron source to induce fission primarily in the fissile material of a spent fuel assembly. The DDA technique had originally been developed and successfully implemented for assay of drums with radioactive waste for material accountancy.<sup>2-5</sup> More recently, the DDA technique has also been proposed for detection of the illicit trafficking of special nuclear material.<sup>6</sup> The application of the DDA technique for spent fuel characterization and verification is however fairly novel and is primarily associated with the onset of the Next Generation Safeguards Initiative Spent Fuel project (NGSI-SF) sponsored by the U.S. National Nuclear Security Administration's (NNSA) Defense Nuclear Nonprolifera-



tion (DNN). In contrast to the waste drum assay, the interrogation of entire fuel assemblies face additional challenges mostly associated with the interplay of neutron producing and neutron absorbing materials in a generally highly multiplying environment. The initial research of DDA application to spent fuel thus led to development of novel analytical approaches that rely on measurement of the DDA signal in time domains significantly closer to the initial interrogation pulse than in the waste drum assay application. Based first on the Monte Carlo N-Particle eXtended (MCNPX)<sup>7</sup> simulations of the spent fuel assay by a conceptual DDA instrument, the results suggested that this adapted DDA technique can accurately characterize or verify a variety of spent fuel assembly (SFA) properties,<sup>8</sup> such as its multiplication, effective fissile content, total plutonium content, initial enrichment and burnup, and even identify certain types of fuel pin diversions.<sup>9</sup>

Overall, the DDA technique for nuclear fuel assay has been extensively researched through coupled projects sponsored by the NGSF-SF focused on spent fuel and the NNSA's DNN Office of Research and Development focused on fresh fuel. The fresh fuel research project includes further simulation work<sup>10</sup> and laboratory experiments with a prototype DDA instrument assaying fresh nuclear fuel<sup>11</sup> at Los Alamos National Laboratory. The purpose of the fresh fuel DDA project is to investigate potential development and deployment challenges faced by the spent fuel project, including operating in very high count rate environments due to detector proximity to the neutron generator and fuel assembly.<sup>12</sup> In addition, benchmarking of the fresh fuel DDA experimental data against the MCNPX simulated results provide additional validation of the previously performed spent fuel simulations which showed the capabilities of the DDA instrument to act as a robust NDA safeguards technique.

The motivation for the investigation of the fresh fuel diversion scenarios presented in this paper is to perform proof-of-concept DDA pin substitution detection. For fresh fuel, the overall fissile content is well known from the fuel manufacturing process, allowing the detection of substituted pins to be measured directly without the need of a reference or operator declaration burdened by uncertainty associated with irradiation history and burnup. Additionally, fresh fuel pins have significantly higher multiplication than pins from non-nuclear material or pins from the most readily available nuclear substitutes such as depleted (DU) or natural uranium (NU). Therefore it is expected that diversions in fresh fuel assemblies should be more

easily identifiable than diversions in the spent fuel assemblies where multiplication of spent fuel pins is comparable to that of pins from NU or DU due to the highly multiplying environment and lack of neutron absorbers in the fuel rods. From this perspective, fresh fuel diversion scenarios can offer a "limiting case" with likely a highest probability of detecting an illicit diversion of several fuel rods and provide a venue to optimize data analysis for such detection. If a certain type of diversion is not identifiable in the fresh fuel case, then the likelihood of detecting diversions in the spent fuel case by means of the active interrogation involving the DDA technique is improbable.

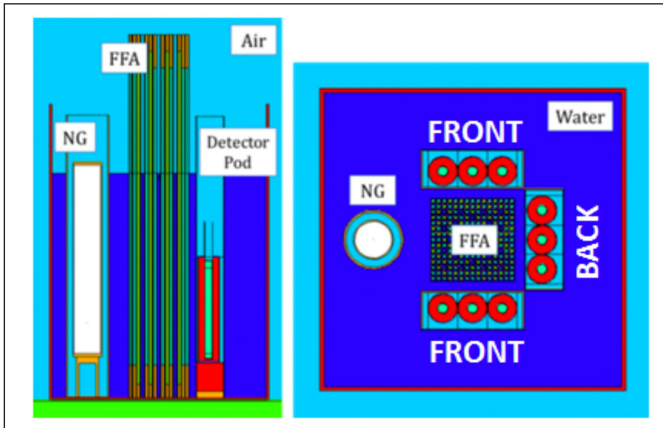
## Fresh Fuel Simulations

The previously benchmarked DDA MCNPX model using fresh fuel<sup>11</sup> was used for the following diversion scenario study. Overall, this DDA fresh fuel benchmark showed good agreement between the experimental and simulated signals which typically differed from one another only by 1-2 percent.<sup>13</sup> These results thus showed that the DDA instrument signal and its decay times could be modeled sufficiently accurately for multiple detector positions and fresh fuel enrichments.<sup>11</sup> During the benchmarking of the fresh fuel experiments and MCNPX simulations, a variety of sensitivity studies were also performed to determine the effects on the DDA signal.<sup>13</sup>

Quantifying the sensitivity of the DDA instrument is an essential step in determining whether the changes we observe in the recorded DDA signal can be correlated to changes in the material being assayed or are an artifact of the uncertainty of the measurement itself. The simulation study evaluated in this paper focuses solely on examining differences created by modifying the quantity of fissile material in the fresh fuel assembly by a virtual pin substitution. Besides the material definition changes, the geometry, nuclear data, and other simulation parameters remain constant for the respective assayed enrichments. Thus, the main source of uncertainty in these simulations is due to the statistical uncertainties in the MCNPX tally results. The substantial cost in computational time required for the MCNPX simulations allows us to simulate only several seconds of an actual measurement with the neutron generator which translates into  $5 \cdot 10^8$  neutron histories per simulation. Therefore our simulation results are burdened by higher statistical fluctuations than a real world measurement that is expected to last for about five to ten minutes. MCNPX sensitivity studies in Reference 13 included evaluation of statistical uncertainty in the time-binned tally results and the DDA signal



**Figure 1.** Cross sectional and top view of the simulated DDA instrument setup used in the simulations of fresh fuel assay



die-away time in different time domains. The results of that study showed that in the early time domains (70-100  $\mu$ s and 100-150  $\mu$ s) standard deviation of the mean in the die-away time for multiple detector positions and fresh fuel enrichments did not exceed 2 percent.<sup>11</sup> Additionally, the statistical variation in the integral of the DDA signal in the same time domains did not exceed 1 percent.

In comparison to anticipated real world scenarios, the statistical uncertainty of the measurement will be 1-2 orders of magnitude smaller depending on the actual time of the measurement, intensity of the neutron generator, and the exact design of the instrument. However, the results of experimental measurements are affected by additional sources of uncertainty such as geometrical reproducibility, thermal instability, variations in background, and others that are under control in the simulations. A previously performed DDA instrument experiment and simulation benchmark campaign included a sensitivity study which examined some of these effects such as small geometry discrepancies, deadtime corrections, neutron generator pulse wrap-around effects (room return), and neutron generator output reproducibility.<sup>11, 13</sup> We found that the magnitudes of the associated systematic experimental uncertainties are on par with the statistical uncertainties of the simulated DDA signal, i.e. typically about 2 percent.

Therefore, should there be no modification to the DDA setup between assays, changes of more than  $\pm 2$  percent to the simulated DDA die-away time and integral signal in the early time domains (70-100  $\mu$ s and 100-150  $\mu$ s) are considered to be significant and can be attributed to the effects of various diversion scenarios. In reality, this threshold for flagging fuel assem-

blies as suspect may vary depending on the actual experimental setup, measurement procedure, and overall context of the assay (e.g., ensemble of fuel assemblies from same reactor discharge or random screening in the interim repository). Such complex evaluation however exceeds the scope of this paper; the intention of this paper is to provide a base case of a DDA system performing assays of well documented diversion scenarios. It is the conviction of the authors that such results can be easily scaled or extrapolated for a great variety of other possible diversion scenarios where different numbers of pins are removed, or different types of material are used as the substitute.

The benchmarked fresh fuel DDA instrument setup consists of a Thermo Scientific P 385 DT neutron generator and nine  $^3\text{He}$  detectors inserted into 23.5 mm radially thick high-density polyethylene (HDPE) cylinders wrapped with 1-mm thick Cd foil positioned around a PWR-like 15x15 fuel lattice filled with low enriched (LEU) and depleted (DU) uranium dioxide fuel rods all submerged in water. The detectors and neutron generator are contained inside waterproof stainless steel pods within the water tank (Figure 1).

## Fresh Fuel Diversion Scenarios

The benchmarked DDA simulation results with no diversion of fuel pins were used as a reference for the diversion scenarios. The simulated diversion scenarios consisted of removing ten fresh LEU fuel rods (3.19 percent  $^{235}\text{U}$ ) and replacing them with 10 NU rods (0.72 percent  $^{235}\text{U}$ ), 10 DU rods (0.22 percent  $^{235}\text{U}$ ), or ten stainless steel (SS) rods. The positions of the fuel pin replacements were kept constant for each effective fuel assembly  $^{235}\text{U}$  enrichment. The location of the fuel pin diversions were distributed throughout the assembly and are shown in Figure 2. The specifications of the fuel rods and the PWR-like fuel assembly are provided in Table 1. The effective enrichments of the No Diversion and pin diversion cases (with ten LEU pins replaced with NU, DU, or SS) are listed in Table 2.

## Analysis & Results

When comparing the No Diversion case with the three diversion scenarios in which ten LEU rods were replaced with NU, DU, or SS pins, three characteristics of the DDA signal were assessed. These were (1) the overall dynamic evolution of the DDA signal, (2) the integral of the DDA signal in the 70-100  $\mu$ s time domain, and (3) the signal die-away time recorded by individual detectors in the 70-100  $\mu$ s time domain. The 70-100  $\mu$ s time domain was chosen as the equivalent of the so-called



**Figure 2.** The schematics of the fresh fuel assembly composition matrix with indicated positions of diverted LEU pins substituted by pins with NU, DU, or SS, with red = LEU fuel rod, blue = Diversion position (natural, depleted, or stainless steel rod), yellow = DU, and green = Guide Tube. For the No Diversion scenario, blue = LEU.

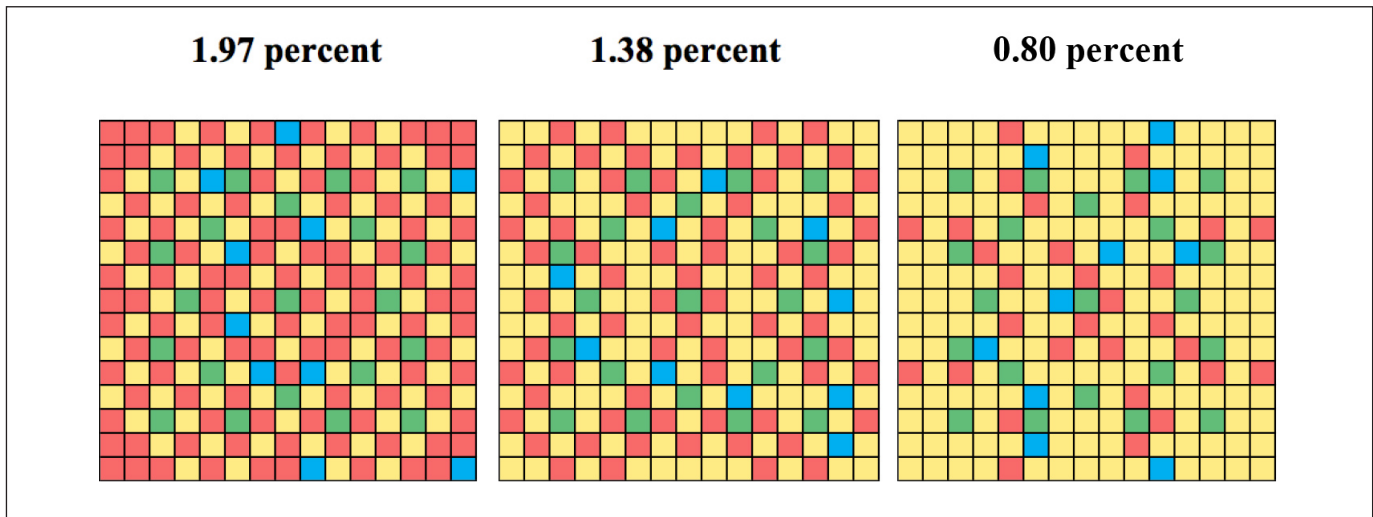


**Table 1.** LANL PWR-like 15x15 fresh fuel assembly and pin specifications

| PWR Assembly               |         |
|----------------------------|---------|
| Lattice geometry           | 15 x 15 |
| Assembly width             | 21.5 cm |
| Fuel pin pitch             | 1.4 cm  |
| Number of fuel pin slots   | 204     |
| Number of guide tube slots | 21      |

| Fuel Pins                                  |                         |                         |                         |                       |
|--|-------------------------|-------------------------|-------------------------|-----------------------|
|  | LEU                     | NU                      | DU                      | SS                    |
| Fuel type                                  | UO <sub>2</sub>         | UO <sub>2</sub>         | UO <sub>2</sub>         | N/A                   |
| Cladding type                              | Zircaloy-2              | Zircaloy-2              | Zircaloy-2              | SS                    |
| Avg. enrichment (percent <sup>235</sup> U) | 3.19 percent            | 0.72 percent            | 0.22 percent            | 0                     |
| Fuel pellet density                        | 10.48 g/cm <sup>3</sup> | 10.48 g/cm <sup>3</sup> | 10.48 g/cm <sup>3</sup> | 8.0 g/cm <sup>3</sup> |
| Fuel pellet radius                         | 0.4525 cm               | 0.4525 cm               | 0.4525 cm               | 0.4525 cm             |
| Cladding thickness                         | 0.0875 cm               | 0.4525 cm               | 0.4525 cm               | 0.4525 cm             |
| Outer pin radius                           | 0.54 cm                 | 0.54 cm                 | 0.54 cm                 | 0.54 cm               |
| Total fuel rod length                      | 130 cm                  | 130 cm                  | 130 cm                  | 130 cm                |
| Active fuel length                         | 102 cm                  | 102 cm                  | 102 cm                  | 102 cm                |
| Inert fuel regions                         |                         |                         |                         |                       |
| Top  | 17 cm                   | 6 cm                    | 6 cm                    | N/A                   |
| Bottom                                     | 12 cm                   | 5 cm                    | 5 cm                    | N/A                   |

**Table 2.** Effective enrichment of entire fresh fuel assembly for each diversion scenario

|              | Enrichment (percent <sup>235</sup> U) |              |              |
|--------------|---------------------------------------|--------------|--------------|
|              | 1.97 percent                          | 1.38 percent | 0.80percent  |
| No Diversion | 1.97 percent                          | 1.38 percent | 0.80percent  |
| NU           | 1.85 percent                          | 1.26 percent | 0.68 percent |
| DU           | 1.82 percent                          | 1.24 percent | 0.66 percent |
| SS           | 1.81 percent                          | 1.23 percent | 0.65 percent |

“magic time window” of 100-200 μs identified as the key time domain for spent fuel characterization in conceptual DDA study in Reference 9. As an additional benefit, the early time domain (directly following the neutron generator pulse) experiences the highest recorded count rates which correlate to improved counting statistics and lower uncertainties. Using the three observables, the relationships between enrichment, DDA signal, and die-away time were evaluated.

### Dynamic Evolution of the DDA Signal

From the very principle of the DDA method, and as observed in previously performed simulations and experiments,<sup>11</sup> the DDA signal is expected to be sensitive to the fissile content within the fresh fuel assembly. As the amount of fissile material in the fresh fuel assembly increases with higher enrichment, the probability of inducing fission by thermal neutrons increases; thus, more neutron generations within the same fission chain can be created and thereby prolong the lifetime of the entire





neutron population. This naturally leads to higher magnitude and longer die-away times of the DDA signal observed by individual neutron detectors.

The DDA signal of the No Diversion case was compared to the ten LEU pin diversion scenarios using NU, DU, and SS replacement pins. The dynamic evolutions of the DDA signals for three different effective enrichments (1.97 percent, 1.38 percent, and 0.80 percent  $^{235}\text{U}$ ) were plotted for a Front (closest to neutron generator) and Back (furthest from neutron generator) detector position (Figure 3). Qualitatively, the three 10-pin replacement scenarios showed distinguishable differences compared to the No Diversion case with the magnitude of the DDA signal gradually decreasing with the effective enrichment of the fuel assembly. In other words, in case of the fresh fuel, even small variations ( $\pm 0.1\text{-}0.2$  percent of  $^{235}\text{U}$ ) of the fuel enrichment are in principle observable with the described DDA system, where however the Back detectors seem more sensitive than the Front detectors.

### DDA Signal in 70-100 $\mu\text{s}$ Time Domain

For a quantitative comparison, the integrals of the No Diversion DDA signal in the 70-100  $\mu\text{s}$  time domain for Front and Back detectors were compared to the integrals of the DDA signals of the three diversion scenarios (NU, DU, and SS rods). The relative differences between the No Diversion and diversion scenarios were determined for the three enrichments (Figure 4). The Back detectors (furthest from the neutron generator) showed a larger relative difference in the summed DDA signal than the Front detectors, with the differences ranging from 4-10 percent and 2-5 percent, respectively, for the NU, DU, and SS cases. The larger impact on the Back detectors is due to their increased sensitivity to the overall fuel assembly fissile content, as discussed in Reference 10, while the Front detectors are more sensitive to regional changes. These different sensitivities of the detectors positioned around the fresh fuel assembly may be of use when evaluating diversion scenarios that include clusters of pins substituted simultaneously by comparing Front-to-Back ratios, which have been investigated in Reference 14. However, the Front-to-Back comparison approach is not very sensitive to scenarios used in this paper, where positions of diverted pins are nearly evenly distributed across the entire fuel assembly.

Overall, the results in Figure 4 for the Back detectors suggest that the change in the magnitude of the DDA signal is well above the 2 percent threshold for considering the assembly

suspect even when only 10 pins are substituted for all three substitution materials. The sensitivity of the Front detectors is lower, and in the case of the NU and DU substitution, the difference in magnitude of the DDA signal is comparable to expected experimental errors, thus would yield inconclusive results.


### DDA Signal Die-Away Time in 70-100 $\mu\text{s}$ Time Domain

The DDA signal die-away times in the 70-100  $\mu\text{s}$  time domain were determined for all nine detectors for the three enrichments for the four simulations (No Diversion, NU, DU, and SS). The characteristic "Empire State" effect<sup>13</sup> was observed, reflecting that the enrichment and detector position relative to the neutron generator impact the DDA signal die-away time (Figure 5). A gradual decrease in the die-away time for each respective detector position was evident as the effective enrichment in the fuel assemblies decreased.

**Keywords:** differential die-away, non-destructive assay, fresh fuel, missing pins

### References

1. IAEA. 2015. Safeguards Mission, March 2015. Online. Available: <https://www.iaea.org/safeguards/about.html>. Accessed May 2015.
2. Caldwell, J., and W. Kunz. 1982. Experimental Evaluation of the Differential Die-away Pulse-Neutron Technique for the Fissile Assay of Hot Irradiated Fuel Waste, LA-UR-82-788, Los Alamos National Laboratory.
3. Caldwell, J., R. Hastings, G. Herrera and W. E. A. Kunz. 1986. The Los Alamos Second-Generation System for Passive and Active Neutron Assays of Drum Size Containers, Los Alamos National Laboratory, LA-10774-MS.
4. Coop, K. 1989. Neutron Die-away Methods for Criticality Safety Measurements of Fissile Waste, *American Nuclear Society Winter Meeting*, San Francisco, 1989.

- 
5. Clark, P., M. Wilson, J. Rackham, K. Stephenson and J. Simpson. 1999. Improved Assay of Highly Active Reprocessing Waste by the Use of a Linear Accelerator Based Neutron Source, *Proceedings of the 40th INMM Annual Meeting*.
  6. Favalli, A., H. Mehner, J. Crochemore, and B. Pedersen. 2009. Pulsed Neutron Facility for Research in Illicit Trafficking and Nuclear Safeguards, *IEEE*, vol. 56, no. 3.
  7. Pelowitz, D., et al. 2011. MCNPX User's Manual, Version 2.7.0, Los Alamos National Laboratory, LA-UR-11-00438.
  8. Humphrey, M., S. Tobin, and K. Veal. 2012. The Next Generation Safeguards Initiative's Spent Fuel Nondestructive Assay Project, *Journal of Nuclear Materials Management*, vol. 40, no. 3.
  9. Henzl, V., M. Swinhoe, S. Tobin, H. Menlove, J. Galloway, and D. Won Lee. 2012. Direct Measurement of Initial Enrichment, Burn-up and Cooling Time of Spent Fuel Assembly with a Differential Die-Away Technique Based Instrument, *Proceedings of the 53<sup>rd</sup> INMM Annual Meeting*.
  10. Martinik, T., V. Henzl, S. Grape, S. Jacobsson Svard, P. Jansson, M. Swinhoe, and S. Tobin. 2014. Simulation of Differential Die-Away Instrument's Response to Asymmetrically Burned Spent Nuclear Fuel, submitted for publication in *Nuclear Instruments and Methods in Physics Research A*.
  11. Goodsell, A., V. Henzl, M. Swinhoe, C. Rael, D. Desimone and W. Charlton. 2015. Comparison of fresh fuel experimental measurements to MCNPX results using the differential die-away instrument for nuclear safeguards applications, *ESARDA Symposium 2015*, Los Alamos National Laboratory, LA-UR-15-23252.
  12. Goodsell, A., M. Swinhoe, V. Henzl, K. Ianakiev, M. Iliev, C. Rael and D. Desimone. 2014. Differential Die-Away Instrument: Report on Neutron Detector Recovery Performance and Proposed Improvements, Los Alamos National Laboratory, LA-UR-14-27369.
  13. Goodsell, A., V. Henzl, M. Swinhoe, C. Rael and D. Desimone. 2015. Differential Die-Away Instrument: Report on Comparison of Fuel Assembly Experiments and Simulation, Los Alamos National Laboratory, LA-UR-15-20242.
  14. Henzl, V. 2014. Evaluation of Differential Die-Away Technique Potential in Context of Non-Destructive Assay of Spent Nuclear Fuel, Los Alamos National Laboratory, LA-UR-14-29224.



## Book Review

By Mark L. Maiello, PhD

Book Review Editor

### Building the H Bomb A Personal History

**Kenneth W. Ford**

Softcover, 222 pages

ISBN 978-9814618793

World Scientific Publishing Co.,

Singapore, 2015

Personal memoirs can be interesting for their personal point of view especially when the events discussed are at the nexus of some world-changing event. In the right hands, it can be a very visceral experience with unique claims to the story based on eye-witness observations, personal conversation, friendship, and perhaps even more intimate relationships with the players who changed history. Successful telling these kinds of stories depends on much — not the least of which is one's role or station at the moments defining the story. And of course, one must be able to nimbly relate these accounts interweaving an on-scene perspective into the overall historical account. In *Building the H Bomb*, we fall somewhere between accomplishment and failure.

This memoir is an honest accounting of Dr. Kenneth Ford's experiences helping to build some of the world's first thermonuclear weapons, but it's a bit bereft of excitement. The approach throughout is very light-hearted, no doubt a reflection of the author's personality. As are many memoirs, the story is speckled with side trips concerning mentors, family, friends, and in this case, some of the big names in weapons development:

Fermi, Teller, and Oppenheimer. But, these little vacations from both the grind and the excitement of weapons development don't necessarily reveal earth-shattering facts about a physicist's life during the late 1940s and '50s or the major players he orbited around. There isn't a new definitive revelation of Edward Teller's heavy hand in H-bomb development (though the author speculates from a firm basis about who is to be credited with the H-bomb's implosion design). The author verifies Fermi's kindly and positive disposition. Oppenheimer, perhaps too far up the chain of command for the author to have had much contact, is commented upon from afar. Others lower in the chain, part of Ford's working group and less publicly known are given quite properly, more ink. But they are less interesting. Ordinary life outside the office (and outside the 1950s computer room) — superficially at least — is given its due. But, is that enough for a reader seeking insight about life as a theoretical physicist on one the biggest game-changing projects in human history?

Ford projects much humility and honesty. He lets you know from what vantage his perspective lies. He was a team member at this time, not a team leader. He was stationed at Los Alamos for part of this story — a place he loves — but was also assigned through the tenacity and influence of his supervisor to the relative comforts of Princeton, New Jersey, USA. He sat in on many high-level meetings that included some of the

major H-bomb luminaries, but was also excluded from some too. He will honestly state that in some instances, he does not recall why he was allowed to remain present or even what he was doing at some of these encounters. As the guy who did not mind working at night, he was often assigned computing time when most of his contemporaries were asleep. He was not the guy who made decisions but the one who helped those that did. Perhaps he is best described as the fly on the wall, though the wall was not always in proximity to where all the action was.

To compliment this romp through a few of the nuclear playgrounds of the mid-twentieth century is Ford's internal scuffle with loyalty oaths, and, eventually, with his own ethics as a result of being involved with the H-bomb. He reveals that he was initially not a politically conscience man. After the first dedicated H-bomb test, the "Mike" shot of 1952, his feelings vacillated between the euphoria of success and the dread associated with the bomb's power, but he was not ready to act on the latter. Scientists had been conflicted about working on the bomb since Hiroshima and Nagasaki. Many, for example, quit their jobs at the uranium separation operations at Oak Ridge once the secrecy ended and they found out what had been created there. Admittedly, descriptions of the human suffering as a result of the atomic bombings was suppressed in the U.S. but, in the small world of physics, the conscientious objection to the bomb



wouldn't have been news to Ford had he been paying it much attention. Instead, his revelations came along slowly, buoyed by the anti-war sentiments of the Vietnam era that eventually pushed him away from weapon's development entirely. But as a tepid contributor to the anti-war movement, his internal rebellion comes across as equally lukewarm narrative. He found his way but in a private, rather quiet, methodical manner (to each his own). Older readers may sympathize with the reality of holding a job, growing into it and then being profoundly changed by the circumstances of one's times. Younger readers should take note that such evolutions do occur. Work thought at first to be interesting and exciting may, through the vicissitudes of national or world events or even very local ones, can become a burden — sometimes of conscience.

Ironically, this straightforward, well-meaning memoir has its share of controversy. The U.S. Department of Energy contends that Ford's book contains secret material. For all the consternation that caused the author, there is little that a lay reader — and that includes scientists from other professions — will find clandestine. The purported secret material is not obvious (Dr. Ford assures us that he was careful not to print anything that could not be found elsewhere), and there is little payoff here for those seeking a thrill associated with this controversy.

Will one be bored? Simply put: No. There is a good story here about a young aspiring Princeton PhD who accepted an offer in 1950 to assist with weapons development in Los Alamos. These honest musings and recollections of a dedicated man devoted to his science provide enough substance to keep one turning

the page. The reader will immediately perceive the framework of the memoir: a devoted, talented scientist seeking to hone his craft with the ultimate intent to make his way into the larger world of research becomes part of one the most controversial and unprecedented feats of physics ever imagined — (initially one with dim prospects of success until the Teller-Ulam breakthrough of radiation implosion). Ford both worked to live and lived to work. Along the way he met some notables, traveled parts of the nation he later fell in love with, and found that despite the satisfaction he obtained from his contributions to the hydrogen bomb development work, his nation's conduct in Vietnam — not notably at Hiroshima or Nagasaki — drove him to reconsider his relationship to his government.

These are the recollections of a talented physicist who was fortunate to have experienced the heady atmosphere of those days when nuclear physics was nascent. He led a life that some might consider chancy — where he worked and what he worked on was not a traditional career path (it was however, a life changing experience). But it's a quiet memoir. The language is simple, straightforward; the sentences short and to the point. There is little embellishment here. When Ford talks about working overnights at an IBM office in New York City, and of his fondness for a neighborhood deli that sustained him, that is all the detail you get. There was apparently no dramatic self-revelation, no epiphany, not even a funny anecdote associated with the lateness of the hour and the endless computer runs done in near solitude. Frequently, the author will journey down other arcane paths with similar lack of entertaining payoff. In particular, he men-

tions the several vehicles he owned, the trips he took with them — one or two admittedly with memorable but not out-of-the-ordinary consequences — and what eventually became of these machines: most found endings that you would expect (sold). Ford applied for and obtained the P.O. box number for what eventually became the Princeton Plasma Physics Laboratory (a direct descendant of the H-bomb development project) — a box number that is apparently still current. These tangents provide but mild diversions. However, the author's daily in-the-trenches efforts and his modest off-work activities as a weapons physicist do not detract from the back-story — the historic game-changing moment he had the privilege to be part of.

The banal is balanced a bit by the personal side of the story. Among the other notables already mentioned, Ford also encountered Von Neumann, the great mathematician and computer architect. He even orbited in the vicinity of the Nobel-prize winning Cornell University physicist Hans Bethe who postulated stellar fusion cycles. But his writing is enlivened, quite naturally, when Ford delves into his relationship with lesser known personalities such as his mentor John Wheeler who so influenced the young physicist. Friend and colleague John Toll is treated equally well. Others also are revered: Princeton assistant professor David Bohm, a roommate and colleague of the author, is given several pages because he ran afoul of the "red scare" promulgated by the House Un-American Activities Committee of the 1950s. The mention of these colleagues, physicists of Project Matterhorn (the hydrogen bomb development effort), do help to invigorate Ford's effort.

The book is well-designed and includes several useful illustrations and many black-and-white (some striking) archival photographs of the work places, physicists, and events that remain near and dear to the author. The sections of the book are cleverly divided by a classy graphic illustrating the deuterium-tritium fusion reaction and its products. The

writing moves along at a reasonably fast pace and can be engaging if not sophisticated. You need not seek long for the author's forthright sentiment — it will charm and disarm many readers. A chapter of descriptive thermonuclear physics is included in the early third of the book that does not distract from the memoir. It complements the narrative but can be

skipped as the author courteously mentions. It is preceded by a review of the discoveries of radioactivity and early atomic physics. Overall, and despite its heady title, *Building the H Bomb* is a good, light, airy read that is straightforward, compact, and sincere if just a tad short on emotional impact.



# Taking the Long View in a Time of Great Uncertainty

## Rehearsing Possible Futures

By Jack Jekowski  
Industry News Editor and Chair of the Strategic Planning Committee



In last quarter's column, I described how scenario planning, a strategic planning tool that is being implemented by many organizations, can be used to rehearse, and prepare for possible alternative futures in the context of the complex world we live in today. In particular, when we look across the geo-political landscape of the global security environment today<sup>1</sup>, one can become quickly overwhelmed with many uncertainties, and lose sight of the big picture strategies that might be useful to prepare for alternative futures. When carefully identified, critical uncertainties, or combination of critical uncertainties, can provide insight into events or actions that might dramatically change the path to the future. If an organization has sufficient spheres of influence, such as the National Laboratories, or national or international organizations including the International Atomic Energy Agency (IAEA), or the United Nations itself, it may even be possible to change the direction that the world is headed if it is determined that the end point of any particular future path is undesirable.

### Creating Scenarios of Interest to the Institute

The nuclear environment that the INMM works within has many interrelated complexities, lending itself to characterization using scenario techniques. The stories created of future worlds using these scenario techniques help stimulate strategic discussions that are different than those which take place during traditional strategic planning activities. These discussions might include, for example, the technical challenges of verification requirements under the Joint Comprehensive Plan of Action (JCPOA)<sup>2</sup>, the policy challenges that lie ahead addressing the nuclear ambitions of North Korea, or the societal impact of the Fukushima recovery effort.

Many indicators point to these challenges, as described in the recent announcement by the Bulletin of Atomic Scientists, updating their "Doomsday Clock",<sup>3</sup> and by former U.S. Secretary of Defense, William J. Perry who has suggested the risk of a nuclear catastrophe is greater today than at any time during the Cold War.<sup>4</sup> One only has to look at

the monumental, decadal technical challenges facing Japan today in the aftermath of the Fukushima nuclear incident, to wonder "What if management had rehearsed an improbable seismic event and resulting unprecedented tsunami during the design of their facility plan? Could they have avoided or mitigated the event that occurred?"

This is the world of scenario planning — stretching the imagination of managers and leaders so they can discuss possible responses and solutions to "what if" questions about future events in a controlled environment, and by rehearsing those discussions, be better prepared for the unexpected.

### Critical Uncertainties for Scenario Axes

In last quarter's column, I posited two current critical uncertainties that one could envision creating a set of future worlds in which strategic discussions pertinent to the future of the INMM could occur. Those future worlds would be created by the nexus of these two critical uncertainties on an orthogonal set of axes, where the extremes of each axis reflect end points of the critical uncertainty, representing on one end an ideal state and on the other end a troubling, undesirable, or even nightmarish state. Let's take the two critical uncertainties that we identified and examine them in more detail for possible end state descriptors:

*This column is intended to serve as a forum to present and discuss current strategic issues impacting the Institute of Nuclear Materials Management in the furtherance of its mission. The views expressed by the author are not necessarily endorsed by the Institute, but are intended to stimulate and encourage JNMM readers to actively participate in strategic discussions. Please provide your thoughts and ideas to the Institute's leadership on these and other issues of importance. With your feedback we hope to create an environment of open dialogue, addressing the critical uncertainties that lie ahead for the world, and identify the possible paths to the future based on those uncertainties that can be influenced by the Institute. Jack Jekowski can be contacted at [jjekowski@aol.com](mailto:jjekowski@aol.com).*





## The Advancement and Control of Nuclear Technologies

- In a positive future world one might envision continuing breakthroughs in monitoring and security technologies that would allow treaty verification by national technical means, and verification of compliance requirements. The deployment of the world-wide seismic monitoring system by the Comprehensive Test Ban Treaty Organization (CTBTO)<sup>5</sup> is an example of how technology can be used to further the confidence of the world in monitoring for clandestine nuclear tests. Similarly, technologies developed by the U.S. national laboratories and International agencies have been used effectively to implement remote monitoring and verify compliance to treaty requirements. Efforts for remote detection and characterization of clandestine activities have proven to be more difficult to achieve, as is the complex world of nuclear forensics as a method to deter the use of nuclear materials, or in the worst case scenario, to affix responsibility. However, breakthroughs in these technologies could dramatically change the dialogue for arms control treaties. New technologies can also be envisioned that will lead to an inherently safer and more prosperous future, such as the development of more secure and inherently-safe nuclear reactor concepts, such as the advancements promised by Small Modular Reactors<sup>6</sup>, mentioned in last quarter's column.
- In a negative future world, one might envision malevolent parties utilizing the technologies of the 21<sup>st</sup>

century to achieve their agendas, not the least of which would include the use of nuclear materials, or new paths for the acquisition of nuclear materials or the surreptitious manufacture of those materials<sup>7</sup>, as also mentioned in last quarter's column. The technologies of the 21<sup>st</sup> century might also lead to the use of cyber techniques to access restricted information or even disrupt physical operations of nuclear facilities. In fact, cyber intrusions for nefarious purposes have become a common headline in the media today, and has recently driven a new U.S. national security cyber strategy,<sup>8</sup> as well as special Presidential attention, with multi-\$B increases in the U.S. Federal budget proposed for FY2017.<sup>9</sup> In a nightmare scenario a small band of non-nation state actors might take control of a poorly-protected nuclear reactor resulting in a catastrophic event impacting a large population and shaking the confidence of the public, turning them further against "all things nuclear".<sup>10</sup> This has led some to equate cyber activities to warfare, and even to draw an analogy to nuclear deterrence.<sup>11</sup>

## Global Nuclear Security Threats

- In a positive future world, the efforts of the current U.S. administration to rally world leaders through commitments made at the four Nuclear Security Summits leads to the enhanced protection of nuclear materials and facilities.<sup>12</sup> The completion and demonstration of the CTBTO seismic network and enhanced atmospheric monitoring technologies, as well as breakthroughs in nuclear forensics and related monitoring and

verification techniques provide world governments with the confidence they need to proceed with multi-lateral nuclear agreements and treaties. Combined with efforts by non-governmental organizations (NGOs), public interest in a "new world" is raised, and helps to drive policymakers to establish new goals to the elusive concept of "global zero," which for now, at least, seems farther away than ever.<sup>13</sup>

- In a negative future world, the geopolitical and religious conflicts that are shaking the world intensify, and a new Cold War emerges, this time with more nuclear players, as the "dominoes fall"<sup>14</sup> and more nations join the "nuclear club."<sup>15</sup> The once optimistic future that the end of the Cold War offered suffers setbacks as every Nuclear Weapons State pursues modernization efforts for their stockpiles and delivery systems<sup>16</sup>, and as once-tempered political rhetoric has been overtaken by frightening words of nuclear confrontations.<sup>17</sup> The divisions of the major powers into ideologies that become more and more incompatible create a backdrop for uncontrolled conflicts that ultimately triggers a global conflict, with nations teetering on the brink of nuclear war. One can envision any one of several nuclear "tipping points" leading to a nuclear exchange, from the Middle East to East Asia. The spread of extremist terrorism events grow exponentially as the world is unable to address the indoctrination of new generations into those doctrines, and the global community is wracked with a "hundred-year" war.



### *The Advancement and Control of Nuclear Technology*

- |   |  |            |
|---|--|------------|
| <p>(-)</p> <ul style="list-style-type: none"><li>• New technologies allow for fabrication of weapons components by non-state entities</li><li>• Cyber intrusions proliferate including attacks on physical infrastructure</li><li>• Classified information is routinely disclosed</li></ul> | <ul style="list-style-type: none"><li>• New techniques emerge for treaty verification</li><li>• CTBTO completes network and demonstrates effectiveness</li><li>• National Technical Means emerge that can be used for “stand-off” analysis of surreptitious weapons tests</li><li>• Nuclear forensics techniques are enhanced and widely publicized</li><li>• New safe, secure nuclear power technologies are deployed and replace older installations</li></ul> | <p>(+)</p> |
|---|--|------------|

### *Global Nuclear Security Threats*

- |   |   |            |
|---|---|------------|
| <p>(-)</p> <ul style="list-style-type: none"><li>• Nuclear materials are stolen</li><li>• Nuclear states proliferate</li><li>• Terrorists detonate a dirty bomb in a large Western city</li><li>• Nuclear tensions rise amid modernization efforts</li><li>• New generation of international terrorists expand world wide</li></ul> | <ul style="list-style-type: none"><li>• Nuclear Security Summits lead to protection of nuclear materials</li><li>• NGOs help with disseminating the success of the new technologies and sway public opinion</li><li>• UN and other international efforts stem the rise of international terrorism</li><li>• Economic stability reduces the impact of political divisiveness</li><li>• Global Zero initiatives take hold as the NPT Section VI goals are actively worked</li></ul> | <p>(+)</p> |
|---|---|------------|

The selection of the proper set of critical uncertainties for each axis is very important to the development of robust scenarios that challenge the mindset of leadership, yet are not so outrageous that discussions are shut down because of the implausibility of the future worlds that are created. Often, the process becomes one of trial and error, where engaged participants walk through discussions of future worlds, and realize that the axes are not truly orthogonal, or that a previously unidentified critical uncertainty might lend itself to richer, more impactful discussions. This sometimes repetitive process is not wasted, for each attempt will routinely raise new perspectives, drive the need for additional research, and further strengthen the confidence of the leadership involved that they are developing a sense for handling any eventuality. It is not uncommon for major organizations to engage

science fiction writers to help with the development of stories of these future worlds, so that the imagination of the organization is captured in the strategic discussions.

### **Development of Scenario Axes**

From the discussion above, we can create two potential axes that might lead to future worlds that challenge the mindset of the Institute’s membership. These are portrayed below, with end point descriptors.

In future columns I will explore the development of other critical uncertainty axes, and then use them to develop “future world stories” that will allow us to better understand the role the Institute can play in this very complicated world. As always, I would welcome thoughts and ideas that can help shape those future world stories.

### **Endnotes**

- 1 See “Terrorism and Terraforming”, Aviation Week and Space Technology, January 4-17, 2016, pp. 46-48.
- 2 See “Nuclear Inspectors Have Snazzy New Tools to Catch Iran Cheating”, [http://foreignpolicy.com/2016/02/04/nuclear-inspectors-have-snazzy-new-tools-to-catch-iran-cheating/?utm\\_source=Saithru&utm\\_medium=email&utm\\_campaign=New%20Campaign&utm\\_term=%2ASituation%20Report](http://foreignpolicy.com/2016/02/04/nuclear-inspectors-have-snazzy-new-tools-to-catch-iran-cheating/?utm_source=Saithru&utm_medium=email&utm_campaign=New%20Campaign&utm_term=%2ASituation%20Report)
- 3 See <http://thebulletin.org/it-still-three-minutes-midnight9107> and <http://thebulletin.org/sites/default/files/2016%20doomsday%20clock%20statement%20-%20final%5B5%5D.pdf> for the final report for this year.



- 4 See [http://www.huffingtonpost.com/william-jperry/nuclear-catastrophe-risk\\_b\\_9019558.html](http://www.huffingtonpost.com/william-jperry/nuclear-catastrophe-risk_b_9019558.html) and <http://www.wjperryproject.org/>
- 5 See <https://www.ctbto.org/>
- 6 See <http://www.energy.gov/ne/nuclear-reactor-technologies/small-modular-nuclear-reactors> for more information on the U.S. Department of Energy's programs to stimulate the development of these new energy sources.
- 7 See NNSA Report "Prevent, Counter and Respond – A Strategic Plan to Reduce Global Nuclear Threats", [https://nnsa.energy.gov/sites/default/files/NPCR%20Report\\_FINAL\\_\(with%20signatures\)\\_3-18-15.pdf](https://nnsa.energy.gov/sites/default/files/NPCR%20Report_FINAL_(with%20signatures)_3-18-15.pdf)
- 8 See [https://www.whitehouse.gov/sites/whitehouse.gov/files/documents/2016\\_Federal\\_Cybersecurity\\_Research\\_and\\_Development\\_Strategic\\_Plan.pdf](https://www.whitehouse.gov/sites/whitehouse.gov/files/documents/2016_Federal_Cybersecurity_Research_and_Development_Strategic_Plan.pdf)
- 9 See <https://www.whitehouse.gov/the-press-office/2016/02/09/fact-sheet-cybersecurity-national-action-plan><https://www.whitehouse.gov/the-press-office/2016/02/09/fact-sheet-cybersecurity-national-action-plan>
- 10 For an interesting perspective on where the "Cyber War" may be headed, see <http://thehill.com/policy/national-security/269594-us-said-to-have-had-detailed-cyberattack-plan-for-iran> and <http://www.nytimes.com/2016/02/17/world/middleeast/us-had-cyberattack-planned-if-iran-nuclear-negotiations-failed.html>
- 11 See "The flawed analogy between nuclear and cyber deterrence," <http://thebulletin.org/flawed-analogy-between-nuclear-and-cyber-deterrence9179>
- 12 See <https://www.whitehouse.gov/blog/2015/08/05/announcement-nuclear-security-summit-2016> for information on the fourth Nuclear Security Summit that will be held in Washington, D.C., March 31-April 1, 2016.
- 13 See "Today's Nuclear Dilemma" by Eric Schlosser, <http://thebulletin.org/2015/november/todays-nuclear-dilemma8839>
- 14 See "Taking the Long View: Sometimes Life Seems to be too Complicated," Journal of Nuclear Materials Management, Vol. 44 No.2, for a discussion of how an earlier scenario development created by the author utilized a term coined by Dr. Sig Hecker to describe a world in which more and more nuclear armed states emerge.
- 15 The term "Nuclear Club" is term often used in the media to refer to countries that are deemed to have a nuclear weapons capability – typically the five Nuclear Weapons States (the U.S., U.K, France, Russia and China), and Pakistan, India, Israel and North Korea (although the latter could be deemed not to have a "weaponized" or deliverable weapon at this time). See <http://www.usatoday.com/story/news/world/2016/01/06/nine-nations-possess-nuclear-weapons/78350588/> for a recent article in *USA Today* using that terminology in the aftermath of the announcement by the DPRK (North Korea) that it had tested a Hydrogen bomb. North Korea withdrew from the NPT on January 10, 2003, but at that time indicated "it had no intention of producing nuclear weapons."
- 16 See "Disarm and Modernize," <http://foreignpolicy.com/2015/03/24/disarm-and-modernize-nuclear-weapons-warheads/>
- 17 See "A New Arms Race Threatens to Bring the U.S. and Russia Back to the Nuclear Brink," [http://www.huffingtonpost.com/joe-cirincione/arms-race-us-russia-nuclear\\_b\\_8557526.html](http://www.huffingtonpost.com/joe-cirincione/arms-race-us-russia-nuclear_b_8557526.html), and "North Korea Threatens U.S. Nuclear Attack", <http://www.washingtontimes.com/news/2015/sep/15/l-todd-wood-north-korea-threatens-us-nuclear-attack/>



**July 24–28, 2016**  
INMM 57th Annual Meeting  
Atlanta Marriott Marquis  
Atlanta, GA USA

**September 18–23, 2016**  
PATRAM 2016  
Kobe Portopia Hotel  
Kobe, Japan

**December 5–9, 2016**  
IAEA International Conference  
on Nuclear Security:  
Commitments and Actions  
International ATomic Energy  
Agency  
Vienna, Austria

**January 10–12, 2017**  
32nd INMM Spent Fuel  
Management Seminar  
Washington Marriott Georgetown  
Washington, DC USA

**July 16–20, 2017**  
INMM 58th Annual Meeting  
Renaissance Indian Wells  
Indian Wells, California USA

For more information, visit the INMM Events Page.

## Author Submission Guidelines

The *Journal of Nuclear Materials Management* is the official journal of the Institute of Nuclear Materials Management. It is a peer-reviewed, multidisciplinary journal that publishes articles on new developments, innovations, and trends in safeguards and management of nuclear materials. Specific areas of interest include facility operations, international safeguards, materials control and accountability, nonproliferation and arms control, packaging, transportation and disposition, and physical protection. *JNMM* also publishes book reviews, letters to the editor, and editorials.

Submission of Manuscripts: *JNMM* reviews papers for publication with the understanding that the work was not previously published and is not being reviewed for publication elsewhere. This restriction includes papers presented at the INMM Annual Meeting. Papers may be of any length. All papers must include an abstract.

The *Journal of Nuclear Materials Management* is an English-language publication. We encourage all authors to have their papers reviewed by editors or professional translators for proper English usage prior to submission.

Papers should be submitted as Word or ASCII text files only. Graphic elements must be sent in TIFF, JPEG or GIF formats as separate electronic files.

Submissions may be made via email to Managing Editor Patricia Sullivan at [psullivan@inmm.org](mailto:psullivan@inmm.org). Submissions may also be made via regular mail. Include a CD with all files. These submissions should be directed to:

Patricia Sullivan  
Managing Editor  
Journal of Nuclear Materials Management  
One Parkview Plaza, Suite 800  
Oakbrook Terrace, IL 60181 USA

Papers are acknowledged upon receipt and are submitted promptly for review and evaluation. Generally, the corresponding author is notified within ninety days of submission of the original paper whether the paper is accepted, rejected, or subject to revision.

Format: All papers must include:

- Corresponding author's complete name, telephone number and email address
- Name and address of the organization where the work was performed
- Abstract
- Tables, figures, and photographs in TIFF, JPEG, or GIF formats. **Color is encouraged.**
- Numbered references in the following format:  
1. Jones, F.T., and L. K. Chang. 1980. Article Title. *Journal* 47(No. 2): 112–118. 2. Jones, F.T. 1976. *Title of Book*, New York: McMillan Publishing.
- Author(s) biography and photos
- **A list of keywords**

The *Journal of Nuclear Materials Management* does not print "foot notes." We publish references and/or end notes. If you choose to include both references and notes, you may combine them under the same heading or you may keep them separate, in which case you must use numbers for the References (1., 2., 3., etc.) and letters (A., B., C., etc.) for the End Notes.

*JNMM* is published digitally in full color. Color graphics and images are encouraged.

Peer Review: Each paper is reviewed by at least one associate editor and by two or more reviewers. Papers are evaluated according to their relevance and significance to nuclear materials safeguards, degree to which they advance knowledge, quality of presentation, soundness of methodology, and appropriateness of conclusions.

Author Review: Accepted manuscripts become the permanent property of INMM and may not be published elsewhere without permission from the managing editor. Authors are responsible for all statements made in their work.

